Synthesis and Characterization of Hydrogels prepared by Free Radical Polymerization

Dissertation

With the Aim of Achieving the Doctoral Degree
at the Faculty of Mathematics, Informatics and Natural Sciences

Department of Chemistry
University of Hamburg

Submitted by

Helena Paulsen

Hamburg 2018

The experimental work described in this thesis was carried out at the Institute for Technical and Macromolecular Chemistry of the University of Hamburg in the group of Professor Dr. Gerrit A. Luinstra from November 2014 to November 2017.

There's something that doesn't make sense.
Let's go and poke it with a stick.

The Doctor

Table of Contents

List of Abbreviations

[M]	monomer concentration
$[M]_0$	monomer concentration at time 0
$[M]_t$	monomer concentration at time t
[P·]	the concentration of the growing polymer chains
$\|\eta^*\|$	complex viscosity
$1-x$	amount of relaxation controlled processes
a	edge length
AA	acrylic acid
AIBN	azobisisobutyronitrile
APS	ammonium persulfate
ATRP	atom transfer radical polymerization
BPO	dibenzoylperoxide
$c(AA)$	concentration of acrylic acid
$c(KPS)$	concentration of KPS
$c(PEGda)$	concentration of crosslinking agent PEGda
CFRP	controlled free radical polymerization
CTA	chain transfer agent
d	particle diameter
D	diffusion coefficient
Di-Cup	dicumyl peroxide
dV	normalized volume change
ESI-MS	electrospray ionization mass spectrometry
f	radial efficiency, factor of ionic sensitivity
F	factor considering the interparticle volume
FRP	conventional free radical polymerization
FT	Fourier Transformation
g	ratio of the swelling degree after and before the vacuum treatment
G'	storage modulus
G''	loss modulus
G_w	gain in weight
I·	initiator radical
I_2	initiator
IPN	interpenetrating network
IR	infrared
k'	initiator-dependent rate constant
k_{add}	addition rate constant
k_{-add}	fragmentation rate constant
k_d	decay of the initiator
k_D	rate constant of Fickian diffusion controlled sorption
k_i	initiation rate constant

k_p	propagation rate constant
KPS	potassium persulfate
k_R	rate constant of relaxation controlled sorption
k_{re-in}	re-initiation rate constant
k_t	termination rate constant
k_{tc}	termination/recombination rate constant
k_{td}	termination/disproportionation rate constant
k_β	fragmentation rate constant
LAMs	"less-activated" monomers
LCST	lower critical solution temperature
$\ln([M]_0/[M]_t)$	pseudo-first order plot
L_x	ligands
m	weight of the composite sample swollen with solvent
M	monomer
m/ρ_s	composite volume in pure organic solvent
m/ρwater	composite volume in pure water
M:CTA:I	ratio of monomer, CTA and initiator
$M_{\infty,D}$	equilibrium amount of diffusion controlled sorption
$M_{\infty,R}$	equilibrium amount of relaxation controlled sorption
MADIX	macromolecular design via the interchange of xanthates
MAMs	"more-activated" monomers
MBA	*N,N'*-methylenebis(acrylamide)
m_{Bas}	weight of the dried original Basotect® sample
m_{eq}	equilibrium weight of the water-swollen sample
m_{gel}	weight of the swollen gel
$m_{gel,dry}$	weight of the dried gel
MGluBX	methyl α-D-glucopyranoside-6-(*S*-benzyl)xanthate
MMBX	methyl α-D-mannopyranoside-6-(*S*-benzyl)xanthate
MMPX	methyl α-D-mannopyranoside-6-(*S*-2-propionic acid)xanthate
M_n	number average molecular weight
m_s	weight of the solvent bound in the gel
$m_{s,gel}$	weight of absorbed solvent in the gel
$m_{s,int}$	weight of the interstitial solvent in the gel
m_{SAP}	weight of the dried SAP
$m_{SAP,as}$	weight of the dry SAP composite after swelling
$m_{SAP,bs}$	weight of the dry SAP composite before swelling
M_t	time-dependent weight of solvent entering/leaving a gel
$M_{t,D}$	time-dependent weight of solvent controlled by Fickian diffusion process
$M_{t,R}$	time-dependent weight of solvent controlled by relaxation process
M_t/M_∞	normalized time-dependent swelling
MWD	molecular weight distribution

ND	degree of neutralization
NMP	nitroxide mediated radical polymerization
NMR	nuclear magnetic resonance
NVP	*N*-vinyl pyrrolidone
O	surface
P	measure for the swelling and modification with hydrogel of the original Basotect® sample
PAA	poly(acrylic acid)
PDI	polydispersity index
PEGda	poly(ethylene glycol) diacrylate
P_i	polymer
P_{m+n}	high molecular mass polymer
$P_m\cdot$	growing polymer chain
$P_m^=$	unsaturated polymer
$P_n\cdot$	growing polymer chain
P_n^H	saturated polymer
PNIPAm	poly(*N*-isopropylacrylamide)
PVP	poly(*N*-vinyl pyrrolidone)
Q	swelling capacity
Q_{real}	real weight dependent swelling degree
Q_{vac}	swelling degree after applying vacuum
R group	initiating group
R·	alkyl radical
RAFT	reversible addition fragmentation chain transfer
R-X	alkyl halide
SAP	superabsorbent polymer
SEC	size exclusion chromatography
SEM	scanning electron microscopy
t	time
TEMPO-R	2,2,6,6-tetramethylpiperidine 1-oxyl derivatives
TLC	thin-layer chromatography
V	volume
V/V_{eq}	normalized volume
VA-044	1,2-bis(2-(4,5-dihydro-1H-imidazol-2-yl)propan-2-yl)diazene dihydrochloride
w_{gel}	gel content
w_{os}	weight fraction organic solvent
w_{sol}	sol content
x	factor of thickness variation, amount of diffusion controlled processes
X_i	monomer conversion
Z group	stabilizing group
δ	chemical shift

ρ	density
ρ_s	density of an organic solvent
ρ_water	density of water
ω	angular frequency

Zusammenfassung

Hydrogele sind im täglichen Leben allgegenwärtig. Sie können aufgrund ihrer verschiedenen chemischen und physikalischen Eigenschaften in den unterschiedlichsten Anwendungsgebieten eingesetzt werden. Im Folgenden werden zwei unterschiedliche Ansätze für die Herstellung verschiedener Hydrogele vorgestellt.

Der erste Ansatz fokussiert die Synthese und Charakterisierung von Poly-*N*-isopropylacrylamid (PNIPAm) und Poly-*N*-vinylpyrrolidon (PVP) unter Verwendung eines *reversible addition fragmentation chain transfer* (RAFT, reversibler Additions-Fragmentierungs-Kettentransfer) Mechanismus.

N-Isopropylacrylamid (NIPAm) and *N*-Vinylpyrrolidon (NVP) wurden kontrolliert mit RAFT-Agentien auf Monosaccharid-Basis polymerisiert. Auf diese Weise konnten PNIPAm und PVP mit maßgeschneiderten Endgruppen, die von dem verwendeten RAFT-Agens abhingen, hergestellt werden. Auf diese Weise wurden Mannose- und Glukose-basierte RAFT-Agentien in die Polymere eingebracht. Die Anwesenheit der „Z"- und „R"-Gruppen des RAFT-Agens als Endgruppen in kontrolliert hergelltem PNIPAm konnte, je nach funktioneller Gruppe, über ^{13}C-NMR-Spektroskopie und/oder chemische Methoden nachgewiesen werden.

Die Reaktionsgeschwindigkeiten der kontrollierten Polymerisationen wurden mittels Reaktionsverfolgung über ^{1}H-NMR-Spektroskopie bestimmt. Diese Reaktionsgeschwindigkeiten wurden mit den Reaktionsgeschwindigkeiten der konventionellen freien radikalischen Polymerisation unter gleichen Bedingungen verglichen. Der Anteil an Polymer ohne funktionelle RAFT-Gruppen an den Kettenenden, die bei der RAFT-Polymerisation gebildet wurden (auch als „totes" Polymer bezeichnet), konnte durch die Synthese von Poly-NIPAm-*co*-NIPAm-Diblockcopolymeren und anschließender Integrierung der Gelpermeationschromatogramme der PNIPAm-Blöcke bestimmt werden. Der Anteil an totem Polymer betrug 19 % für Carboxyl-terminiertes PNIPAm und 36 % für Benzyl-terminiertes PNIPAM.

Der zweite Ansatz, der in dieser Arbeit beschrieben wird, behandelt Copolymere aus Polyacrylsäure und Natriumpolyacrylat. Superabsorbierende Komposite aus teilweise neutralisierter Polyacrylsäure (PAA), einem Polyethylenglykoldiacrylat (PEGda) als Vernetzer und dem offenzelligen Melamin-Formaldehyd-Schaumstoff Basotect® als Matrix wurden in einer Eintopf-Synthese hergestellt. Die Zusammensetzung der Anfangs-Monomerlösung beeinflusste die Veränderung des Verhältnisses aus Oberfläche und Volumen der Basotect®-Matrix nach der Kompositsynthese, die Gewichtszunahme des Schaumstoffs durch Modifikation mit PAA und die Quelleigenschaften des entstandenen Kompositmaterials. Die Gewichtszunahme des Schaumstoffs stieg mit steigendem Hydrogelanteil. Quellexperimente wurden sowohl in demineralisiertem Wasser als auch in Salzlösungen und organischen Lösemitteln wie Ethanol und Dimethylsulfoxid (DMSO) durchgeführt. Die höchste Quellung konnte dabei in demineralisiertem Wasser festgestellt werden. Ein Lösungsmittelaustausch von Wasser zu DMSO oder Ethanol führte zu einem Schrumpf der Proben, wobei der Schrumpf für Ethanol größer war als bei DMSO. Elektronenmikroskopische (SEM) Aufnahmen der Proben konnten nach Trock-

nung mit überkritischem Kohlendioxid für DMSO-gequollene und für Wasser-gequollene Gele nach Gefriertrocknung erhalten werden.

Es wurde festgestellt, dass die Zusammensetzung aus Monomer und Vernetzer genau wie die Dicke der Matrix einen großen Einfluss auf die Quellung und die Quellkinetik hat. Der Hydrogelanteil und die Quellung stiegen mit steigender Konzentration an Acrylsäure in der Anfangs-Monomerlösung und sanken mit steigendem Vernetzungsgrad. Eine geringe Konzentration sowohl an Vernetzer als auch an Acrylsäure führte zu vermehrten Auswaschungen des Hydrogels aus der Matrix und demzufolge zu glitschigen Gelen. Die Matrixdicke hatte ebenfalls einen Einfluss auf das Quellverhalten der SAP-Hydrogele. Dies liegt an der behinderten Diffusion im Falle dicker Matrices und einer geringeren Anzahl an Vernetzungspunkten bei sehr dünnen Matrices mit einem hohen Oberfläche-zu-Volumen-Verhältnis. Die Quellung in salzhaltigen Lösungen führte zu einer verminderten Quellung im Vergleich zur Quellung in demineralisiertem Wasser.

Rheologische Messungen der gequollenen Hydrogele zeigten, dass eine Zunahme der Quellung zu einer Vergrößerung des Netzpunktabstandes (einer Verringerung der Netzpunktdichte) und demzufolge zu einer Verringerung der Speicher- und Verlustmoduli führte.

Abstract

Hydrogels are omnipresent in daily life. They are also used in diverse fields of application with various chemical and physical properties. This thesis reports on two routes of synthesis of hydrogels.

The first approach focuses on the synthesis and characterization of poly(*N*-isopropylacrylamide) (PNIPAm) and poly(*N*-vinylpyrrolidone) (PVP) along a reversible addition fragmentation chain transfer (RAFT) mechanism.

The polymerization of *N*-isopropylacrylamide (NIPAm) and *N*-vinylpyrrolidone (NVP) was carried out with RAFT agents based on carbohydrate molecules in a controlled manner. PNIPAm and PVP were thus equipped with tailor-made functional end groups in form of the RAFT agents. Mannose or glucose-based RAFT agents could thus be introduced into the polymers. The presence of the "Z" and "R" group of the RAFT agent as end groups in PNIPAm was detected by ^{13}C NMR spectroscopy and/or with chemical methods, depending on the type of functional group.

The polymerization rates were determined by monitoring the reaction offline, using ^{1}H NMR spectroscopy. A comparison was made to the polymerization rates of the conventional free radical polymerization. The amount of polymer without RAFT groups at the chain ends, referred to as "dead" polymer, was obtained by synthesis of poly(NIPAm-*co*-NIPAm) diblock copolymers and subsequent integration of the SEC elugram. The amount of dead polymer was 19 % for carboxyl-terminated PNIPAm and 36 % for benzyl-terminated PNIPAm.

The second approach concerns poly(acrylic acid) and sodium polyacrylate copolymers. Superabsorbent composites of partially neutralized poly(acrylic acid) (PAA), the crosslinking agent poly(ethylene glycol) diacrylate (PEGda) and an open-cell melamine/formaldehyde foam (Basotect®) as matrix were synthesized in one-pot. The composition of the initial monomer solution affected the change in surface/volume ratio of the matrix after synthesis, the gain in weight relative to unmodified Basotect® and consequently the swelling behavior of the composites. The gain in weight increased with increasing hydrogel content. Swelling experiments were carried out in demineralized water as well as in saline solution and organic media like ethanol and dimethyl sulfoxide (DMSO). The highest swelling was obtained by swelling in demineralized water. Solvent exchange from water to DMSO or ethanol led to sample shrinkage, especially if ethanol was used. Scanning electron microscopy (SEM) images of the samples were obtained for composites swollen in DMSO after drying with supercritical CO_2 and for samples swollen in water after lyophilization.

It was discovered that the composition of monomer content and the amount of crosslinking agent as well as the thickness of the matrix have a large influence on the swelling behavior and its kinetics. The hydrogel content and degree of swelling increased with increasing concentration of acrylic acid in the initial monomer solution, but decreased with increasing degree of crosslinking. A low concentration of both crosslinking agent and acrylic acid led to an increase of mass washout and to slippery gels. The thickness of the Basotect® matrix had an

influence on the water uptake of the hydrogels because diffusion was hindered in thick samples and thin samples with high surface to volume ratios were less crosslinked. Swelling in salt solutions led to a lower swelling than swelling in demineralized water.

Rheological measurements of the hydrogels showed that an increase of the degree of swelling leads to an increased netpoint distance (a decreased crosslink density) and consequently to a decrease of the storage and loss moduli.
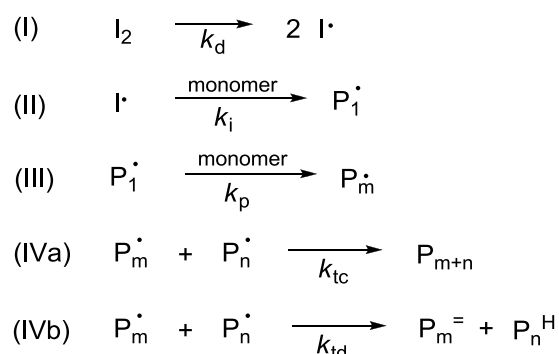
1. Introduction

Nowadays, polymers are omnipresent in every branch of daily life. Plastics are not only used as all sorts of packaging materials, but also as high-performance materials. Many specialized materials are stable even under extreme conditions without loss of their mechanical properties. Polymers are widely used in medical applications like wound dressings, disposable syringes, catheters, artificial heart valves, joints or suture material. Furthermore, polymers are used for drug delivery and tissue engineering. The mechanical, physical and chemical properties of polymers can be tailored to their application area. Besides water-insoluble, durable materials like common packaging materials, there are biodegradable and/or water-soluble polymers and biomolecule polymer conjugates or biopolymers. Some polymers form hydrogels by addition of water. Hydrogels can be used in many different applications, e. g. in wound dressings or hygiene products or in drug delivery applications. Hydrogels with large water absorption capability like superabsorbent polymers are useful materials for hygiene products, whereas stimuli-responsive hydrogels like poly(*N*-isopropylacrylamide) are suitable for application in drug delivery.

1.1 Free Radical Polymerization

Two types of poly reactions can be distinguished, the chain-growth polymerization and step-growth polymerization.[1,2] In contrast to step-growth polymerization, the chain-growth polymerization takes place by addition of a monomer to an active growing polymer chain and subsequent addition of further monomers to the active center of the growing chain. Termination takes place by deactivation of the active center. High molecular weights are obtained almost immediately because of the fast addition of monomers to the growing polymer chain.[1,2] Besides ionic polymerization and insertion polymerization, the radical polymerization is a common chain-growth polymerization technique.[2] Radical polymerizations are fast and relatively insensitive to impurities and can be carried out as bulk, solution (also in water), emulsion and suspension or precipitation polymerization.

The radical polymerization begins with the decay of an initiator (Scheme 1, step I: initiator decay) followed by the radical attack on the monomer species (Scheme 1, step II: initiation). The radical decay can be initiated thermally, chemically, electrochemically or photochemically.[2] Typical non-reversible thermal initiators are diazo compounds like azobisisobutyronitrile (AIBN) and 2,2'-azobis[2-(2-imidazolin-2-yl)propane]dihydrochloride (VA-044)[3] or peroxides like dicumyl peroxide (Di-Cup) and dibenzoylperoxide (BPO).[2,4] Persulfates like potassium persulfate (KPS) fragment reversibly into radicals under basic or neutral conditions.[2] Monomers used for radical polymerizations typically contain C=C double bonds like molecules with vinyl, vinylidene, acryl, methacryl or allyl groups.[2] In the third step of a radical polymerization, the activated monomer attacks further monomers resulting in a growing polymer chain (Scheme 1, step III: propagation). The monomer molecules that are attacked by the growing polymer chain can either be the same monomer species as the original monomer (homopolymerization) or be different from the original monomer (copolymerization). In case of a copolymerization, the incorporation of the monomers into the growing polymer chain is

random if the polymerization of one species is not kinetically or thermally preferred. If monomers have more than one polymerizable functional group, they form crosslinked polymers. The degree of crosslinking depends on the amount of the monomer, its conversion and its functionality. Reactions of two radicals, e. g. two growing polymer chains, lead to the deactivation of the radicals and consequently to the termination of the growing polymer chain (Scheme 1, step IVa: recombination or step IVb: disproportionation).[2]
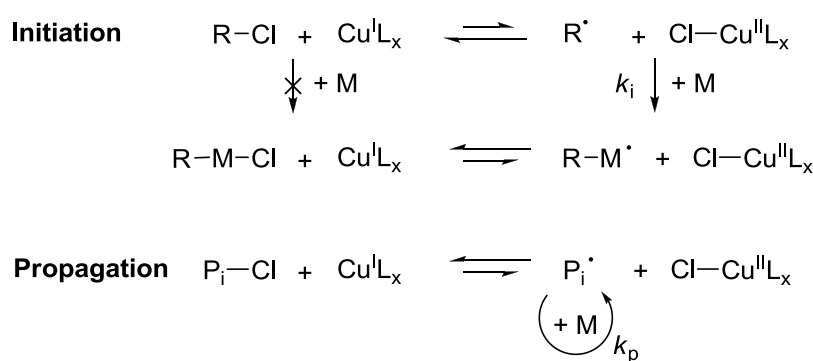
$$(\text{I}) \qquad \text{I}_2 \xrightarrow{\ k_d\ } 2\ \text{I}\cdot$$

$$(\text{II}) \qquad \text{I}\cdot \xrightarrow[k_i]{\text{monomer}} \text{P}_1^{\cdot}$$

$$(\text{III}) \qquad \text{P}_1^{\cdot} \xrightarrow[k_p]{\text{monomer}} \text{P}_m^{\cdot}$$

$$(\text{IVa}) \qquad \text{P}_m^{\cdot} + \text{P}_n^{\cdot} \xrightarrow{\ k_{tc}\ } \text{P}_{m+n}$$

$$(\text{IVb}) \qquad \text{P}_m^{\cdot} + \text{P}_n^{\cdot} \xrightarrow{\ k_{td}\ } \text{P}_m^{=} + \text{P}_n^{H}$$

Scheme 1. Radical polymerization. (I) Initiation; (II) start reaction; (III) propagation; (IV) termination by a) recombination and b) disproportionation. k_d k_i, k_p, k_{tc} and k_{td} are rate constants.

1.1.1 Controlled Free Radical Polymerization

It is possible to obtain polymers with adjusted molecular mass, narrow molecular weight distribution (small polydispersity index PDI) and defined end groups by radical polymerization. In the controlled free radical polymerization (CFRP), the advantages of living polymerizations are combined with the advantages of the free radical polymerization. This is achieved by minimization of termination steps. The concentration of the active species (radical species) is kept low. This reduces the probability of the deactivating reaction of two active growing polymer chains. The polymer chain ends are still active after complete conversion of the monomers. This leads to easily accessible block copolymers by addition of a second monomer species after conversion of the first monomer species.[5]

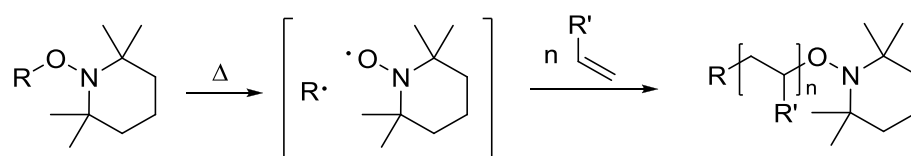#### *Atom Transfer Radical Polymerization*

The atom transfer radical polymerization (ATRP) uses alkyl halides and transition metals or transition metal complexes like copper complexes to control the polymerization.[6] The metal complex abstracts a halide radical from the alkyl halide R-X to form the oxidized species. The activated radical species R· attacks the monomer M and can be deactivated by reversible abstraction of the halide radical from the metal complex or form a growing polymer chain by addition of monomer (Scheme 2). The redox equilibrium is on the side of the alkyl halide and reduced metal complex. This provides a low concentration of the active radical species.[6] The disadvantage of the ATRP is the necessary removal of the metal catalysts because of their toxicity or interference in specific applications.[7]

Initiation

$$R-Cl \ + \ Cu^IL_x \ \rightleftharpoons \ R^\bullet \ + \ Cl-Cu^{II}L_x$$

$$\times + M \qquad\qquad k_i \downarrow + M$$

$$R-M-Cl \ + \ Cu^IL_x \ \rightleftharpoons \ R-M^\bullet \ + \ Cl-Cu^{II}L_x$$

Propagation $\quad P_i-Cl \ + \ Cu^IL_x \ \rightleftharpoons \ P_i^\bullet \ + \ Cl-Cu^{II}L_x$

$$\left(+ M \right) k_p$$

Scheme 2. ATRP mechanism.[6] R: alkyl group; L_x : ligands of the copper complex; M: monomer; P_i: polymer; k_i: initiation rate constant; k_p: propagation rate constant.

Nitroxide Mediated Radical Polymerization

The nitroxide mediated radical polymerization (NMP) controls the polymerization using nitroxide containing initiators like 2,2,6,6-tetramethylpiperidine 1-oxyl (TEMPO) derivatives. TEMPO-R thermally decomposes reversibly into the stabilized TEMPO radical and the active radical species. The active radical attacks the monomer and initiates a growing polymer chain. The growing polymer chain is terminated and deactivated reversibly by TEMPO and re-activated by homolytic cleavage.[5]

Scheme 3. NMP mechanism with TEMPO.[5] R, R': alkyl groups.

Reversible Addition Fragmentation Chain Transfer Polymerization

Like the NMP, the reversible addition fragmentation chain transfer (RAFT) polymerization is based on stabilized radicals that reduce the concentration of the active species to control the molecular weight and its distribution.[8] It is possible to synthesize block copolymers[9–13], star-like[14–16], comb-like[17] and dendritic[14] polymeric structures. The advantage of the RAFT polymerization over the other controlled/living polymerization methods is a high tolerance towards various reaction conditions and monomers including hydroxyl, carboxyl and amine groups.[8] Furthermore, RAFT allows the introduction of tailor-made functionalities at the chain ends of the polymers.[18]

The RAFT agent controls the polymerization by reversible deactivation of the growing polymer chain. It acts as chain transfer agent (CTA). CTAs used in RAFT polymerization contain a thiocarbonylthio group, a stabilizing group (Z group) and a re-initiating group (R group) (Figure 1). The Z and R group form the α and ω ends of the polymer chain.[8,9]
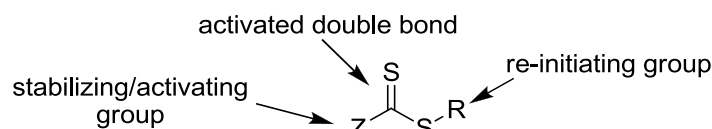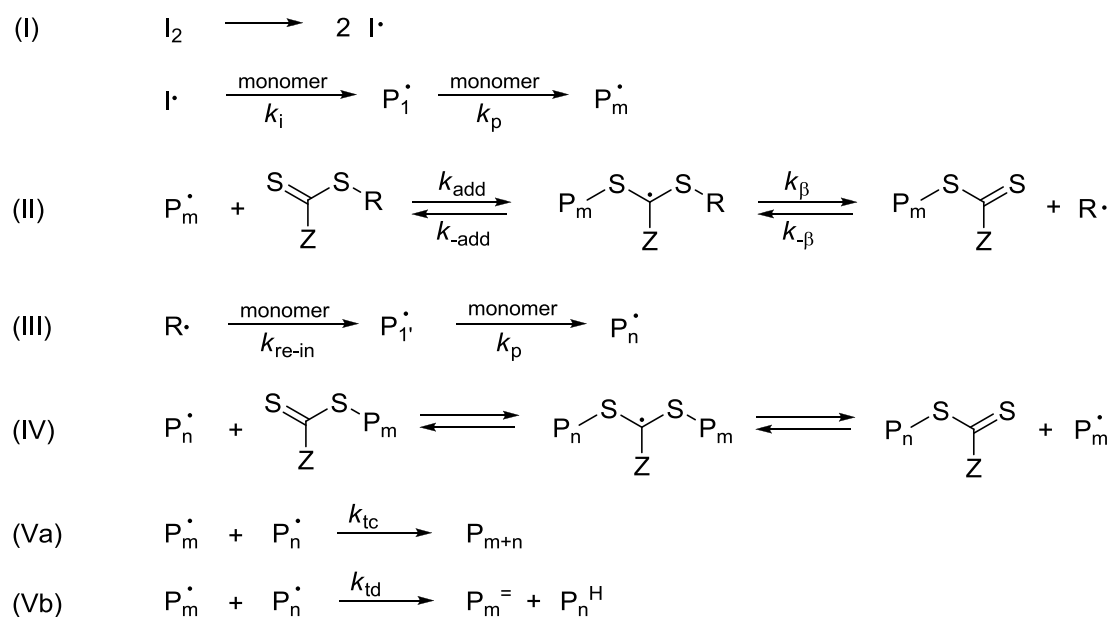
Figure 1. General structure of a RAFT agent containing a thiocarbonylthio group with activated double bond, Z group and R group.

The RAFT polymerization starts with the decay of the initiator species I_2 into the radicals $I\cdot$ (Scheme 4, step I). These radicals initiate the active growing polymer chain by reaction with monomer (k_i, k_p). It is possible that the radicals add to the RAFT agent, but it is less likely because the monomer concentration is larger than the concentration of the RAFT agent.

The activated growing polymer chain $P_m\cdot$ is rapidly deactivated by addition to the C=S double bond of the RAFT agent (Scheme 4, step II, k_{add}) to form a stabilized tertiary CTA radical (dormant polymer chain). This tertiary CTA radical may either re-fragment towards the initial active growing polymer chain $P_m\cdot$ and the original CTA (k_{-add}) or fragment into the radical $R\cdot$ of the R group and the polymer-containing macro CTA (k_β).

The $R\cdot$ group can re-initiate monomer to form another active growing polymer radical $P_n\cdot$ (Scheme 4, step III, k_{re-in}, k_p). After consumption of the initial CTA, only macro CTA is present and the main equilibrium is established as addition-fragmentation mechanism (Scheme 4, step IV). The active growing polymer radical $P_n\cdot$ adds to the macro CTA to form a tertiary radical CTA containing a dormant polymer chain bound to both sulfur atoms. Rapid fragmentation and re-addition of the polymer chains $P_n\cdot$ and $P_m\cdot$ lead to equal probabilities of the polymer chains to grow and consequently to a controlled polymerization with narrow molecular weight distribution.

In contrast to the living polymerization, termination can occur by reaction of two active growing polymer chains $P_m\cdot$ and $P_n\cdot$ in a recombination (Scheme 4, step Va, k_{tc}) to a high molecular mass polymer P_{m+n} or disproportionation (Scheme 4, step Vb, k_{td}) to an unsaturated polymer $P_m^=$ and a saturated polymer P_n^H. [9,18,19]

(I) $\quad I_2 \longrightarrow 2\ I^{\bullet}$

$\quad I^{\bullet} \xrightarrow[k_i]{\text{monomer}} P_1^{\bullet} \xrightarrow[k_p]{\text{monomer}} P_m^{\bullet}$

(II) $\quad P_m^{\bullet} + $ [dithioester structure: S=C(Z)–S–R] $\underset{k_{-add}}{\overset{k_{add}}{\rightleftharpoons}}$ [structure: P_m–S–C$^{\bullet}$(Z)–S–R] $\underset{k_{-\beta}}{\overset{k_{\beta}}{\rightleftharpoons}}$ [structure: P_m–S–C(Z)=S] $+ R^{\bullet}$

(III) $\quad R^{\bullet} \xrightarrow[k_{re\text{-}in}]{\text{monomer}} P_{1'}^{\bullet} \xrightarrow[k_p]{\text{monomer}} P_n^{\bullet}$

(IV) $\quad P_n^{\bullet} + $ [structure: S=C(Z)–S–P_m] $\rightleftharpoons$ [structure: P_n–S–C$^{\bullet}$(Z)–S–P_m] $\rightleftharpoons$ [structure: P_n–S–C(Z)=S] $+ P_m^{\bullet}$

(Va) $\quad P_m^{\bullet} + P_n^{\bullet} \xrightarrow{k_{tc}} P_{m+n}$

(Vb) $\quad P_m^{\bullet} + P_n^{\bullet} \xrightarrow{k_{td}} P_m^{=} + P_n^{H}$

Scheme 4. Proposed mechanism of the RAFT polymerization. (I) Initiation; (II) addition/fragmentation of the growing polymer radical to the RAFT agent; (III) re-initiation; (IV) main equilibrium; (V) termination by a) recombination or b) disproportionation.[18–20]

In contrast to other controlled radical polymerizations, the radical concentration in the RAFT process is not reduced. Mechanistically, there is no reason for a rate retardation in comparison to the polymerization rate of the free radical polymerization as soon as the RAFT equilibrium is established, provided that the RAFT steps are sufficiently fast.[21] Nonetheless, there are many reports on rate retardation during the RAFT progress.[21–23] Reasons for this retardation may be a poor choice of the R group of the RAFT agent as well as impurities in the chemicals or a slowdown of the gel effect by limitation of the maximum molecular weight accompanied by a relatively low viscosity of the reaction mixture.[21] Additionally, there can be an inhibition phase, e. g. caused by a slow transformation of the RAFT agent into a macro RAFT agent. Usually, the more RAFT agent is used, the slower is the polymerization.[21,22] The big challenge in RAFT polymerizations is to find and synthesize suitable RAFT agents, which polymerize the required monomers at acceptable polymerization rates with narrow molecular weight distributions and adjustable average molecular weight since most RAFT CTAs are not commercially available. A plurality of RAFT agents is required for different classes of monomers. On the other hand, this can be a benefit because the RAFT agent remains in the polymer as chain ends. Therefore, different RAFT agents allow the synthesis of polymers with tailor-made functionalities at the chain ends. Usually, RAFT agents contain dithioester, xanthate, trithiocarbonate or dithiocarbamate functionalities (Scheme 5).[8,18]
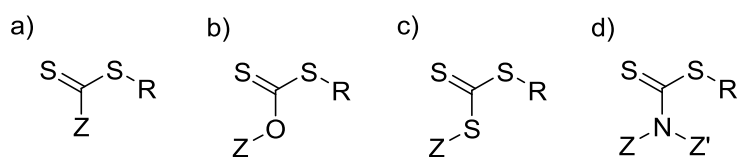
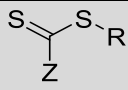**Scheme 5.** CTAs used in RAFT polymerization. a) Dithioester; b) xanthate; c) trithio-carbonate; d) dithiocarbamate.
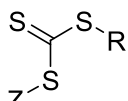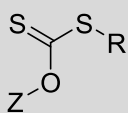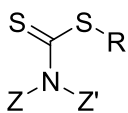
The polymerization by macromolecular design via the interchange of xanthates (MADIX) is a special case of the RAFT mechanism using xanthates as RAFT agent.[24] Just like dithiocarbamates, xanthates have a decreased reactivity of the S=C double bond toward addition of the growing polymer radical on account of the delocalization of the non-bonded electron pair of the oxygen atom of the CTA for xanthates or the nitrogen atom for dithiocarbamates (Scheme 6). This decreased rate of radical addition leads to a poor control over the molecular weight distribution because the concentration of active growing polymer chains is large when using "more-activated" monomers (MAMs) like methacrylic, acrylic and styrenic monomers.[24,25] Dithioesters or trithiocarbonates are generally used for the control of MAMs (Table 1).[25]

Nonetheless, MADIX is suitable for the controlled polymerization of fast propagating "less-activated" monomers (LAMs) like vinyl amides and vinyl esters (e. g. vinyl acetate).[25–27] Such poorly stabilized radicals can add on the C=S double bond, which allows some control over the reaction, whereas the polymerization is inhibited in the presence of dithiobenzoates.[20,27] Xanthates and dithiocarbamates decelerate the addition of radicals to the RAFT agent and promote subsequent fragmentation ($k_{add} < k_{-add}$). Therefore, fragmentation is not the rate determining step in the chain transfer that leads to control over the polymerization of LAMs (Table 1).[25]
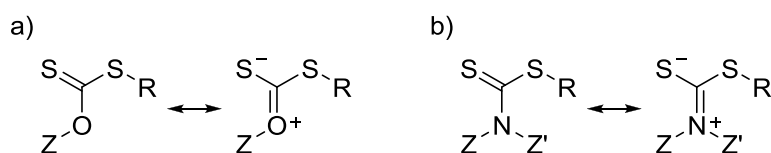
Scheme 6. Delocalization of the non-bonded electron pair of the a) oxygen atom of a xanthate and of the b) nitrogen atom of a dithiocarbamate with the S=C double bound.[18]

Table 1. RAFT agents and monomers polymerized with these CTAs.

RAFT agent		Monomers (selection)
dithioesters	S=C(S-R)(Z)	• acrylic acid/acrylates/methacrylates (acrylic acid[8], benzyl methacrylate[28], butyl acrylate[8,29], butyl methacrylate[8], *N*,*N*-dimethylaminoethyl methacrylate[8], hydroxyethyl methacrylate[8], methyl methacrylate[8,30]) • acrylamides/methacrylamides (*N*-(2-hydroxypropyl) methacrylamide[28], *N*-isopropylacrylamide[31]) • acrylonitril[8] • styrene[8]/styrene derivatives[8] • vinyl benzene sulfonates (pentafluorophenyl 4-vinyl-benzene sulfonate[32], phenyl 4-vinylbenzene sulfonate[32]) • vinyl benzoate[8]
trithiocarbonates	S=C(S-R)(Z-S)	• acrylic acid[33]/methacrylates (poly(ethylene glycol) methyl ether methacrylate[34], methyl methacrylate[34,35]) • acrylamides (*N*,*N*-dimethylacrylamide[36], *N*,*N*-dimethylpropionamide[36], *N*-isopropylacrylamide[34,37]) • styrene[33]
xanthates	S=C(S-R)(Z-O)	• acrylates (methyl acrylate[26], ethyl acrylate[26]) • vinyl esters (vinyl acetate[15,26,38], vinyl pivalate[15]) • *N*-vinyl pyrrolidone[38–40] • *N*-vinylcarbazole[41] • styrene[26]
dithiocarbamates	S=C(S-R)(Z-N-Z')	• *N*,*N*-dimethylacrylamide[25] • vinyl acetate[42] • *N*-vinylcarbazole[25] • *N*-vinyl pyrrolidone[43] • styrene[42]

1.2 Polymer Gels

Gels are differentiated in polymer gels and solid particulate gels like silica gels.[44] Gels are widely used in medicine and biotechnology[45], as carrier for the electrophoresis of proteins[46] and for gel chromatography[47], as thickeners[44] and as gelling agents in food products[48].

A gel is defined as a three-dimensional network whose pores are filled with liquids (lyogel) or gas (xerogel or aerogel).[44] Lyogels can be transformed into xerogels or aerogels by drying (Figure 2). The "normal" drying process causes a change in the structure compared to the lyo-

gel and leads to a xerogel. The structural change can be circumvented by supercritical drying, e. g. with supercritical carbon dioxide. In this way, aerogels can be obtained.[49]
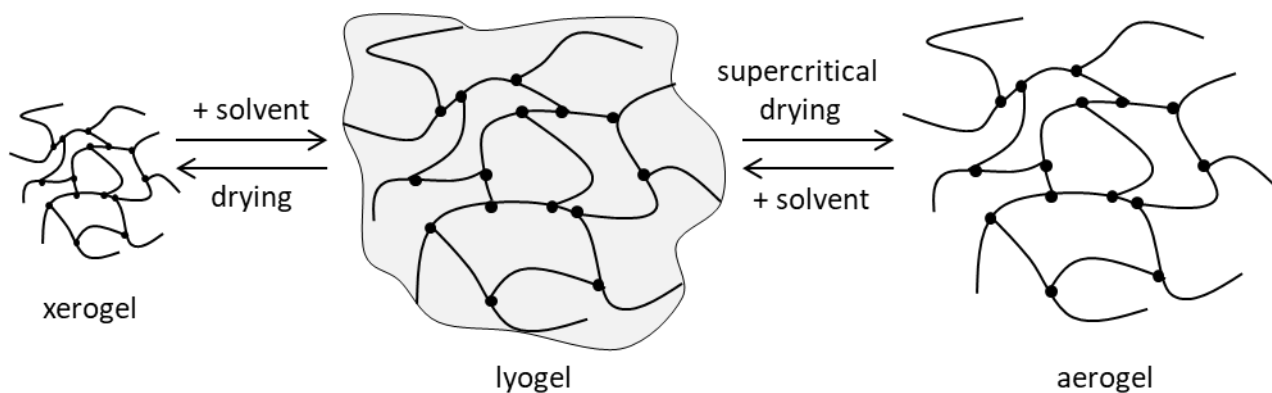

Figure 2. Synthesis of a xerogel or an aerogel from a lyogel by drying under air (xerogel) or by supercritical drying (aerogel).

Lyogels have both properties of liquids as well as of solid materials. Therefore, they are viscoelastic. Whether the behavior is more like a viscoelastic solid or liquid depends on the applied stress.[44] The three-dimensional network may either be physical or chemical in character. Physical networks can be formed by molecule-molecule interactions like hydrogen bonds, van-der-Waals interactions and Coulomb forces or by entanglements (Figure 3a). Chemical networks contain covalent bonds between the single molecules (Figure 3b). They can be obtained by polymerization in the presence of a crosslinking agent, which has at least two reactive functional groups. Monomers containing two or more reactive C=C double bonds like diacrylates or bis-acrylamides are commonly used as crosslinking agents. Linear polymers can be post-crosslinked by reaction of functional groups that are already present in the polymer or by addition of crosslinking agents like sulfur containing molecules for vulcanization.[44,50,51]
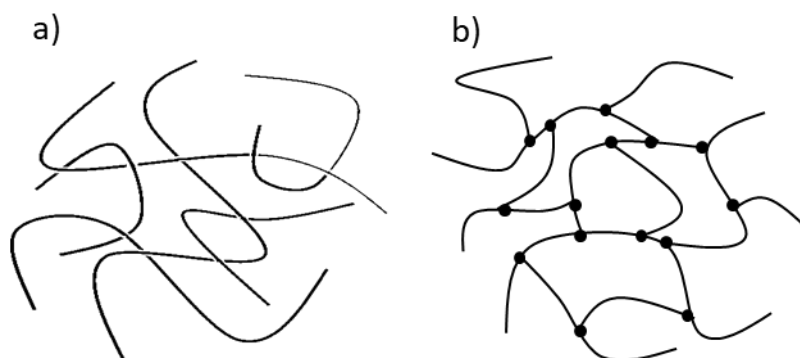
Figure 3. Structure of crosslinked polymers. a) Physical networks, e. g. by entanglements, hydrogen bonds, van-der-Waals interactions or Coulomb forces. b) Chemical network with covalent bonds.

Polymer chains between the crosslinks in chemically crosslinked gel networks are stretched by swelling. Therefore, swelling is hindered by elastic forces generated from non-equilibrium

condition. The osmotic pressure of the swelling and the counteracting elastic forces cancel each other in equilibrium.

The determination of a molecular mass is not useful in crosslinked polymers. The material behaves like one large molecule. Useful parameters for gels are the net bow molecular mass, the network density and the distance between two crosslinks. Close-meshed gels are hard, brittle and often more temperature resistant. Wide-meshed networks, e. g. natural rubber, soften above their glass transition temperature. Aging processes can affect the gels. This often leads to solvent release.[50]

1.2.1 Hydrogels

Hydrogels are water containing lyogels. They can be defined as water-swollen, crosslinked polymeric networks or as hydrophilic polymers that swell in water, but do not dissolve on account of the crosslinks between the polymer chains.[51] The hydrophilicity of these polymers is given by hydrophilic functional groups at the polymer backbone like hydroxyl, carboxyl, sulfonate or amide groups (Scheme 7).[52–54]
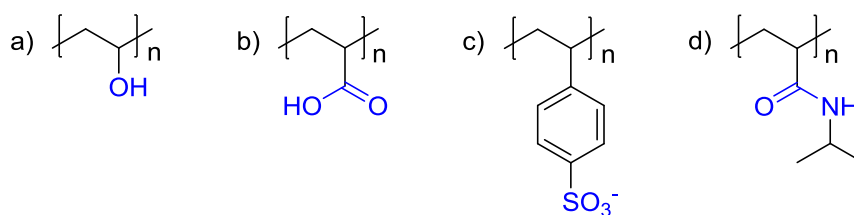
Scheme 7. Chemical structure of hydrophilic groups found in hydrogels.[52] a) Hydroxyl; b) carboxyl; c) sulfonate; d) amide functionality.

Besides synthetic hydrogels, there is a large number of natural hydrogels based on polysaccharides or peptides, e. g. starch[55], guar gum[56] or alginate[57] derivatives. Nonetheless, for most applications the synthetic materials are superior to natural hydrogels since they have a higher water absorption capacity and gel strength, which is why natural hydrogels are increasingly replaced by synthetic materials.[51]

The structure of synthetic polymers can be tailor-made and therefore, the properties can be adjusted. The swelling of hydrogels depends on the monomers and comonomers used, the crosslinking density and the type of crosslinking.[52] Usually, the water content of a swollen hydrogel is larger than the amount of the dry gel itself.[51] High swelling degrees can be achieved with polymers that are water-soluble in their non-crosslinked structure.[51]

Hydrogels can be based on homopolymeric, copolymeric or multipolymer interpenetrating networks. Their physical structure may be crystalline, semi crystalline or amorphous. In addition to non-ionic hydrogels, a number of ionic, ampholytic and zwitterionic hydrogels exists.[51] These often biocompatible materials are used as biomaterials for biomedical and pharmaceutical applications, e. g. as ultrasound gels[58], contact lenses[59], membranes[60], scaffolds for tissue engineering[61,62], in drug delivery[63–65], as superabsorbent polymers (SAP) in

wound dressings[66,67] and hygiene products[68], but also as water storage materials in agriculture[69] and cable sheathings[70].

Some hydrogels respond to environmental influences like temperature[63], pH value[63], light[63], ionic strength[71] or mechanical stress[72] with a change of their properties. These materials are referred to as stimuli-responsive polymers. Possible fields of application are medicine and biotechnology. One of the most studied stimuli-responsive synthetic polymers is poly(*N*-isopropylacrylamide) (PNIPAm). PNIPAm has a liquid-to-solid transition at its lower critical solution temperature (LCST) of about 32 °C.[63,73] Beneath its LCST, PNIPAm is soluble in water, but forms a physically crosslinked hydrogel when the LCST is reached.

1.2.2 Superabsorbent Polymers

Superabsorbent polymers are lightly crosslinked hydrogels, which can absorb large amounts of water or an aqueous medium relative to their own "dry" weight. They can contain more than 99 % water.[61,74] SAPs show similarities to natural tissue on account of their large water content. They are used in many application areas, e. g. hygiene products, medical, food and agricultural industries.[61,69,75,76] The probably most common application of SAPs is the usage of partially neutralized poly(acrylic acid) in infant diapers, in feminine hygiene or incontinence products.[68,74,77–79]

The swelling behavior of superabsorbent polymers is characterized by the amount of absorbed water (swelling capacity), the swelling kinetics and the elastic modulus of the hydrogel. The viscoelastic properties can be determined by rheological measurements in an oscillatory shear experiment. The swelling capacity and kinetics as well as the elastic modulus depend on the crosslink density of the gel network. A large absorption of water is possible in a material of low crosslink density and vice versa. Polymers in hygiene applications usually have a low crosslink density leading to a high swelling capacity.[79,80]

SAPs are usually synthesized by free radical crosslinking polymerization of ionogenic monomers like acrylic or methacrylic acid and their sodium or potassium salts in the presence of crosslinking agents with at least two polymerizable double bonds such as poly(ethylene glycol) diacrylate (PEGda) or *N,N*'-methylenebis(acrylamide) (MBA).[61,74] Generally, SAPs can be non-ionic, ionic, ampholytic or zwitterionic. In addition to synthetic SAPs based on petrochemicals, a number of natural SAPs based on polysaccharides or proteins exists. Nonetheless, commercially available SAPs are usually synthetic polymers with an anionic backbone like sodium polyacrylate and its copolymers.[77]

The water-soluble thermal initiators potassium persulfate (KPS) and ammonium persulfate (APS) or azo initiators like 2,2'-azobis-(4-cyanopentanoic acid) are widely used in solution polymerization in aqueous media or inverse-suspension polymerization. Redox initiator systems like hydrogen peroxide/iron(II), hydrogen peroxide/ascorbate, persulfate/bisulfite, persulfate/thiosulfate or persulfate/ascorbate are also used for polymerization in solution.[80–82]

The monomer concentration in the reaction solution affects the reaction kinetics and the properties of the resulting polymer network.[80] Large concentrations lead to more chain transfer reactions to polymer and consequently to branching and self-crosslinking. Thus, the

polymer network inhibits an increased network density. The use of chain transfer agents can decrease these side reactions.[80]

Acrylic acid is usually partly neutralized in the polymerization, but it is also possible to neutralize the gel network after its synthesis.[83,84] In suspension polymerization, neutralization of acrylic acid is necessary as the protonated form is soluble in the organic phase.[80] The partial neutralization of the polyelectrolyte chain is essential to achieve high swelling. The ions of the polyelectrolyte chains are close to each other in the dried gel, resulting in a large osmotic pressure. The osmotic pressure decreases because the ion concentration is reduced by absorption of water. Therefore, the osmotic pressure in the SAP hydrogel is the main driving force of its swelling. The swelling equilibrium is reached when the restoring forces of the polymer gel and external pressures compensate the osmotic driving force (Figure 4).[78]
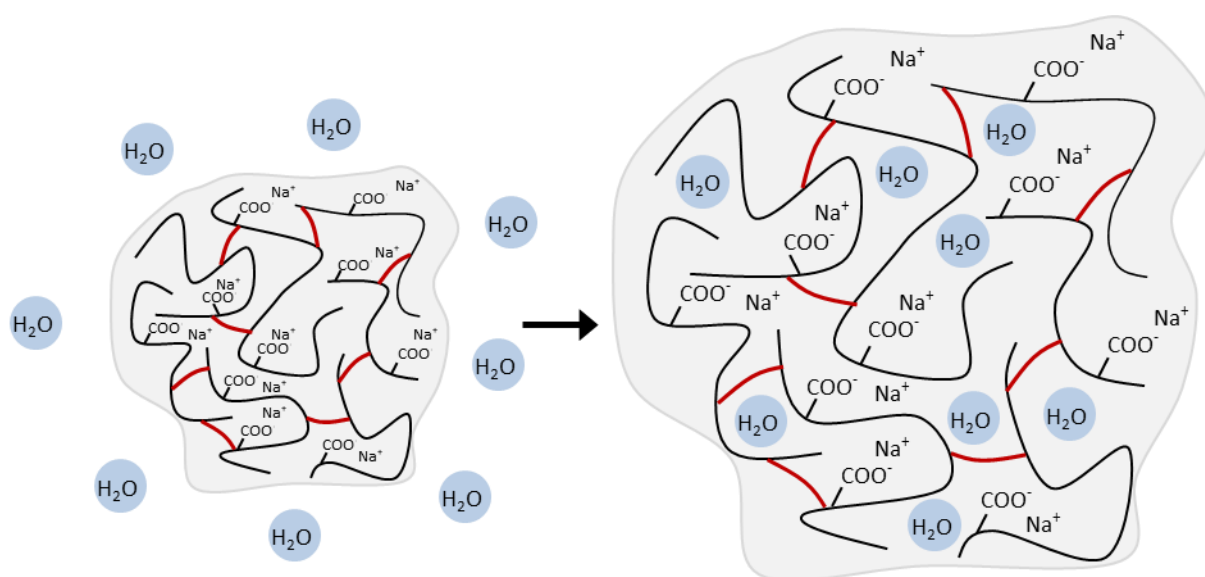
Figure 4. Swelling of a superabsorbent polymer based on crosslinked poly(acrylic acid).[78]

SAPs are not only used to absorb water, but also for the absorption of saline solutions.[85] The swelling of polyelectrolytes in saline solution is different from the swelling in water since the ion concentration inside the gel is less reduced by swelling in saline solution relative to swelling in water. Therefore, the swelling is decreased in aqueous solutions containing salts. The decrease of the swelling capacity is larger in the presence of di- or trivalent cations like calcium ions Ca^{2+} or aluminum ions Al^{3+}. These cations neutralize more than one carboxylate group of the polyelectrolyte and act as crosslinking agents.[78]

The ionic sensitivity can be characterized by the dimensionless factor f.[86] A large loss of the swelling capacity Q in saline solution in comparison to swelling in distilled water results in a high value of f (Equation 1). Negative values of f are obtained for gels with increased swelling in saline solution. This effect could be observed with superswelling hydrogels containing sulfobetaine-sulfonic acid structures.[87]

$$f = 1 - \frac{Q_{\text{saline solution}}}{Q_{\text{distilled water}}} \qquad (1)$$

1.2.3 Superabsorbent Composite Materials

Superabsorbent polymers can be applied onto a carrier material. This can be essential to improve the properties of the SAP, especially its mechanical stability, for a specific application. Carrier materials can be a fabric, foam materials or metal surfaces.

There are different ways to bind the SAP to the carrier material. The SAP can be introduced into an interlayer of the carrier material (DE 10034505) or can be applied on a carrier material (DE 10231356 B4).[88,89] Furthermore, a carrier material can be impregnated with monomers (WO 2009/056543, WO 2011/032862, WO 01/56625) or partially polymerized SAPs (US 2006/0252899) that are afterwards polymerized to a SAP resulting in a SAP composite material[90–93] or the carrier material can be synthesized in the presence of the SAP (WO 2006/066752).[94]

It is a big advantage in hygiene applications if the SAP is firmly bound in the fabric or foam matrix. An easy route to synthesize such composites is the impregnation of the matrix with superabsorbent polymer-forming monomers and subsequent *in situ* polymerization as described in WO 2009/056543.[91] The patent describes a method to obtain composite materials containing at least one superabsorbent polymer and one aminoplast resin as carrier material for application e. g. in hygiene products, desiccants, water reservoirs, sealing materials, insulation materials, packages and artificial plant substrates.[91] The carrier material was impregnated with a monomer solution and the monomers were polymerized in a subsequent step. An aqueous solution of acrylic acid and sodium acrylate was used as monomer solution (Table 2).

Table 2. Chemicals and amount used in WO 2009/056543.[91]

Chemicals	Amount [wt%]
Acrylic acid	33.9
Water	4.3
Sodium acrylate (pH 9.5)	13.2
Poly(ethylene glycol) diacrylate ($M_w \approx 400$ g/mol)	2.7
Lutensol AT 80® (non-ionic surfactant)	4.2
Triethanolamine	39.1
V 50® (water soluble initiator)	2.6

The monomer solution was prepared by mixing the chemicals shown in Table 2 under cooling and degassing of the solution. A foam sheet of the aminoplast carrier material, a melamine/formaldehyde foam, was impregnated with the monomer solution until the foam sheet was completely filled with liquid. The foam sheet was allowed to drain for 10 minutes. The

polymerization was carried out at 80 °C in a vacuum drying oven with a nitrogen stream of 150 L/h and a pressure of about 100 mbar. It was also possible to moisten the foam sheet with the monomer solution by spraying. In this case, the solution was further diluted with water.

Melamine/formaldehyde foams can by synthesized by reaction of melamine and formaldehyde and physical foaming (WO 2005/103107). A melamine/formaldehyde precondensate with a melamine/formaldehyde ratio of 1:3 and a molecular weight of about 500 g/mol is added to an aqueous solution of formic acid and the emulsifier *Bayer* K 30. K 30 is mixture of the sodium salts of alkyl sulfonates with 12–18 carbon atoms. Under stirring, *n*-pentane is added and the dispersion is coated onto a Teflon-coated fiber glass, foamed in a drying oven at 150 °C and tempered at 180 °C.[95] The resulting foam had an open-pored structure of 99.6 %, a density of 13 kg/m^3, a mean pore diameter of 210 μm, a BET surface of 6.4 m^2/g and 93 % acoustic absorption.[95]

A commercially available melamine/formaldehyde foam is Basotect®. It is an elastic web-foam with an open-pored structure. Basotect® is sterilizable with alcohol, formalin and water vapor (WO 2007/118803).[96] Basotect® has a low flammability on account of its high amount of nitrogen atoms, an application temperature of up to 240 °C including constant physical properties in a wide range of temperature, a high resistance against many chemicals like organic solvents and it is abrasive. The open-pored structure assures a low density of about 9 g/L, low-temperature flexibility, a high acoustic absorption and heat insulation.[97]

Basotect® is available in six different types.[97]

- Basotect® G: The gray color of Basotect® G prevents staining of the foam. It has a low thermal conductivity, low flammability and mineral-fiber-free processing. Possible applications are in construction and industry.[97]

- Basotect® G+: In addition to the properties of Basotect® G, Basotect® G+ meets the Oeko-Tex® standard in product class I and is interesting for interior architects and designers. The gray color is lighter than the color of Basotect® G and the luminous reflection is 30 % higher.[97]

- Basotect® TG: The dark gray colored Basotect® TG can be thermoformed and offers opportunities for special applications like use in vehicle construction.[97]

- Basotect® UF: The gray colored Basotect® UF has a very high elasticity and optimized flammability properties. It is applied in construction and rail cars.[97]

- Basotect® UL: The ultra-light Basotect® UL is used in aerospace applications.[97]

- Basotect® W: Basotect® W is used in consumer applications, especially for cleaning products. It is tested by Japanese Law 112, which is a strict test for formaldehyde and fulfills the Oeko-Tex® standard in product class I.[97]

Non-colored ("white") Basotect® types like Basotect® W are preferred in applications as carrier material of superabsorbent polymers in hygiene products or wound dressing.

Basotect® can be mechanically modified by multi-dimensional knife cut, sawing and punching, it can be coated or glued, hydrophobized by impregnation with silicon emulsions or impregnated with a thermally reactive adhesive liquid to obtain Basotect® suitable for thermoforming.[97]

1.2.4 Swelling Studies

The swelling properties of superabsorbent polymers are characterized by their swelling capacity Q and the kinetics of the swelling process.[98,99] Often, a high swelling degree correlates with a slow swelling process because of slow water diffusion inside the gel.[100] The swelling degree depends on the crosslink density and the hydrophilicity/functional groups of the polymer.[101] A higher crosslink density leads to more defined particle shapes and lower swelling degrees. Further influences on the swelling degree can be exerted by the pH value, salts in the swelling medium and the temperature.[101,102]

The swelling of gels can be described as volume or as weight dependent swelling degree.[103] Mostly, gravimetric measurements are used to determine the swelling capacity.[80] The swelling degree Q_{real} is consequently defined as ratio of the weight of the gel swollen with solvent m_{gel} and the weight of the dried gel $m_{gel,dry}$ (Equation 2).[55,103] The degree of swelling can be 100 and higher for superabsorbent polymers. The swelling increases with increasing number of charged functional groups.[50]

$$Q_{real} = \frac{m_{gel}}{m_{gel,dry}} = \frac{m_{gel,dry} + m_s}{m_{gel,dry}} = 1 + \frac{m_s}{m_{gel,dry}} \tag{2}$$

Sometimes, it is useful to define the swelling as ratio Q_{real}^* of gel-bound solvent m_s and dry gel weight (Equation 3).[79,80,100]

$$Q_{real}^* = \frac{m_{gel} - m_{gel,dry}}{m_{gel,dry}} = \frac{m_s}{m_{gel,dry}} = Q_{real} - 1 \tag{3}$$

A common method for determining the mass dependent swelling is the tea bag test.[103,104] A certain amount of dry polymer gel is enclosed in a water-wettable foil, put into the swelling solution and allowed to swell.[80] The time-dependent mass m_{gel} can be determined by weighting the swollen polymer wrapped inside the filter.[103]

Usually, interstitial solvent $m_{s,int}$ that is not bound in the gel remains between the gel particles.[103] This leads to an overestimation of the swelling degree Q relative to its real value Q_{real} (Equation 4). The factor F takes the interparticle volume into account and is about 0.7 for monodisperse polyacrylate gel particles.[103]

$$Q = \frac{m_{\text{gel}} + m_{\text{s,int}}}{m_{\text{gel,dry}}} = Q_{\text{real}} + \frac{m_{\text{s,int}}}{m_{\text{gel,dry}}} = \frac{Q_{\text{real}}}{F} \tag{4}$$

Unabsorbed fluid can be removed by centrifugation or blotting with porous paper.[80] However, not the entire interstitial solvent may be removed or water absorbed in the gel may be eliminated, making the method susceptible to large errors.

Kinetics of Swelling Processes

The swelling kinetics of poly(acrylamide-*co*-2-acrylamido-2-methyl-propanosulfonic acid) crosslinked with *N*,*N'*-methylenebis(acrylamide) are described in literature.[99,105,106] The solution for non-steady-state diffusion in a sphere in case of uniform initial concentration[107] was used to model the diffusion and relaxation controlled kinetics in uniform sphere powders.

The swelling process is described as the time-dependent change in weight of solvent M_t entering (swelling process) or leaving (de-swelling process) the sphere as combined model with a term for the mass of solvent controlled by Fickian diffusion process $M_{t,D}$ and a term for the weight of solvent controlled by relaxation process $M_{t,R}$ (Equation 5).[99,106]

$$M_t = M_{t,D} + M_{t,R} \tag{5}$$

The Fickian diffusion process in a sphere is given by Equation 6.[105–107] It depends on the equilibrium amount of diffusion controlled sorption $M_{\infty,D}$, the diffusion coefficient D, the particle diameter d and the time t. The substance-specific constants can be summarized as rate constant of Fickian diffusion k_D.

$$M_{t,D} = M_{\infty,D}\left[1 - \frac{6}{\pi^2}\sum_{n=1}^{\infty}\frac{1}{n^2}\exp\left(-\frac{Dn^2\pi^2 t}{d^2}\right)\right] = M_{\infty,D}\left[1 - \frac{6}{\pi^2}\sum_{n=1}^{\infty}\frac{1}{n^2}\exp\left(-n^2 k_D t\right)\right] \tag{6}$$

The relaxation controlled swelling process depends on the equilibrium amount of relaxation controlled sorption $M_{\infty,R}$ and its rate constant k_R (Equation 7).[106]

$$M_{t,R} = M_{\infty,R}\left[1 - \exp\left(-k_R t\right)\right] \tag{7}$$

The normalized time-dependent swelling M_t/M_∞ is given by addition of the normalized diffusion controlled and the normalized relaxation controlled swelling (Equation 8).[99,106] Normalization causes the equilibrium masses of diffusion controlled processes x and relaxation controlled processes (1–x) to add to 1 (Equation 9).[99]

$$\frac{M_\mathrm{t}}{M_\infty} = \frac{M_{\infty,\mathrm{D}}}{M_\infty}\left[1 - \frac{6}{\pi^2}\sum_{n=1}^{\infty}\frac{1}{n^2}\exp\left(-n^2 k_\mathrm{D}t\right)\right] + \frac{M_{\infty,\mathrm{R}}}{M_\infty}\left[1 - \exp\left(-k_\mathrm{R}t\right)\right] \tag{8}$$

$$\frac{M_\mathrm{t}}{M_\infty} = x\left[1 - \frac{6}{\pi^2}\sum_{n=1}^{\infty}\frac{1}{n^2}\exp\left(-n^2 k_\mathrm{D}t\right)\right] + (1-x)\left[1 - \exp\left(-k_\mathrm{R}t\right)\right] \tag{9}$$

The shape of the initial area of the time-dependent swelling curves obtainable by plotting M_t/M_∞ against the square root of time provides a suggestion if the swelling is mainly relaxation or diffusion controlled. A sigmoidal shape indicates a big amount of relaxation controlled processes (small factor x), whereas a linear shape indicates a big amount of diffusion controlled processes (large factor x).[99]

2. Motivation

Hydrogels are widely used in medical applications, e. g. in drug delivery and wound dressing. There is need for research in the targeted drug release to the body part, in which the drug is to operate. The targeted drug release can be achieved by stimuli responsive behavior of carrier materials. Poly(*N*-isopropylacrylamide) (PNIPAm) is a stimuli responsive and biocompatible polymer and therefore an interesting material for application in drug delivery. Poly(*N*-vinyl-pyrrolidone) (PVP) is also biocompatible and was used e. g. as blood expander. Tailor-made functional groups at the chain ends extent the field of application. The introduction of sugar functionalities is interesting because of their biocompatibility and possible enzymatic reactions. A pathway for the introduction of mannose or glucose and benzyl or carboxyl groups onto the chain ends of PNIPAm and PVP by RAFT polymerization is presented in the following.

Hydrogels in wound dressings are used to absorb blood and/or sore water and to keep the wound moist. The latter is especially important for burns. Commercially available wound dressings containing partially neutralized poly(acrylic acid) wrapped in fabric can enter the wound if the fabric is damaged. This may be prevented by application of a chemically cross-linked superabsorbent composite material consisting of a carrier material and a superabsorbent polymer (Figure 5).
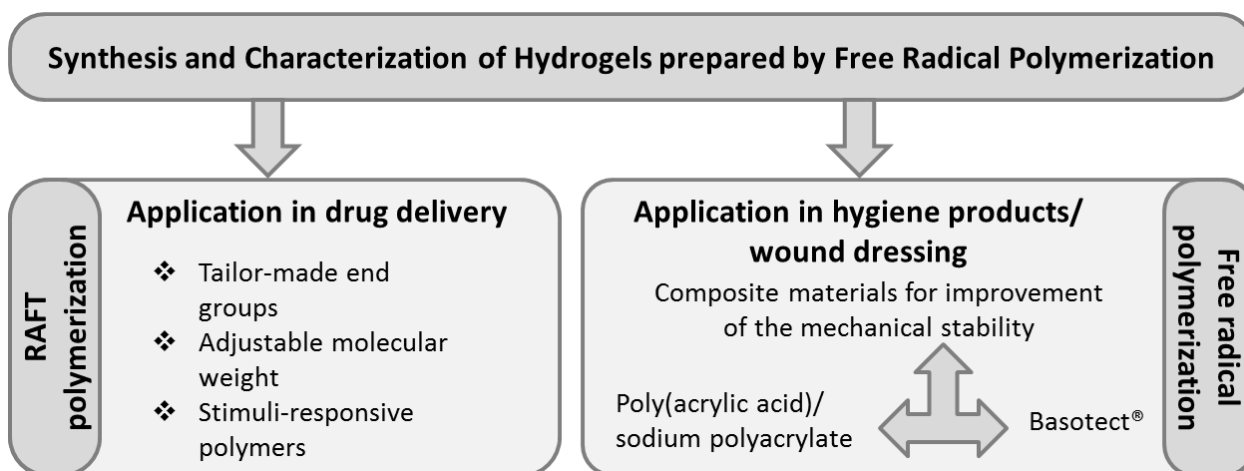
Figure 5. Flowchart presenting the aims of this thesis.

3. Synthesis of RAFT/MADIX Chain Transfer Agents with Monosaccharide Entities

Conjugates of biomolecules and polymers are widespread in medicine and biotechnology applications.[108–110] For these applications, polymers should be biocompatible like poly(*N*-vinyl pyrrolidone) (PVP) or poly(*N*-isopropylacrylamide) (PNIPAm).[40,111] PNIPAm is an interesting material on account of its stimuli-responsive behavior. It undergoes a reversible phase transition in aqueous media from a dissolved, swollen hydrated polymer to a shrunken dehydrated state at its lower critical solution temperature at approximately 32 °C.[112] The existence of the LCST of PNIPAm offers possible applications in biomedical systems like intelligent drug delivery or separation processes.[71,113] PVP is used in pharmaceuticals, in food and cosmetic industries and was used as blood plasma expander.[114]

Living/controlled polymerization techniques have become more and more established in recent years. These techniques allow the synthesis of polymers with adjustable molecular weight and narrow molecular weight distribution (MWD).[8] Besides the atom transfer radical polymerization (ATRP)[6] and nitroxide mediated polymerization (NMP)[5], the reversible addition-fragmentation chain transfer (RAFT) polymerization[8] / macromolecular design via the interchange of xanthates (MADIX)[26] is one of the leading controlled free radical polymerization techniques.[18–20,24,115–118] The RAFT/MADIX process allows the formation of complex molecular architectures such as block copolymers[9–13], star-like[14–16], comb-like[17] and dendritic[14] polymers. RAFT/MADIX is suitable for a variety of different monomers and functional groups and for various solvents including water.[8,40,119,120] This provides the opportunity to use renewable monomers and to produce biodegradable and/or biocompatible polymers.[10,31,40,115,121,122] The RAFT/MADIX polymerization provides easy access to biomolecule-polymer conjugates with one biomolecule bound at the chain end of the polymer.[123] This is on account of the mechanism[20,118,124] of the RAFT/MADIX process (cf. Chapter 1.1.1, Scheme 4).

In the following, a pathway to PNIPAm and PVP with defined molecular weight and tailor-made end functionalities containing saccharide moieties using RAFT/MADIX polymerization is presented. To achieve this goal, different RAFT agents based on mannose or glucose were synthesized and used for the controlled polymerization of NIPAm in 1,4-dioxane with azobisisobutyronitrile (AIBN) as radical starter and *N*-vinyl pyrrolidone (NVP) in aqueous solution with 1,2-bis(2-(4,5-dihydro-1H-imidazol-2-yl)propan-2-yl)diazene dihydrochloride (VA-044) as initiator. The saccharide derivatives at the chain end may be useful for further post-modification of the tailor-made polymers or for enzymatic reactions.

The synthesis routes of three different xanthate RAFT agents will be presented. Methyl α-D-mannopyranoside-6-(*S*-2-propionic acid)xanthate (MMPX) and methyl α-D-mannopyranoside-6-(*S*-benzyl)xanthate (MMBX) are both mannose-based CTAs. Either a carboxyl group (MMPX, Scheme 8a) or a benzyl group (Scheme 8b) acts as R group. Methyl α-D-glucopyranoside-6-(*S*-benzyl)xanthate (MGluBX) is a glucose based RAFT agent with a benzyl group as Z group (Scheme 8c).
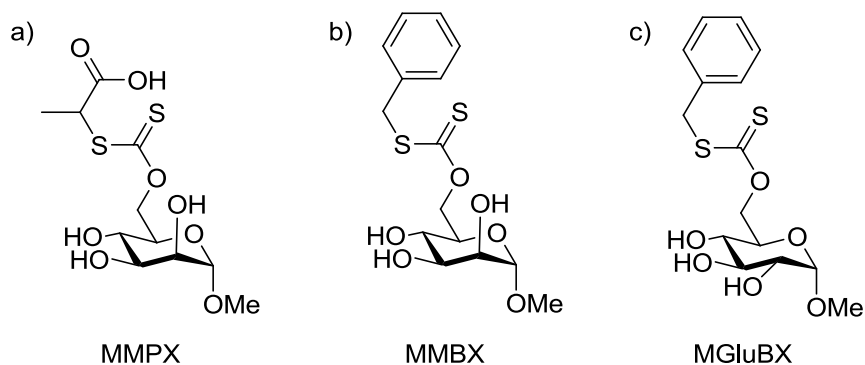
Scheme 8. Saccharide-based xanthate RAFT agents. a) Methyl α-D-mannopyranoside-6-(*S*-2-propionic acid)xanthate; b) methyl α-D-mannopyranoside-6-(*S*-benzyl)xanthate; c) Methyl α-D-glucopyranoside-6-(*S*-benzyl)xanthate.

The polymerization of NIPAm was carried out with MMPX, MMBX and MGluBX to obtain PNIPAm with mannose or glucose and carboxyl or benzyl functionalized end groups (Scheme 9). NVP was polymerized with MMPX (Scheme 10) only; MMBX and MGluBX are not water soluble.
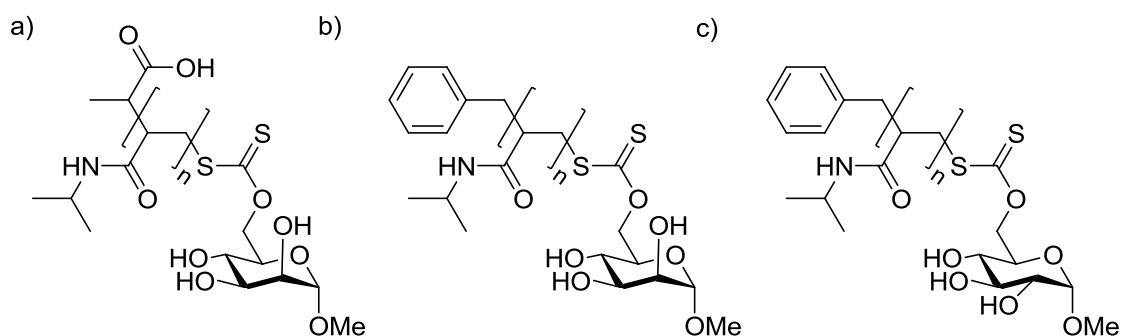
Scheme 9. PNIPAm with defined end groups synthesized by RAFT polymerization with a) MMPX, b) MMBX or c) MGluBX as CTA.
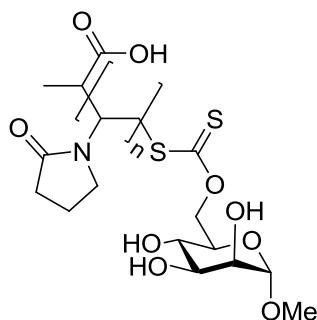
Scheme 10. PVP with defined end groups synthesized by RAFT polymerization with MMPX as CTA.

Important characteristics of the tailor-made polymers are the molecular weight distribution and the kinetics of the polymerization. Both the MWD and kinetics of the RAFT polymerization of NIPAm and NVP with RAFT agents in varying concentrations were compared to the

conventional free radical polymerization without CTA in dependence on the concentration of initiator. The monomer conversion during the polymerizations can be determined by ^{1}H NMR spectroscopy and the molecular weight distribution by size exclusion chromatography (SEC). The amount of "living" polymer chains and "dead" polymer was evaluated by formation of poly(NIPAm-*co*-NIPAm) diblock copolymers. The amount of "dead" polymer can be determined by comparison of the SEC elugrams and integration of the high molecular weight and low molecular weight part of the polymers.

3.1 Synthesis of the RAFT Agents

Methyl α-D-mannopyranoside-6-(*S*-benzyl)xanthate (MMBX) (Scheme 11a) and methyl α-D-mannopyranoside-6-(*S*-2-propionic acid)xanthate (MMPX) (Scheme 11b) were synthesized from methyl α-D-mannopyranoside according to literature.[125] The sodium salt intermediate was obtained by reaction of methyl α-D-mannopyranoside with carbon disulfide in an aqueous sodium hydroxide solution with a subsequent neutralization step. No further protecting groups were necessary since most xanthate groups are formed at position 6 of the pyranoside.[126] The RAFT agents were obtained after addition of benzyl bromide for MMBX or 2-bromopropionic acid for MMPX. Purification was carried out by column chromatography. Methyl α-D-glucopyranoside-6-(*S*-benzyl)xanthate (MGluBX) was prepared in a similar manner[127,128], starting from methyl α-D-glucopyranoside (Scheme 11a). The yields were 25 % for MMBX, 15 % for MMPX and 43 % for MGluPX with respect to carbon disulfide, but as the reactants can be regained the effective yield is larger.
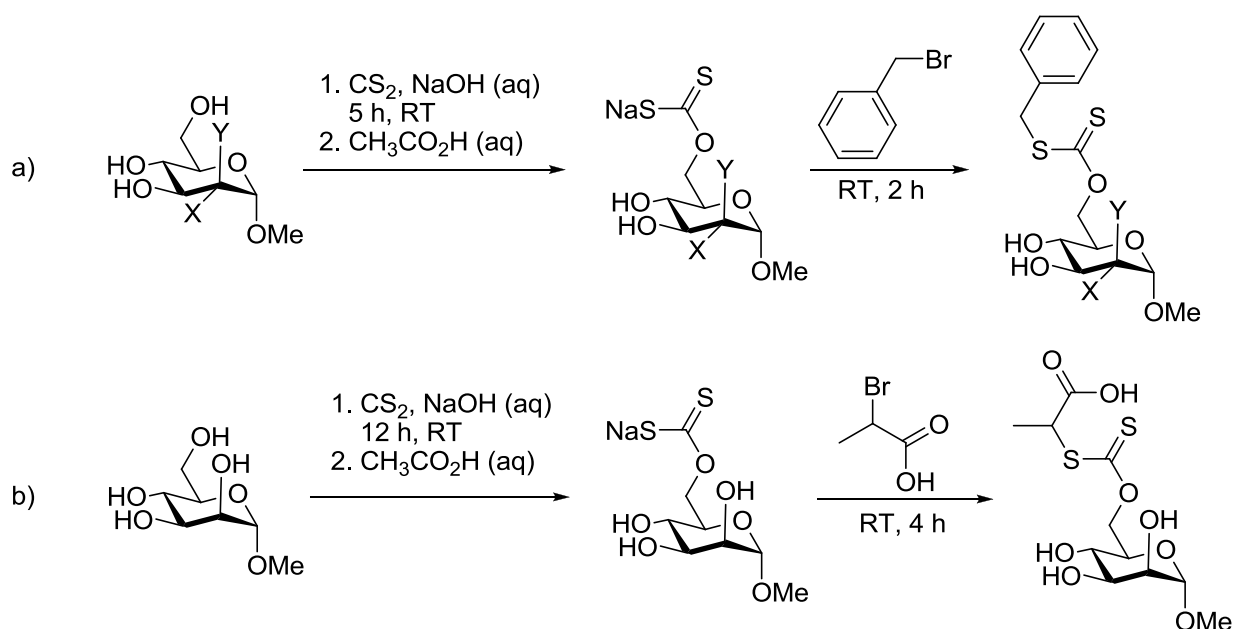
Scheme 11. Synthesis of a) mannose (X=H, Y=OH) or glucose (X=OH, Y=H) and benzyl functionalized RAFT agent MMBX (mannose) and MGluBX (glucose) and b) mannose and carboxylic acid functionalized RAFT agent MMPX.

The RAFT agents were characterized by NMR spectroscopy, electrospray ionization mass spectrometry (ESI-MS) and elemental analysis (Chapter 6.2).

3.2   RAFT Polymerization of NIPAm

3.2.1 Influence of the RAFT Agent

The RAFT polymerizations were compared to the conventional free radical polymerizations (FRP) without RAFT agent to investigate the influence of MMPX, MMBX and MGluBX[128] as CTA on the polymerization of NIPAm (Scheme 12). The polymerizations were carried out under the same reaction conditions at a temperature of 70 °C, a monomer concentration of 1 mol/L and a ratio of monomer, RAFT agent and initiator of M:CTA:I = 100:1:0.2.
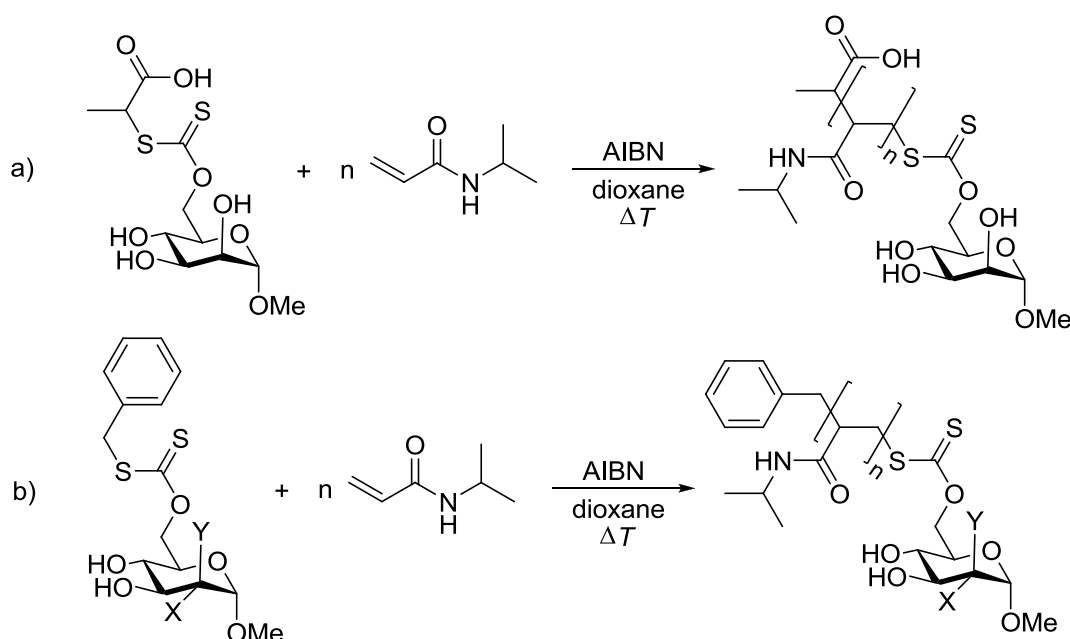
Scheme 12. RAFT polymerization of NIPAm with a) MMPX and b) MMBX (X=H, Y=OH) or MGluBX (X=OH, Y=H) as chain transfer agent.

The monomer conversion X_i could be determined by ^{1}H NMR spectroscopy. From the data, the pseudo-first order plots $\ln([M]_0/[M]_t)$ could be obtained by using Equation 10–12.

The reaction rate R_p of a radical polymerization depends on the concentration of monomer [M] and the concentration of the growing polymer chains [P·]. The concentration of the growing polymer chains depends on the initiator concentration [I_2], the rate of its decay k_d and the radial efficiency f as well as the termination rate constant k_t.

$$R_p = k_p \cdot [M] \cdot [P^\bullet] = k_p \cdot [M] \cdot \sqrt{\frac{f \cdot k_d \cdot [I_2]}{k_t}} \tag{10}$$

$$[M]_t = [M]_0 \cdot e^{-k_p \cdot [P^\bullet] \cdot t} \tag{11}$$

$$\ln\frac{[M]_0}{[M]_t} = \frac{1}{1-X_i} = k_p \cdot [P^\bullet] \cdot t = k_p \cdot \sqrt{\frac{f \cdot k_d \cdot [I_2]}{k_t}} \cdot t = k' \cdot t \qquad (12)$$

The time-dependent monomer conversions and pseudo-first order plots $\ln([M]_0/[M]_t)$ of the polymerization of NIPAm either by RAFT or by conventional free radical polymerization are depicted in Figure 6.
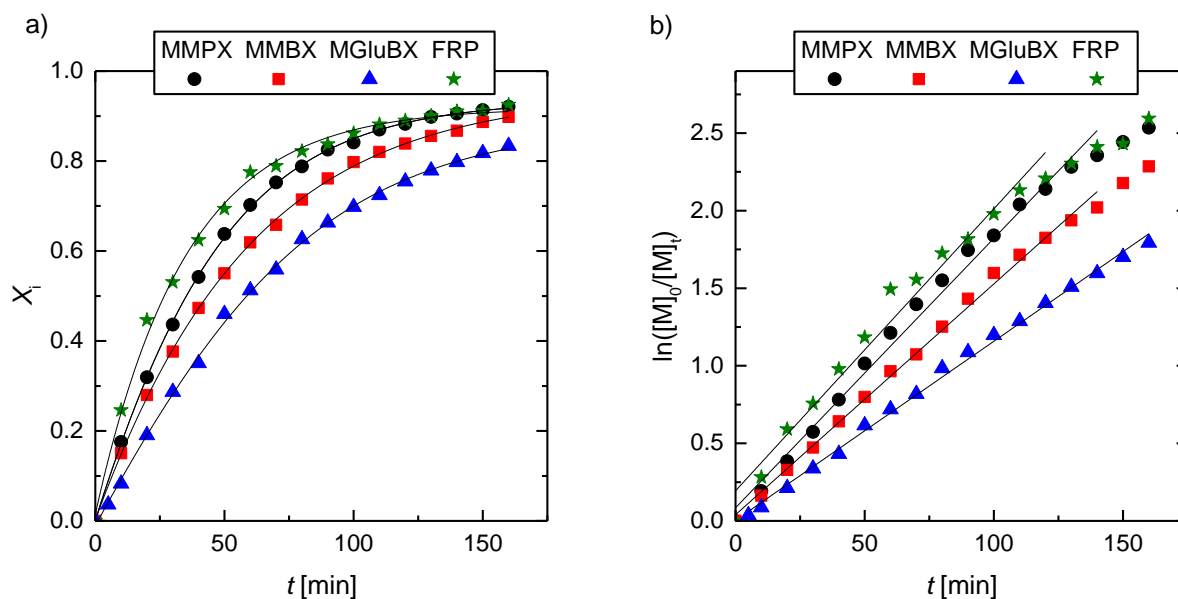
Figure 6. a) Time-dependent conversions X_i and b) pseudo-first-order plots $\ln([M]_0/[M]_t)$ of the polymerization of NIPAm as RAFT process with MMPX, MMBX or MGluBX or as FRP at 70°C obtained by ^{1}H NMR spectroscopy. The ratio of monomer, CTA and initiator was 100:1:0.2.

The polymerization rate was highest for the FRP without RAFT agent, closely followed by RAFT polymerization with MMPX. RAFT with MMBX was slower, whereas RAFT with MGluBX was the slowest polymerization. The polymerizations started immediately after the addition of the initiator. The initiator-dependent rate constants k' were determined from the slope in the pseudo-first-order plots (Table 3).

The RAFT polymers had a lower number average molecular mass M_n and PDI than conventional FRP polymers (Figure 7). The PDIs varied between 1.5 and 1.7 for RAFT polymerizations almost regardless of conversion and of the CTA used; the PDI of polymers synthesized in presence of MMBX was smaller. RAFT polymers had a higher molecular mass than calculated. This may be caused by the fact that the hydrodynamic radius of PNIPAm differs from the hydrodynamic radius of the polystyrene standard used for SEC measurements. Another reason might be a lesser control over the reaction.

The RAFT polymerization with MMPX showed the slightest deviation of M_n from the theoretical values (solid line in Figure 7). PNIPAm synthesized with MMBX or MGluBX displayed a higher dispersity of M_n. Therefore, it can be assumed that the RAFT equilibrium is reached

more quickly in presence of MMPX than in the presence of the other RAFT agents. The usage of MMPX gives a higher control over the polymerization. As the CTAs used are xanthates that usually are used to polymerize less activated MADIX monomers like vinyl esters and vinyl amides[129], and the acrylamide NIPAm is a MAM, it was expected that the control over the polymerization would not be particular large.
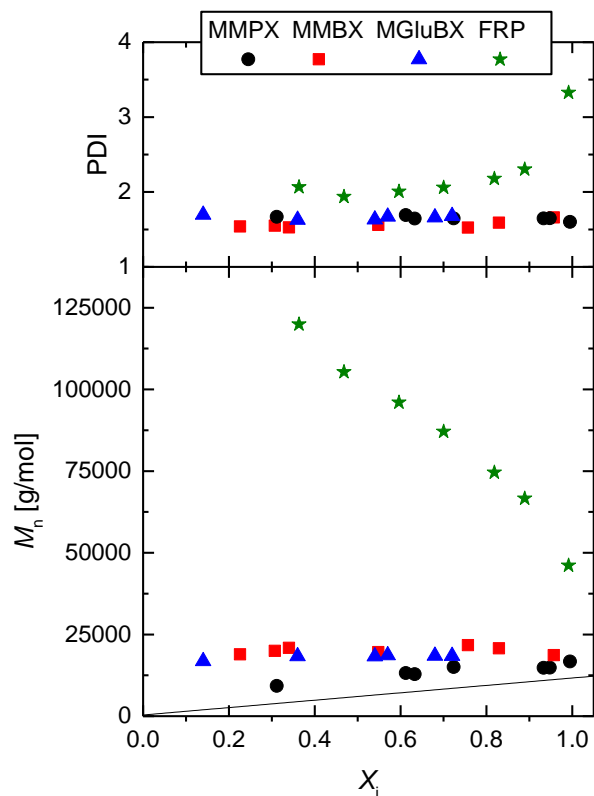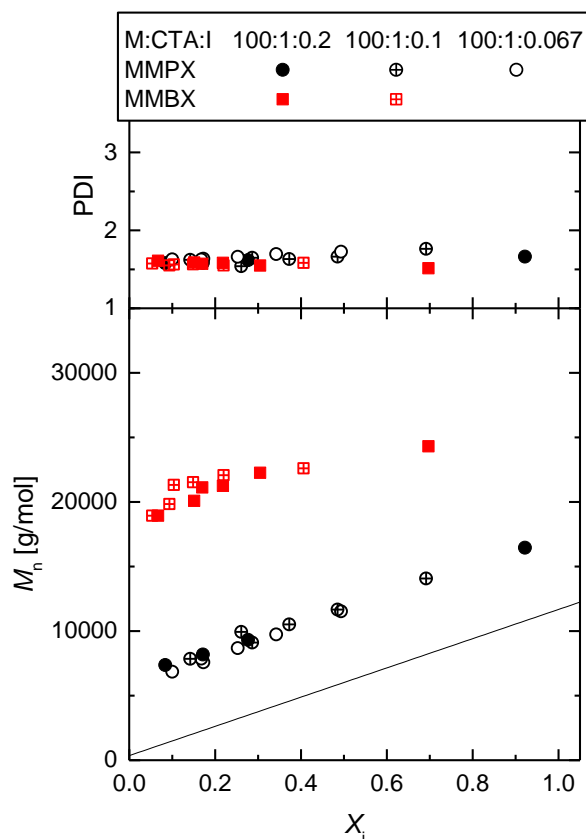

Figure 7. Number average molecular weight M_n and polydispersity index PDI vs. conversion X_i for PNIPAm synthesized by RAFT progress with MMPX, MMBX or MGluBX as CTA or as conventional FRP under same reaction conditions at a reaction temperature of 70 ° and a ratio of monomer, CTA and initiator of 100:1:0.2.

3.2.2 Influence of the Temperature

NIPAm was polymerized both at 70 °C and 50 °C with a ratio of monomer, CTA and initiator of M:CTA:I = 100:1:0.2 and a monomer concentration of 1 mol/L to investigate the influence of the temperature on the polymerization kinetics and the molecular weight distributions. Conversion versus time plots and pseudo-first-order plots for the RAFT polymerizations of NIPAm with MMPX and MMBX are compared to the FRP (Figure 8). Polymerizations at 70 °C lead to high conversions faster than polymerizations at 50 °C. Polymerization rates with MMPX as CTA were in the same range as polymerization rates for the FRP; the rate constants for the RAFT polymerization with MMBX were lower at both 70 °C and 50 °C polymerizations. The difference between the rate constants for the RAFT polymerizations with MMBX and the FRP was larger at lower temperatures (Table 3).
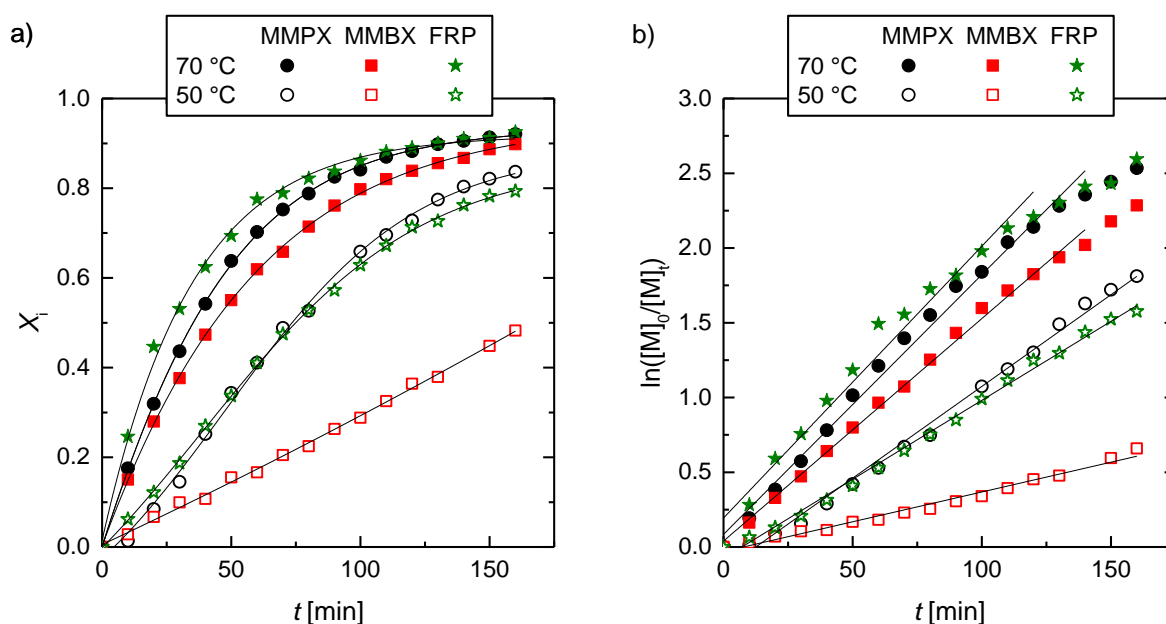
Figure 8. a) Time-dependent conversions X_i and b) pseudo-first-order plots $\ln([M]_0/[M]_t)$ of the polymerization of NIPAm as RAFT process with MMPX or MMBX or as FRP at 70 °C or 50 °C obtained by ^{1}H NMR spectroscopy. The ratio of monomer, CTA and initiator was 100:1:0.2.

Polymers synthesized by RAFT process either at 50 °C or at 70 °C had PDIs between 1.5 and 1.7 (Figure 9). The PDIs of benzyl-terminated PNIPAm were lower than the PDIs of carboxyl-terminated PNIPAm (Figure 7; Figure 9). The average molecular weight of PNIPAm synthesized in presence of MMPX rose with increasing conversion independently of the reaction temperature. Again, PNIPAm synthesized in the presence of MMBX showed a larger deviation of M_n from the theoretical value. The increase of the molecular weight with increasing conversion was easier to recognize at lower temperature. Therefore, it can be concluded that MMPX had a better control over the polymerization of NIPAm than MMBX, and that MMBX worked better at lower temperatures. Further polymerizations were carried out therefore at 50 °C.
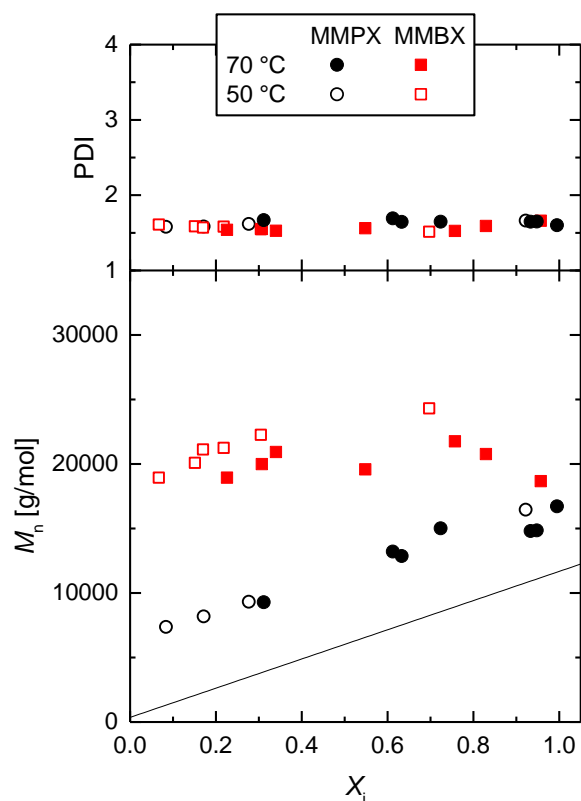
Figure 9. Number average molecular weight M_n and polydispersity index PDI vs. conversion X_i for PNIPAm synthesized by RAFT progress with MMPX or MMBX as CTA at 50 °C or 70 °C. The ratio of monomer, CTA and initiator was 100:1:0.2.

3.2.3 Influence of the Ratio of CTA and Initiator

NIPAm was polymerized with MMPX and MMBX using different ratios of monomer, CTA and initiator at 50 °C. High conversions were reached faster with larger initiator concentrations (lower CTA:I ratio; Figure 10a; Table 3). The linear dependence of the pseudo-first-order plots $\ln([M]_0/[M]_t)$ on the time indicates that the system is in a stationary state in the studied range ($k_p \cdot [P\bullet]$ = constant; Figure 10b). No rate retardation was observed at a lower CTA:I ratio (CTA:I = 1:0.2). Apart from the slow start of polymerization, the initiator dependent propagation rate k' was constant during the reaction time (until the monomer was consumed) for all RAFT polymerizations (Table 3). It is documented in literature that a larger concentration of the RAFT agent leads to a higher rate of retardation, which is also found here.[21]
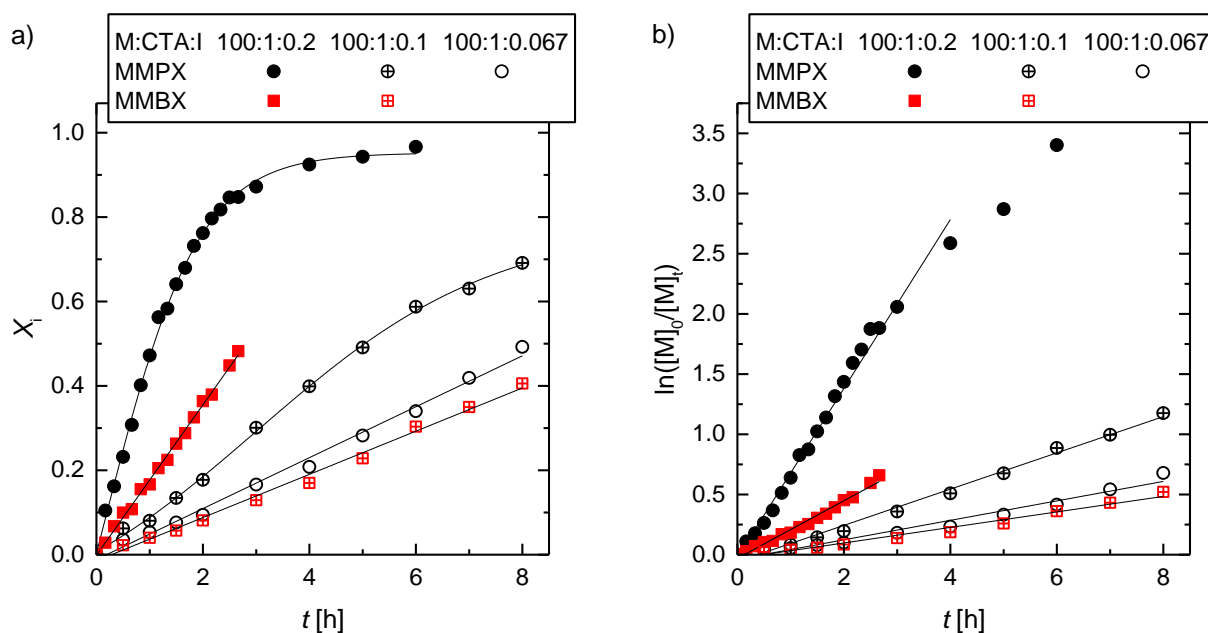
Figure 10. a) Time-dependent conversions X_i and b) pseudo-first-order plots $\ln([M]_0/[M]_t)$ of the polymerization of NIPAm as RAFT process with MMPX or MMBX at 50 °C with different ratios of monomer, CTA and initiator.

The linear increase of M_n with increasing conversion is in the same range for all polymerizations with MMPX (Figure 11). There is no significant difference between the reactions carried out with different ratios of CTA and initiator. The PDIs range between 1.5 and 1.8. A trend of increasing PDI with increasing monomer conversion can be observed. The increase of the PDI with conversion is often discussed.[130]

The PDIs of benzyl-terminated PNIPAm are independent of the monomer conversion and vary between 1.5 and 1.6. Like in the polymerization with MMPX, no difference in M_n with increasing conversion can be noticed with MMBX in dependence on the ratio of CTA and initiator.

Figure 11. Number average molecular weight M_n and polydispersity index PDI vs. conversion X_i for PNIPAm synthesized by RAFT progress with MMPX or MMBX as CTA with different M:CTA:I ratios at 50°C.

Table 3. Initiator-dependent rate constants k' obtained by ¹H NMR spectroscopy for different CTAs and reaction conditions. The NIPAm concentration was 1 mol/L.

Polymerization conditions	Temperature [°C]	M:CTA:I ratio	Initiator-dependent rate constant k' [s⁻¹]
RAFT with MMPX	70	100:1:0.2	$2.90 \cdot 10^{-4}$
RAFT with MMPX	50	100:1:0.2	$2.05 \cdot 10^{-4}$
RAFT with MMPX	50	100:1:0.1	$4.18 \cdot 10^{-5}$
RAFT with MMPX	50	100:1:0.067	$2.25 \cdot 10^{-5}$
RAFT with MMBX	70	100:1:0.2	$2.48 \cdot 10^{-4}$
RAFT with MMBX	50	100:1:0.2	$6.64 \cdot 10^{-5}$
RAFT with MMBX	50	100:1:0.1	$1.79 \cdot 10^{-5}$
RAFT with MGluBX	70	100:1:0.2	$1.92 \cdot 10^{-4}$
Conventional FRP	70	100:1:0.2	$3.03 \cdot 10^{-4}$
Conventional FRP	50	100:1:0.2	$1.76 \cdot 10^{-4}$

3.2.4 Synthesis of NIPAm Diblock Copolymers

NIPAm diblock copolymers were synthesized to determine the amount of "living" chains. Macro RAFT agents (macro MMPX and macro MMBX) were made by RAFT polymerization of NIPAm with MMPX or MMBX with a small ratio of monomer and CTA (cycle 1, Scheme 13a). The macro CTAs could be used as a low molecular weight CTAs after purification by dialysis and freeze-drying (cycle 2, Scheme 13b).
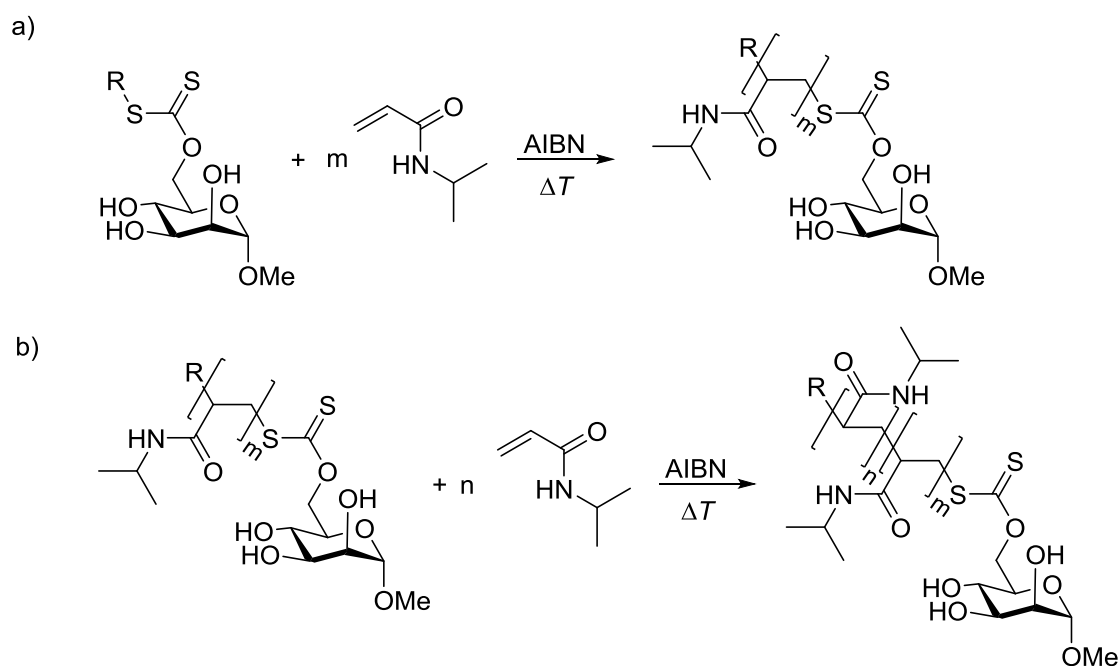
Scheme 13. Synthesis route of a poly(NIPAm-*co*-NIPAm) diblock copolymer; a) Synthesis of a macro CTA (cycle 1), b) synthesis of NIPAm diblock copolymers using a macro CTA (cycle 2).

A shift in molecular weight between cycle 1 and cycle 2 is visible (Figure 12). PNIPAm synthesized in cycle 2 has a higher peak molecular weight, but also a low-molecular shoulder in the area of the MWD of PNIPAm made in cycle 1. This shoulder indicates the amount of "dead" polymer chains. The low-molecular weight shoulder is larger for benzyl-terminated PNIPAm. This again indicates that MMPX leads to a better control over the RAFT polymerization of PNIPAm than MMBX. The low-molecular shoulder of carboxyl-terminated PNIPAm at < 1000 g/mol results from the solvent (Figure 12a).
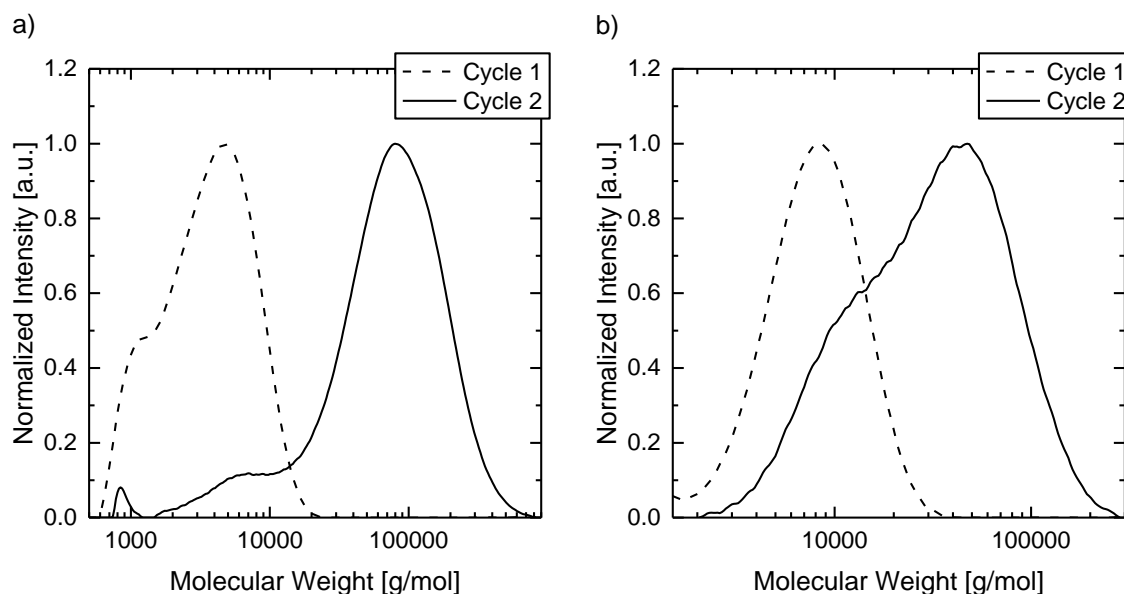
Figure 12. MWD of PNIPAm synthesized by RAFT polymerization with a) MMPX (M:CTA:I = 15:1:0.2; 50 °C; cycle 1) or macro MMPX (M:CTA:I = 200:1:0.07; 50 °C; cycle 2) and b) MMBX (M:CTA:I = 20:1:0.2; 50 °C; cycle 1) or macro MMBX (M:CTA:I = 150:1:0.07; 50 °C; cycle 2) as CTA. The low-molecular shoulder of carboxyl-terminated PNIPAm at < 1000 g/mol is from solvent residuals.

The number of dead chains was quantified from the elugram of poly(NIPAm-*co*-NIPAm) (Figure 13). The amount of dead polymer was determined by the ratio of low molecular weight area A_1 and the overall area A_1+A_2 (Table 4). The amount of dead polymer (19.25 % for MMPX and 36.27 % for MMBX) was larger than reported in literature for controlled RAFT polymerizations[13], but since NIPAm is a MAM and xanthates are usually used to polymerize LAMs and the PDIs are higher than described in literature as well, this is not surprising. Nonetheless, the synthesis of diblock copolymers could prove that there are "living" polymer chains in RAFT/MADIX polymerization with MMPX and MMBX.
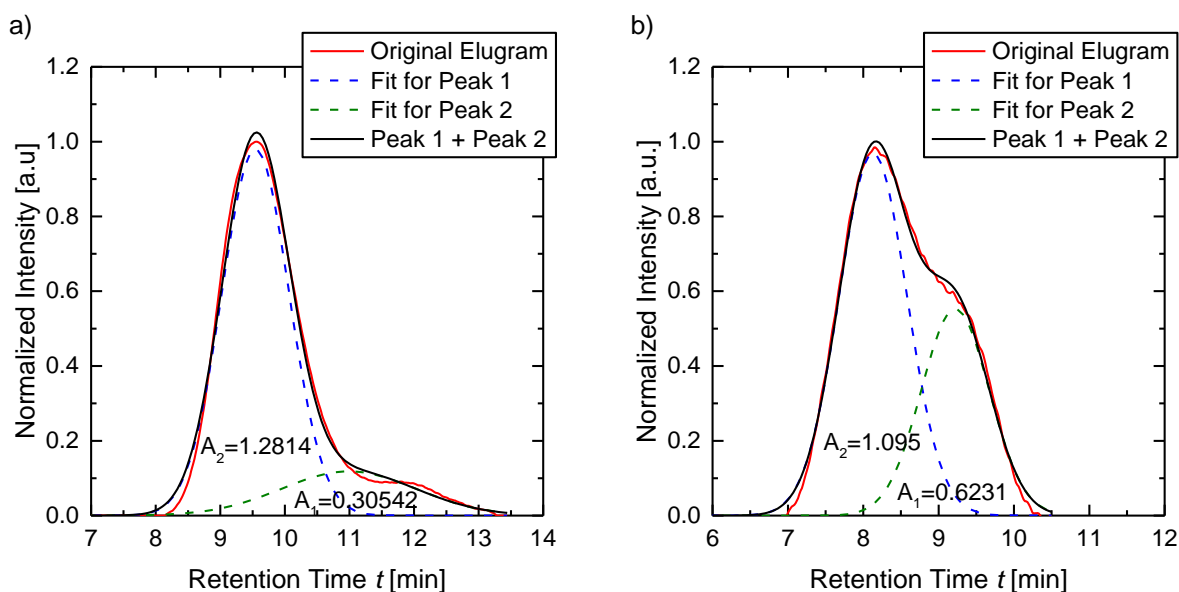
Figure 13. Fitted elugram of poly(NIPAm-*co*-NIPAm) diblock copolymers synthesized by RAFT progress with a) macro MMPX (M:CTA:I = 200:1:0.07; 50 °C) and b) macro MMBX (M:CTA:I = 150:1:0.07; 70 °C).

Table 4. Amount of dead polymer after two cycles of polymerization.

RAFT agent	A_1	A_2	Dead polymer [%]
macro MMPX	0.3054	1.281	19.25
macro MMBX	0.6231	1.095	36.27

3.2.5 Evidence of the End Groups

The advantages of RAFT/MADIX polymerization are the "livingness" of the process and the customizable end groups. Evidence that the benzyl R group is incorporated in benzyl-terminated PNIPAm was provided by ^{13}C NMR spectroscopy (Figure 14b). The benzylic carbons are visible at a chemical shift of $\delta = 128$ ppm. This signal is not visible in the ^{13}C NMR spectrum of PNIPAm synthesized by free radical polymerization without RAFT agent (Figure 14a).
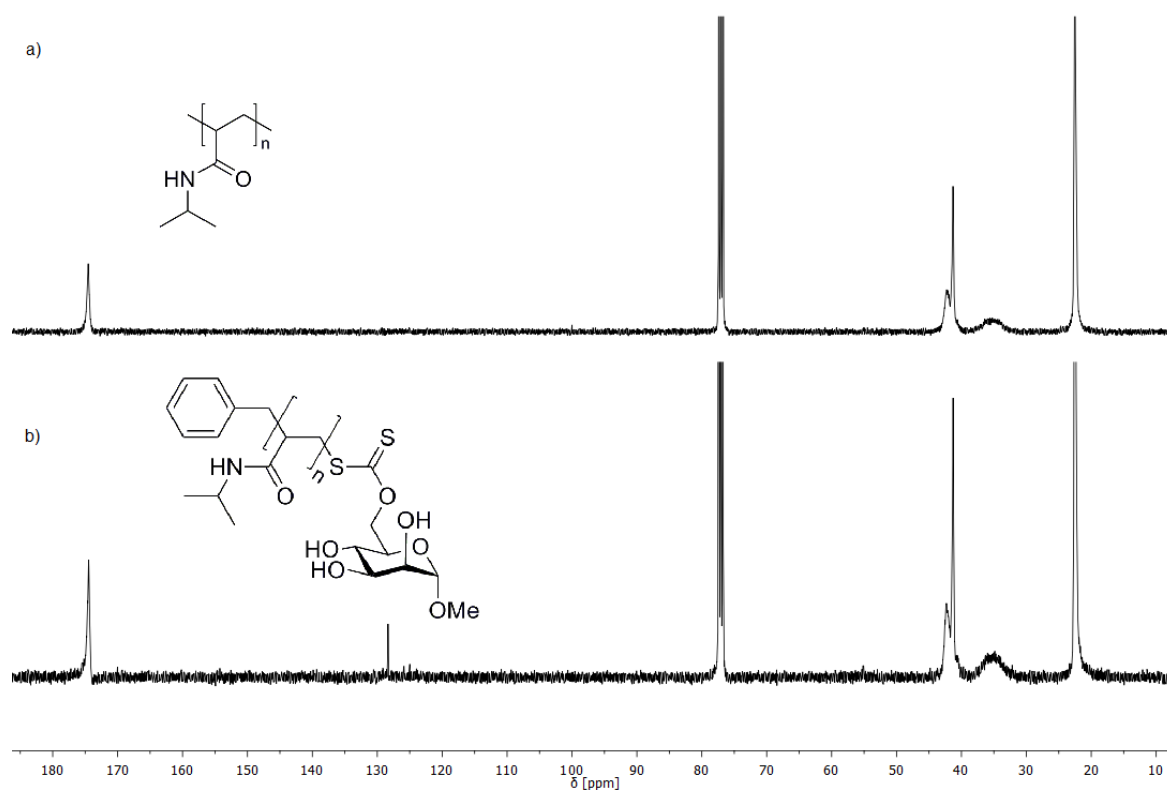
Figure 14. ^{13}C NMR spectra of a) PNIPAm and b) benzyl-terminated PNIPAm in chloroform-*d*.

The presence of the sugar moiety of the Z group was provided by a common sugar test using staining. The solved polymer was applied onto a thin-layer chromatography (TLC) plate, moistened with a mixture of sulfuric acid and ethanol and heated. A brown coloring indicated the presence of sugars in the polymer. The carboxylic acid entity of the R end group was proven by reaction of carboxyl-terminated PNIPAm with furfurylamine (Scheme 14). The furfurylamide function was detectable by ^{1}H NMR spectroscopy (Figure 15).
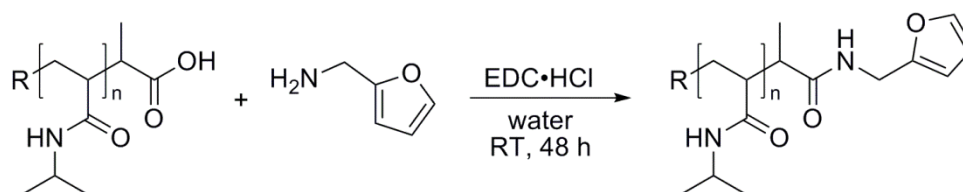
Scheme 14. Post modification of carboxyl-terminated PNIPAm by coupling with furfurylamine.
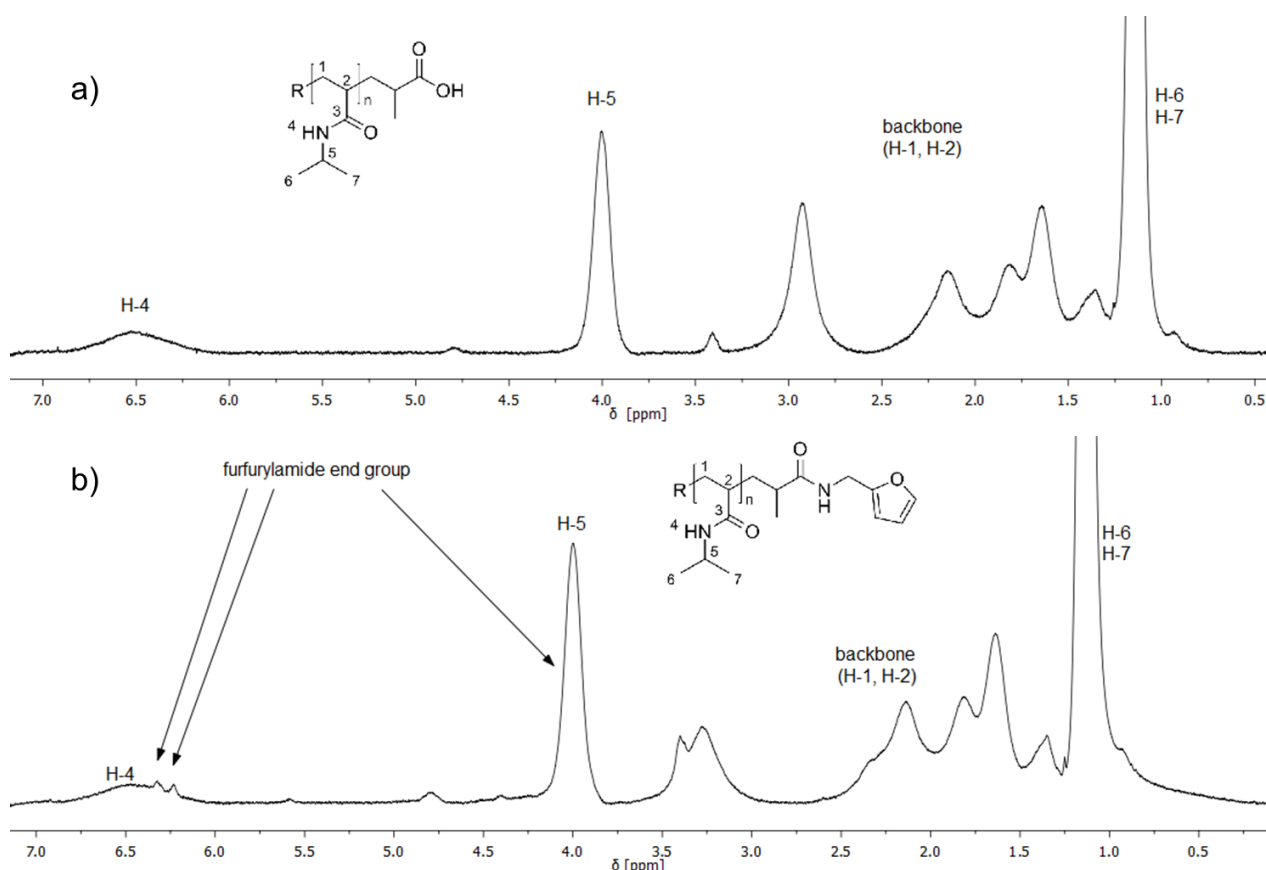
Figure 15. ^{1}H NMR spectra of a) carboxyl-terminated PNIPAm and b) furfurylamide-terminated PNIPAm in chloroform-*d*.

3.3 Polymerization of NVP

NVP was polymerized in water with MMPX as RAFT agent at a temperature of 30 °C or 50 °C (Scheme 15). A ratio of monomer, CTA and initiator of 100:1:0.2 was used.
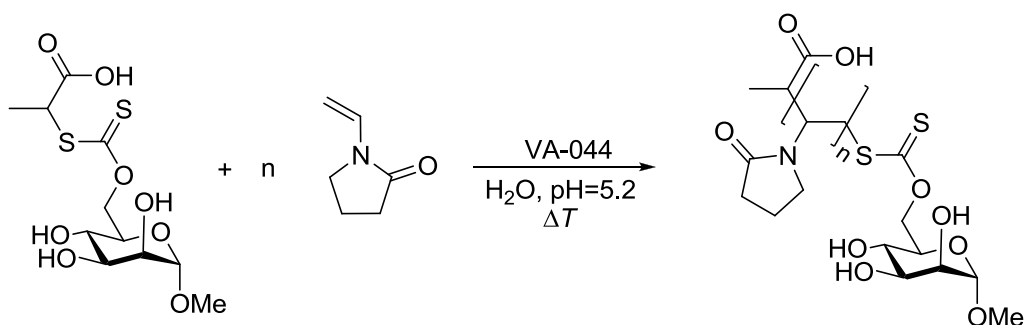
Scheme 15. RAFT polymerization of NVP in aqueous media with MMPX as chain transfer agent.

The influence of the RAFT agent MMPX on the polymerization was investigated by comparison to the conventional free radical polymerization under identical reaction conditions. The rate of polymerization was smaller in the RAFT polymerization than in FRP (Figure 16a). Almost full conversion was obtained after 160 minutes by RAFT polymerization with a ratio of

monomer, CTA and initiator of 100:1:0.2. No inhibition period was observed. The polymerization rate was constant during the reaction for both RAFT and FRP (Figure 16b, Table 5).
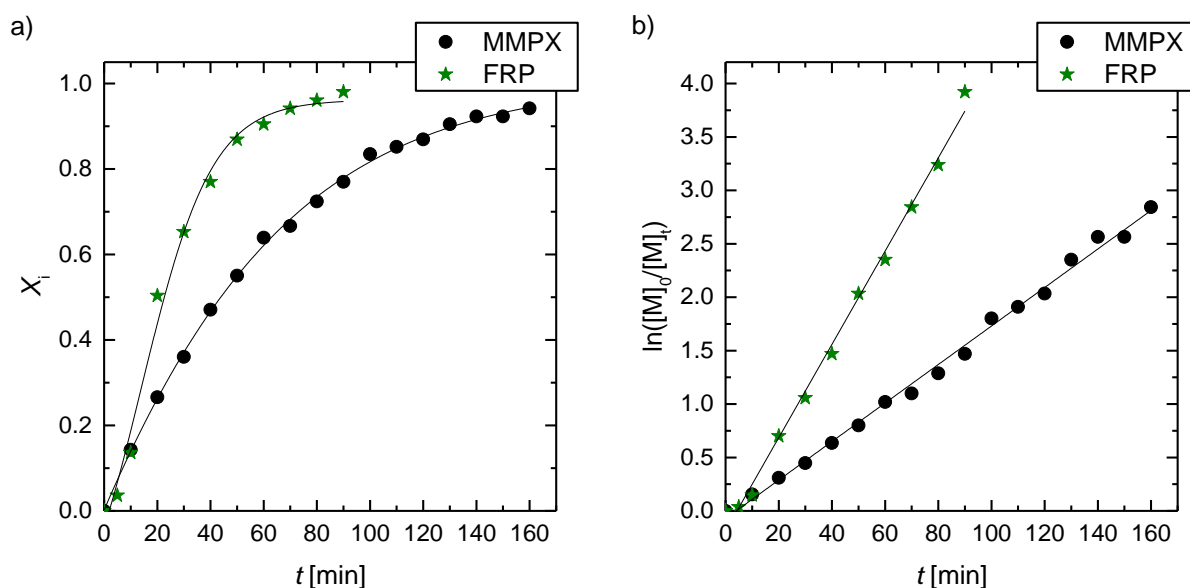
Figure 16. Time-dependent monomer conversions X_i and b) pseudo-first-order plots $\ln([M]_0/[M]_t)$ of the polymerization of NVP as RAFT process with MMPX (M:CTA:I = 100:1:0.2) or as conventional FRP (M:I = 100:0.2) at 50°C obtained by ^{1}H NMR spectroscopy.

Table 5. Initiator-dependent rate constants obtained by ^{1}H NMR spectroscopy for the polymerization of NVP as RAFT process with MMPX or as FRP. The NVP concentration was 1 mol/L for all polymerizations.

Polymerization conditions	Temperature [°C]	M:CTA:I ratio	Initiator-dependent rate constant k' [s^{-1}]
RAFT with MMPX	50	100:1:0.2	$3.00 \cdot 10^{-4}$
FRP	50	100:0.2	$7.03 \cdot 10^{-4}$

The MWDs show large differences between RAFT polymerizations and FRP (Figure 17). M_n and PDI were lower for RAFT polymers compared to conventional polymers. The PDI was independent of the monomer conversion and in the same range for polymerizations at 50 °C and at 30 °C for the RAFT polymerizations. The number average molecular mass shows a wide scattering around the theoretical values (solid line), as was already observed in the RAFT polymerization of NIPAm with MMBX (cf. Chapter 3.2). The PDIs of PVP synthesized by conventional FRP increased with increasing conversion, whereas the molecular weight M_n decreased with increasing monomer conversion. This may be explainable by the increase of the viscosity and the depletion of the monomer at high conversions. It can be concluded that the application of MMPX as RAFT agent does not lead to perfect control over the polymerization of NVP, but it is sufficient to make polymers with PDIs smaller than 1.8 at limited molecular mass.
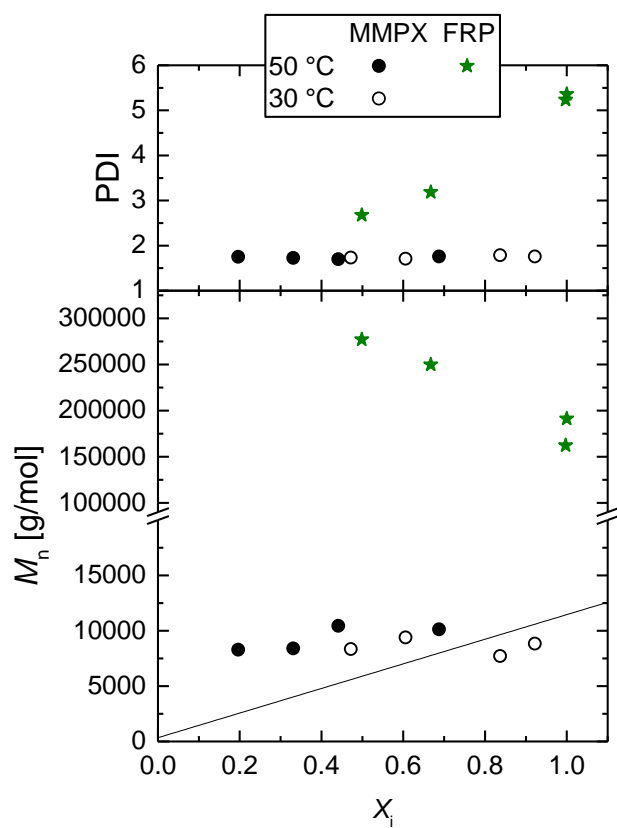
Figure 17. Number average molecular weight M_n and polydispersity index PDI vs. conversion X_i for PVP synthesized by RAFT progress with MMPX with M:I:CTA = 100:1:0.2 at 50 °C or 30 °C or by FRP with M:I = 100:0.2 at 50 °C.

4. Superabsorbent Hydrogel Foams

Hydrogels based on crosslinked poly(acrylic acid) (PAA) derivatives made by free radical polymerization for application as wound dressings or in hygiene products will be presented. Most of the common hydrogels have poor mechanical properties, thereunder low mechanical strength and load capacity, which limits their range of application.[131] An improvement of the mechanical stability can be achieved by formation of double-network hydrogels[132–134] or nanocomposite hydrogels[62,135,136]. Superabsorbent polymers (SAPs) can be bound into an interlayer of the carrier material (DE 10034505)[88] or applied onto the carrier material (DE 10231356 B4)[89]. Another route for composites of SAPs and a carrier material is the *in situ* synthesis of the SAP in the carrier material as matrix (e. g. WO 2011/032862[90] and WO 01/56625[92]).

In this work, the superabsorbent polymer was stabilized by forming an interpenetrating network (IPN) of crosslinked, partially neutralized poly(acrylic acid) in a melamine/form-aldehyde foam matrix (Basotect®) similar to WO 2009/056543.[91] Basotect® is commercially available and inexpensive; it has an open-cell web structure (Figure 18) with a resulting low density of about 9 g/L[97] and high flexibility, hydrophilicity and flame retardancy.[97] The hydrogel composites would have the shape of the Basotect® sample used for the synthesis. In addition, the shape of the SAP composites can be modified by simple cutting of the sample after the synthesis.
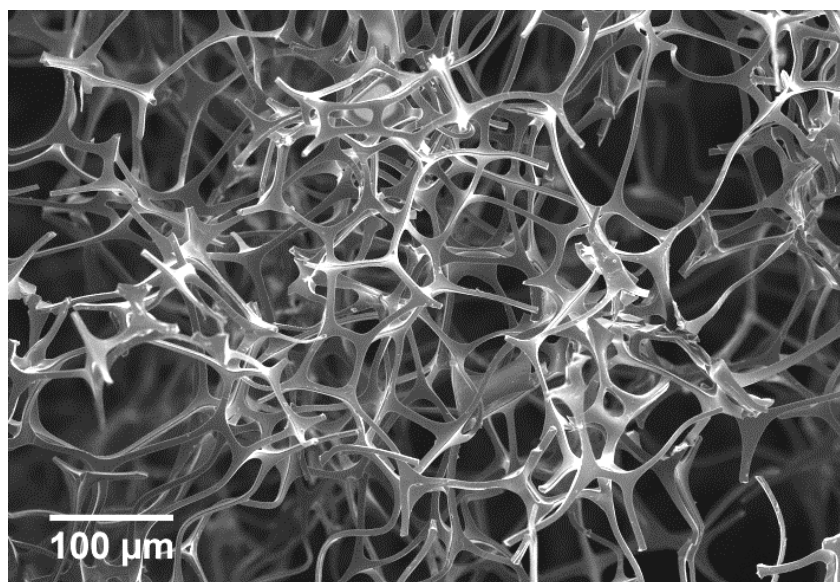
Figure 18. SEM image of the melamine/formaldehyde foam Basotect® with its open-pored web structure.

4.1 Synthesis of Superabsorbent Hydrogel Composites

The superabsorbent polymer PAA was introduced into the melamine/formaldehyde foam by *in situ* polymerization of partially neutralized acrylic acid and a crosslinking agent in aqueous media inside the Basotect® matrix (Figure 19, Scheme 16).[91] The polymerization was carried

out under easily applicable conditions as radical polymerization at 80 °C with potassium persulfate (KPS) as initiator. Poly(ethylene glycol) diacrylate (PEGda) was used as crosslinking agent since it forms a hydrogel itself.[137] The PEGda chain length of about 10 ethylene oxide repeating units ($M_n \approx 575$ g/mol) ensures a higher network flexibility in comparison to small crosslinking agents like *N,N'*-methylenebis(acrylamide).
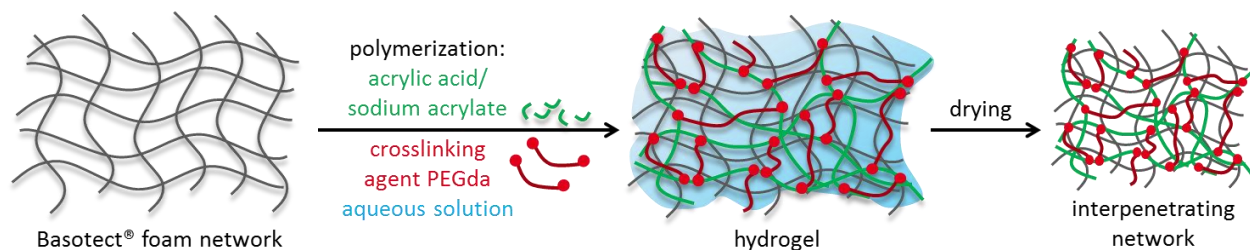
Figure 19. General synthesis path for *in situ* synthesis of superabsorbent polymer composites containing a Basotect® matrix and partially neutralized poly(acrylic acid) crosslinked with PEGda.
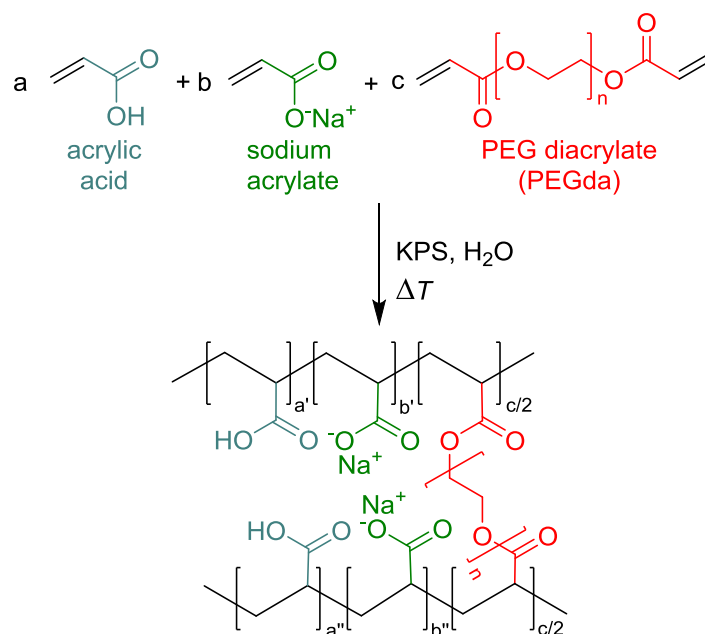
Scheme 16. Free radical copolymerization of acrylic acid, sodium acrylate and PEGda to form a randomly crosslinked superabsorbent polymer.

The appearance of the freshly synthesized SAP-Basotect® composites depends on the amounts of acrylic acid and PEGda in the monomer solution. High conversions and initial monomer concentrations led to a gel-like appearance of the composites at room temperature as well as at 80 °C. Low conversions and initial monomer concentrations led to composites that released a part of the absorbed water. No discoloration of the Basotect® matrix could be detected after six hours of polymerization under Schlenk conditions.

The composition of the initial monomer solution affected the ratio of surface and volume of the Basotect® matrix during the synthesis, the gain in weight of the dry composite relative to unmodified Basotect® and consequently the swelling behavior of the composites.

4.1.1 Investigation of the Monomer Conversion

The monomer conversion was complete after 6–22 h. The progress of the reaction was monitored by FT-IR spectroscopy (Figure 20). The intensity of the C=C bond stretching vibrations at 1636 cm^{-1} decreased with increasing reaction time. A low intensity of the C=C stretching vibration was observable after 6 h of reaction. This signal of the C=C stretching vibration was completely absent after 22 h reaction time. In addition, the monomer signals in the fingerprint area (989 cm^{-1}, 950 cm^{-1}, 899 cm^{-1}, 837 cm^{-1}) disappeared with progressing reaction time.

The reaction of Figure 20 was carried out with an initial acrylic acid concentration of 0.55 mol/L, 7.5 mol% PEGda and 1 mol% KPS with regards to acrylic acid at a degree of neutralization (ND) of 80 %. This was a low concentrated monomer solution. The polymerization of more concentrated monomer solutions is faster. Therefore, the following polymerizations were terminated after 6 h.
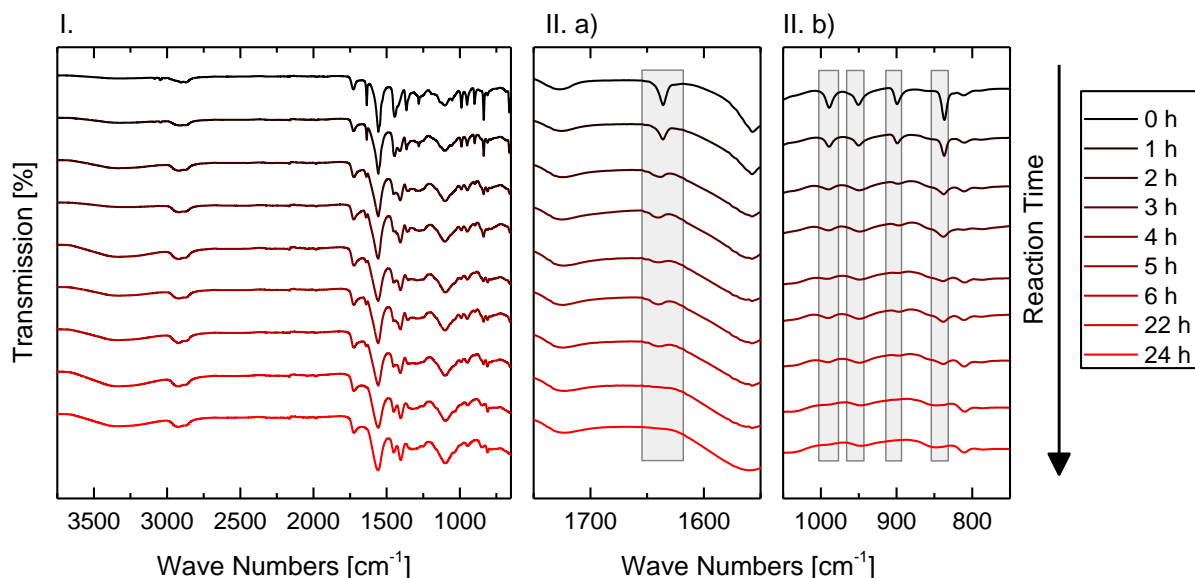
Figure 20. FT-IR spectra of freeze-dried samples taken during the synthesis of a composite of Basotect®, partially neutralized poly(acrylic acid) and PEGda at 80 °C. The initial concentration of acrylic acid was c(AA) = 0.55 mol/L, of crosslinking agent PEGda c(PEGda) = 7.5 mol% and of the initiator KPS c(KPS) = 1 mol%. The degree of neutralization was 80 %. I.) Full spectrum; II. a) section from 1550–1170 cm^{-1}; II. b) section from 1050–750 cm^{-1}.

4.1.2 Influence of the Modification on the Ratio of Surface and Volume

The modification of Basotect® with SAP led to an increased outer surface and a decreased matrix volume of the freshly synthesized composite in comparison to the pure Basotect® before the synthesis (Figure 21). The change in volume and surface of the composite occurred

on account of heating of the aqueous monomer solution accompanied by solution and gel expansion. Solvent could evaporate more easily by stretching in x and y-direction and subsequent surface increase. This led to a decrease of the sample thickness (shrinkage in z-direction). The increase of the ratio of surface and volume was large for composites with small hydrogel content (0.5 mol/L acrylic acid and 10 mol% PEGda in the initial monomer solution). Composites with large hydrogel content bind the solvent stronger, less solvent evaporates and these samples exhibit less change in surface and volume.
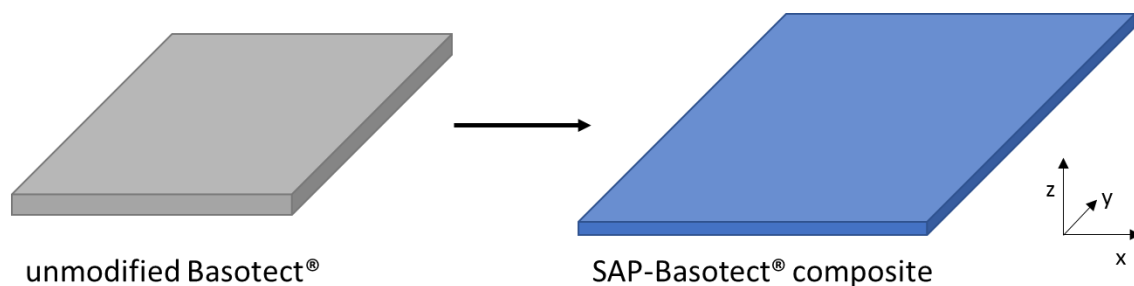
Figure 21. Stretching of the Basotect® sample after *in situ* polymerization of partially neutralized and crosslinked acrylic acid inside the Basotect® matrix.

The surface of composites after the synthesis was larger than the surface of unmodified Basotect® by a factor of 1.04–1.25. The matrix volume was decreased by a factor of 0.37–0.97 (Figure 22a). The ratio of surface A and volume V increased in dependence on the synthesis conditions by a factor of 1.2–2.8 (reaction conditions: factor 1.2: 0.9 mol/L acrylic acid, 10 mol% PEGda; factor 2.8: 0.5 mol/L acrylic acid, 10 mol% PEGda; Figure 22b).
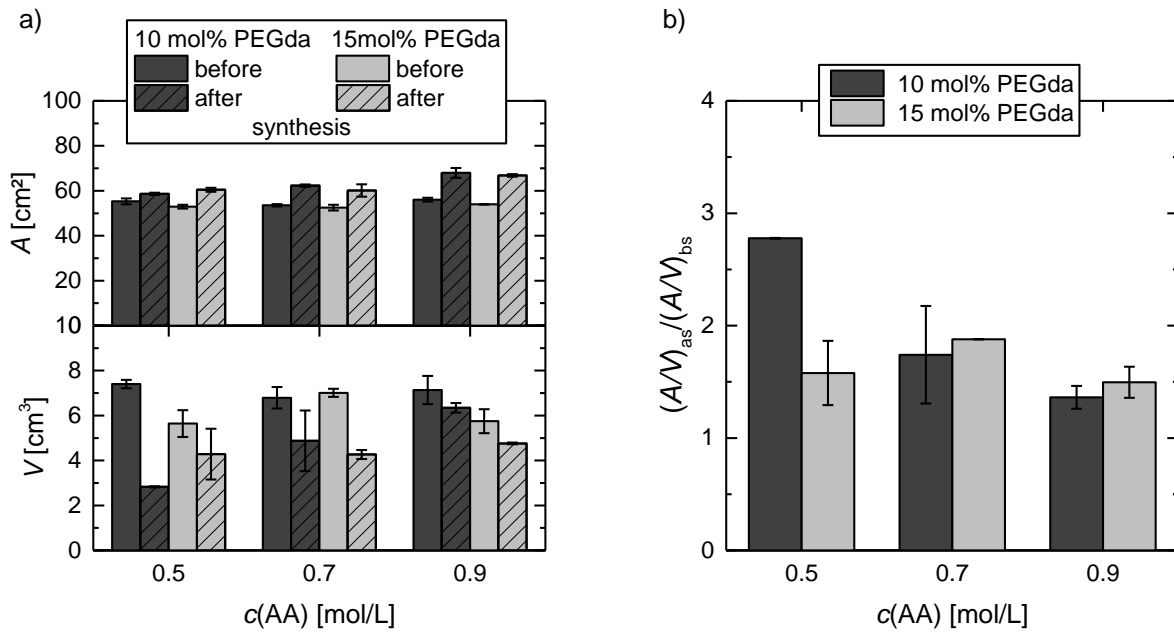
Figure 22. a) Surface A and volume V of Basotect® with SAP. b) Surface/volume ratio before and after modification with 0.5 mol/L, 0.7 mol/L or 0.9 mol/L acrylic acid and 10 mol% or 15 mol% PEGda in the monomer solution. The error bars result from the scattering in three separate samples.

4.1.3 Influences on the Gain in Weight

The gain in weight G_w of the dry hydrogel composites with mass $m_{gel,dry}$ as sum of the mass of the dried original Basotect® sample m_{Bas} and the mass of the SAP m_{SAP} relative to the mass of the dried original Basotect® is an indication for the gel content and consequently an indication for the expected swelling of the sample (Equation 13). The smallest possible value for G_w is 1. A gain in weight of $G_w = 1$ implies that no modification of the Basotect® matrix has taken place.

$$G_w = \frac{m_{gel,dry}}{m_{Bas}} = \frac{m_{Bas} + m_{SAP}}{m_{Bas}} = 1 + \frac{m_{SAP}}{m_{Bas}} \tag{13}$$

The gain in weight increased with increasing concentration of acrylic acid and crosslinking agent PEGda used in the initial monomer solution (Figure 23). G_w only increased for acrylic acid concentrations larger than 0.7 mol/L for composites synthesized with 5 mol% of crosslinking agent with regard to the concentration of acrylic acid. The increase in weight for the samples made with 5 mol% PEGda and 0.7 mol/L acrylic acid or less was with $G_w < 3$ insignificant. The reason for this mediocre increase in weight is that at small concentrations of monomer and crosslinking agent majorly branched, short-chained polymers are formed. These polymers can be washed out of the matrix during washing. There were large error bars for some samples. These result from inhomogeneous impregnation with the monomer solution during synthesis or from non-uniformly cut Basotect®.
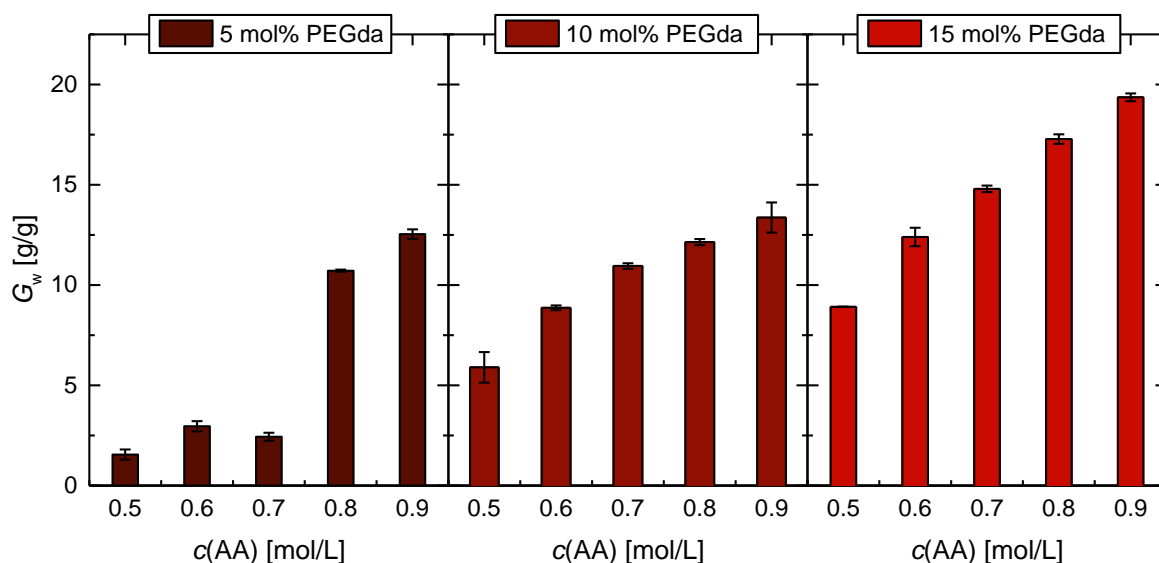
Figure 23. G_w as function of the amount of crosslinking agent PEGda with increasing initial concentration of acrylic acid c(AA) for samples with a thickness d = 0.5 cm. Average of two determinations.

Generally, the gain in weight increased with increasing matrix thickness if there was no change of the crosslinking content, but for a matrix thickness of d = 3 cm, G_w was smaller than for a thickness of d = 1 cm (Figure 24). This is explained by the hindered impregnation with the monomer solution in thick samples on account of impeded diffusion into the inner sample. Again, there were outliers and large error bars because of the uneven thickness of the Basotect® samples. Samples with a thickness of both 0.5 cm and 1 cm exhibited a similar G_w for a concentration of 0.6 mol/L acrylic acid. The reason for this might be that the polymer forms stronger networks and the monomer solution is bound more thoroughly in thicker samples, but the impregnation is faster in thinner samples. Samples with a matrix thickness of d < 0.5 cm were not synthesized with 0.5 mol/L acrylic acid since almost no gel was obtained with 0.6 mol/L. Samples with a thickness of d = 3 cm were synthesized with 0.6 mol/L and 0.7 mol/L acrylic acid in the monomer solution. The time until the swelling equilibrium was reached was more than 3 weeks for higher concentrations. Washout effects increased for less concentrated samples. Furthermore, thick samples are less relevant for application as wound dressing or in hygiene products.
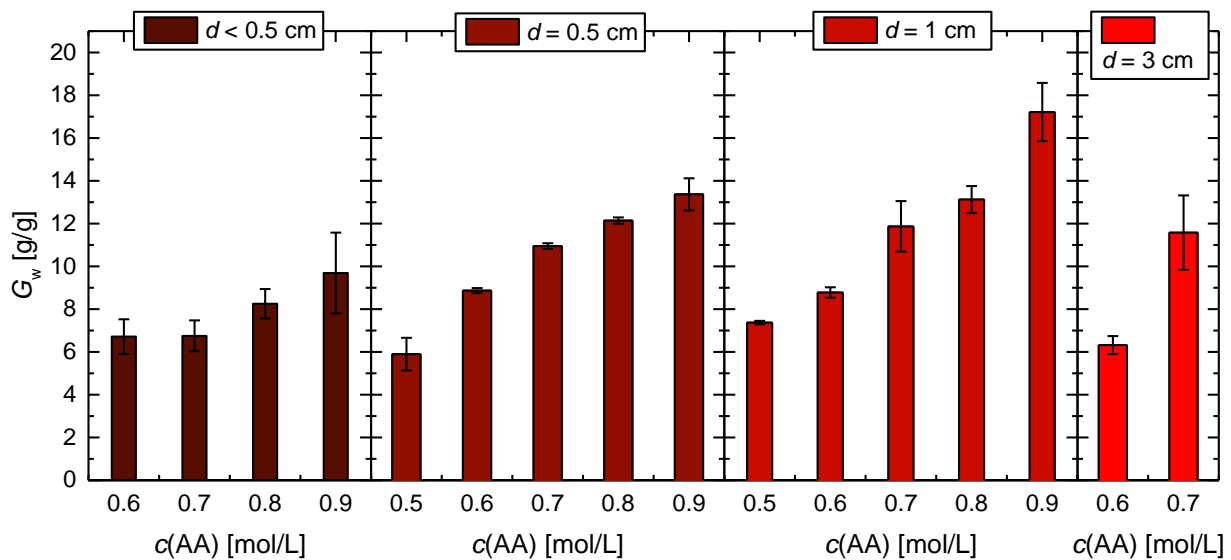
Figure 24. G_w as function of the Basotect® sample and the initial concentration of acrylic acid c(AA) at 10 mol% PEGda with regards to acrylic acid. Average of two determinations.

4.2 Investigation of the Microstructure of the SAP Composites

The microstructure of the samples was investigated by scanning electron microscopy (SEM). SEM images of the samples could be obtained after drying the hydrogels. The superabsorbent composites shrink during drying under air or in a vacuum drying oven and form xerogels. The microstructure of the swollen state of the composites was of special interest. This can be addressed from drying with supercritical carbon dioxide (CO_2) to obtain aerogels. The disadvantage of supercritical drying of hydrogels is that supercritical CO_2 is not soluble in water. Therefore, prior to the supercritical drying, a solvent exchange from water to ethanol or DMSO was carried out.

4.2.1 Solvent Exchange

The weighted dry hydrogel composites were swollen in water until the swelling equilibrium was reached. The swelling solution was gradually exchanged against DMSO or ethanol after 12 days of swelling in water (Figure 25). Most samples underwent a change in structure and volume during the solvent exchange. The carboxylate groups of PAA have a higher solubility in water than in DMSO or ethanol. The expansion of the SAP is decreased in organic media in comparison to water. Consequently, the polymer coils are less expanded.

The volume of the SAP composites is normalized for better comparability of the different samples (Figure 25). The normalized volume V/V_{eq} was calculated from the ratio of the weight of the sample in the solvent mixture m with its density ρ and the equilibrium mass of the water-swollen sample m_{eq} and its approximate density ρ_{water} (Equation 14). The actual density of the samples swollen in different solvent mixtures is unknown, but it can be estimated from the summation of the product of the weight fraction w_{os} of the organic solvent and its density

ρ_s with the theoretical sample volume in pure organic solvent m/ρ_s and the product of the weight fraction $1-w_{os}$ of water with the theoretical sample volume in water m/ρ_{water}.

$$\frac{V}{V_{eq}} \approx \frac{\dfrac{m}{\rho}}{\dfrac{m_{eq}}{\rho_{water}}} \approx \frac{w_{os} \cdot \dfrac{m}{\rho_s} + (1-w_{os}) \cdot \dfrac{m}{\rho_{water}}}{\dfrac{m_{eq}}{\rho_{water}}} \qquad (14)$$

The solvent exchange led to a decreased volume (de-swelling), especially for highly modified and consequently strongly water-swollen samples. This effect was more pronounced for the solvent exchange with ethanol than with DMSO. Only for samples synthesized with 0.5 mol/L acrylic acid and 10 mol% PEGda no volume change was noticeable. The reason for this is that these samples were hardly modified and almost behave like Basotect®. Since Basotect® is compatible with ethanol and DMSO, no change in the structure and consequently no volume change occurred.
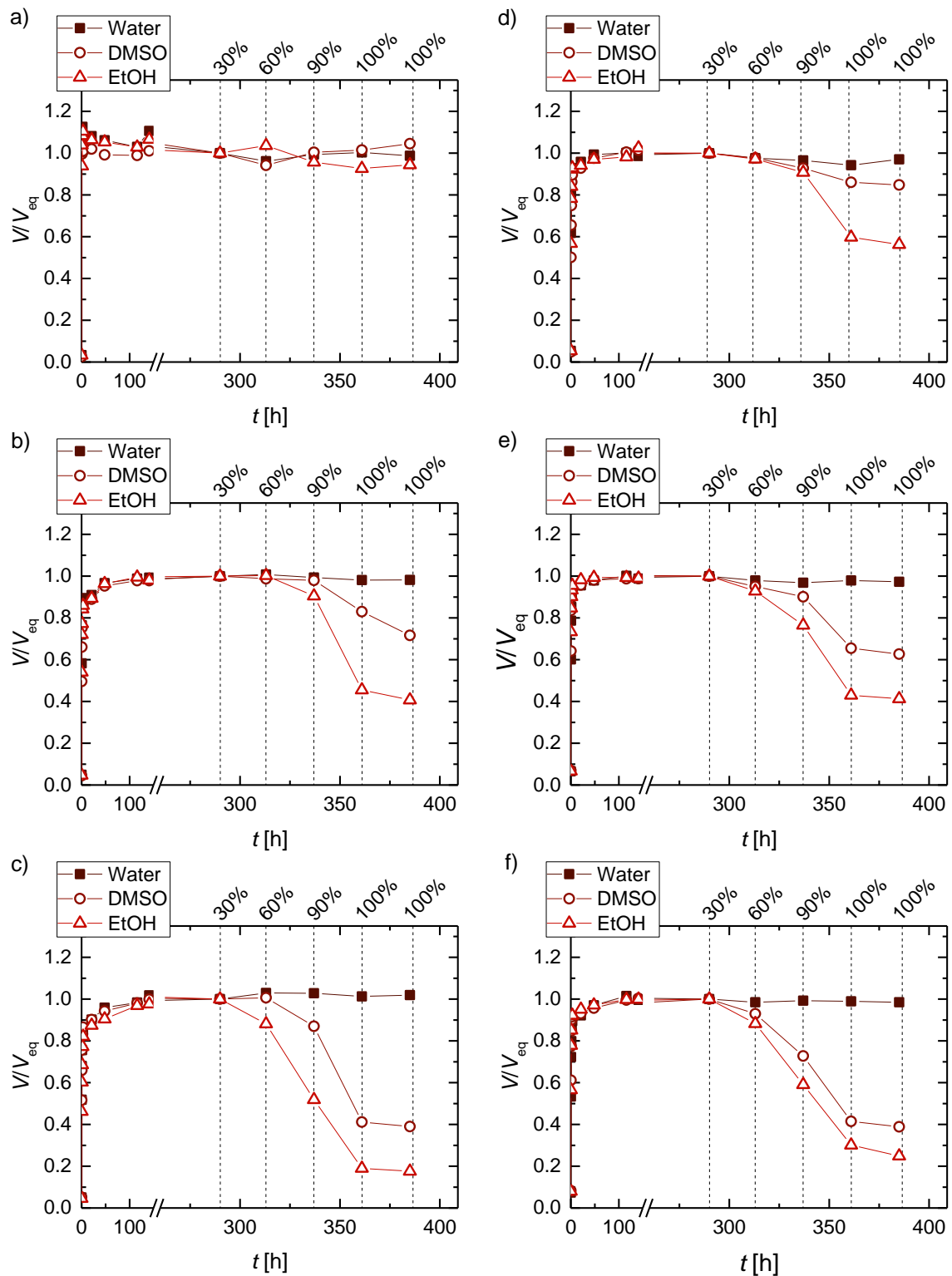
Figure 25. Normalized volume V/V_{eq} during solvent exchange with DMSO and ethanol as function of the swelling time. a–c) 10 mol% PEGda and a) 0.5 mol/L, b) 0.7 mol/L and c) 0.9 mol/L acrylic acid in the initial monomer solution. d–f) 15 mol% PEGda and d) 0.5 mol/L, e) 0.7 mol/L and f) 0.9 mol/L acrylic acid in the initial monomer solution.

The normalized volume change ΔV increased with increasing amount of acrylic acid in the monomer solution (Equation 15, Figure 26).

$$\Delta V = \frac{\left(V / V_{eq}\right)_{w_{os}=0} - \left(V / V_{eq}\right)_{w_{os}=1}}{\left(V / V_{eq}\right)_{w_{os}=0}} = 1 - \frac{\left(V / V_{eq}\right)_{w_{os}=1}}{\left(V / V_{eq}\right)_{w_{os}=0}} \qquad (15)$$

The slope of the increase was large for low-crosslinked samples synthesized with 10 mol% PEGda. The reason for this was the constant volume V of samples synthesized with 0.5 mol/L acrylic acid and 10 mol% PEGda. There was no volume change ($\Delta V = 0$) for these samples, whereas samples synthesized from larger concentrations of acrylic acid showed a volume change larger than the change in volume of samples synthesized with 15 mol% crosslinking agent.
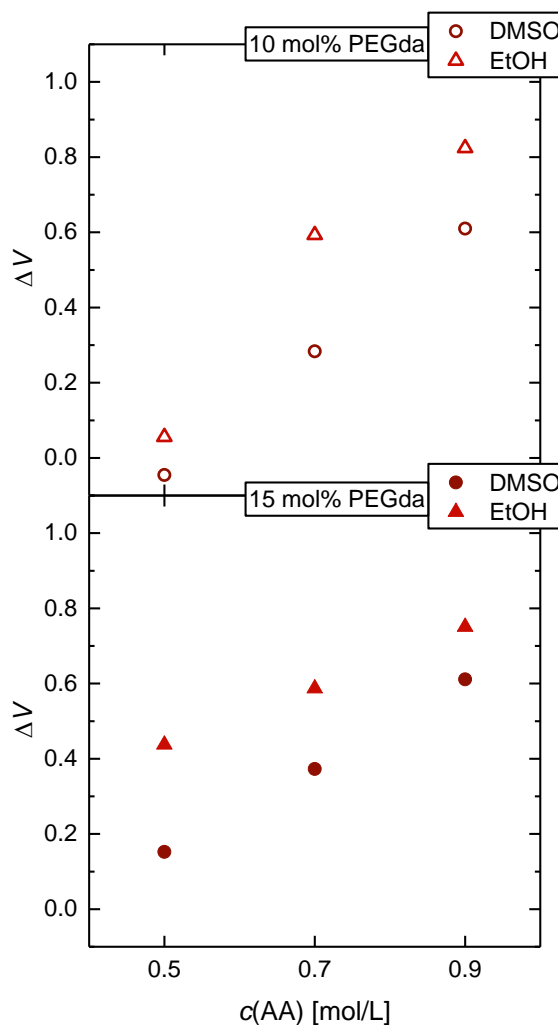
Figure 26. Volume change ΔV after solvent exchange against DMSO ($\circ$) or ethanol (Δ) in dependence on the initial concentration of acrylic acid and the amount of crosslinking agent PEGda in the monomer solution.

A large volume change during swelling changed the structure of the gels. The microstructure of the hydrogels could not be examined by SEM after supercritical drying. This was only possible in their shrunken form.

4.2.2 SEM Images

SEM images of the aerogels obtained from drying with supercritical CO_2 after the solvent exchange from water to DMSO or ethanol were taken to investigate the microstructure of the gels after the swelling measurements. As described above, shrinkage occurred during the solvent exchange. Gels obtained by supercritical drying of the DMSO-swollen samples were used for SEM imaging since the shrinkage was larger with ethanol.

The structure of these aerogels differed from water-swollen composites because of their shrinkage during the solvent exchange. Therefore, freeze-dried water-swollen samples were used to take SEM images as well. It must be considered that a structural change can occur during lyophilization, however, both drying methods give an indication of the "original" microstructure of the composite materials.

The Basotect® matrix is well-recognizable on account of its structure. The SAP is visible as chunks on the surface and in between the matrix structures. The SEM images show a high inhomogeneity within a sample (Figure 27). There are parts of the matrix that are not or just little modified with SAP, whereas other areas contain large amounts of SAP chunks. Therefore, the results discussed in the following should be viewed considering this fact.
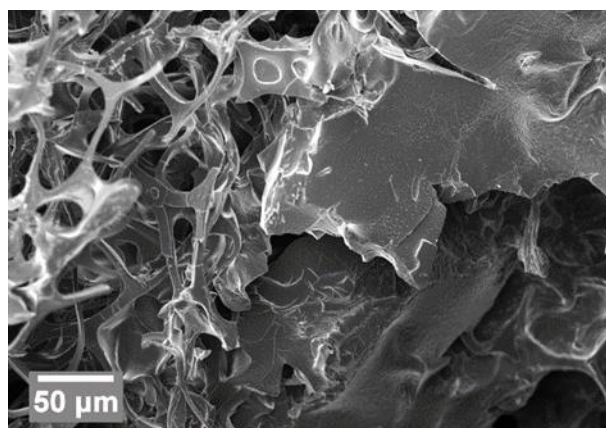
Figure 27. SEM image of a sample with 15 mol% PEGda and 0.9 mol/L acrylic acid in the initial monomer solution.

There were more SAP chunks in between the matrix structures with increasing concentration of acrylic acid in the monomer solution (Figure 28). Furthermore, a higher number of SAP chunks was visible for samples with 15 mol% crosslinking agent PEGda in the monomer solution (Figure 28d–f) in comparison to samples synthesized with 10 mol% PEGda (Figure 28a–c).
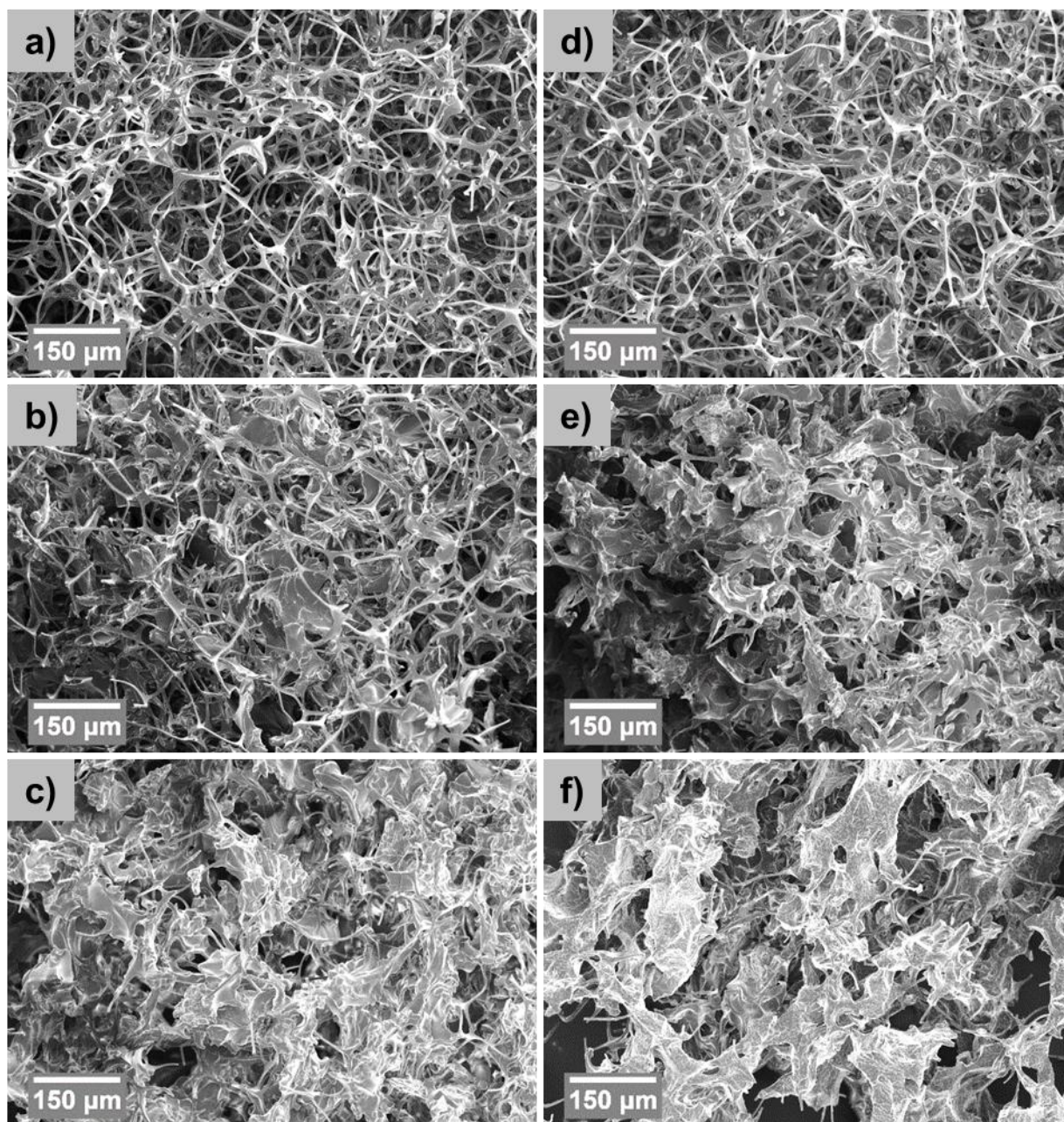
Figure 28. SEM images of SAP-Basotect® composites after swelling in demineralized water and freeze-drying at 300x magnification. The hydrogels were synthesized with 10 mol% PEGda (a–c) or 15 mol% PEGda (d–f) and 0.5 mol/L (a, d), 0.7 mol/L (b, e) or 0.9 mol/L (c, f) acrylic acid in the initial monomer solution.

A difference between the samples dried by lyophilization (Figure 29a–c) or by drying with supercritical CO_2 (Figure 29d–f) cannot be found. The SAP chunk areas seem to be larger for the freeze-dried samples, but it must be taken into account that this impression might be because of the inhomogeneity of the samples. Smaller SAP chunk areas for samples dried with supercritical CO_2 can be explained by shrinkage of the composites during the solvent exchange and consequent shrinkage of the SAP chunks.
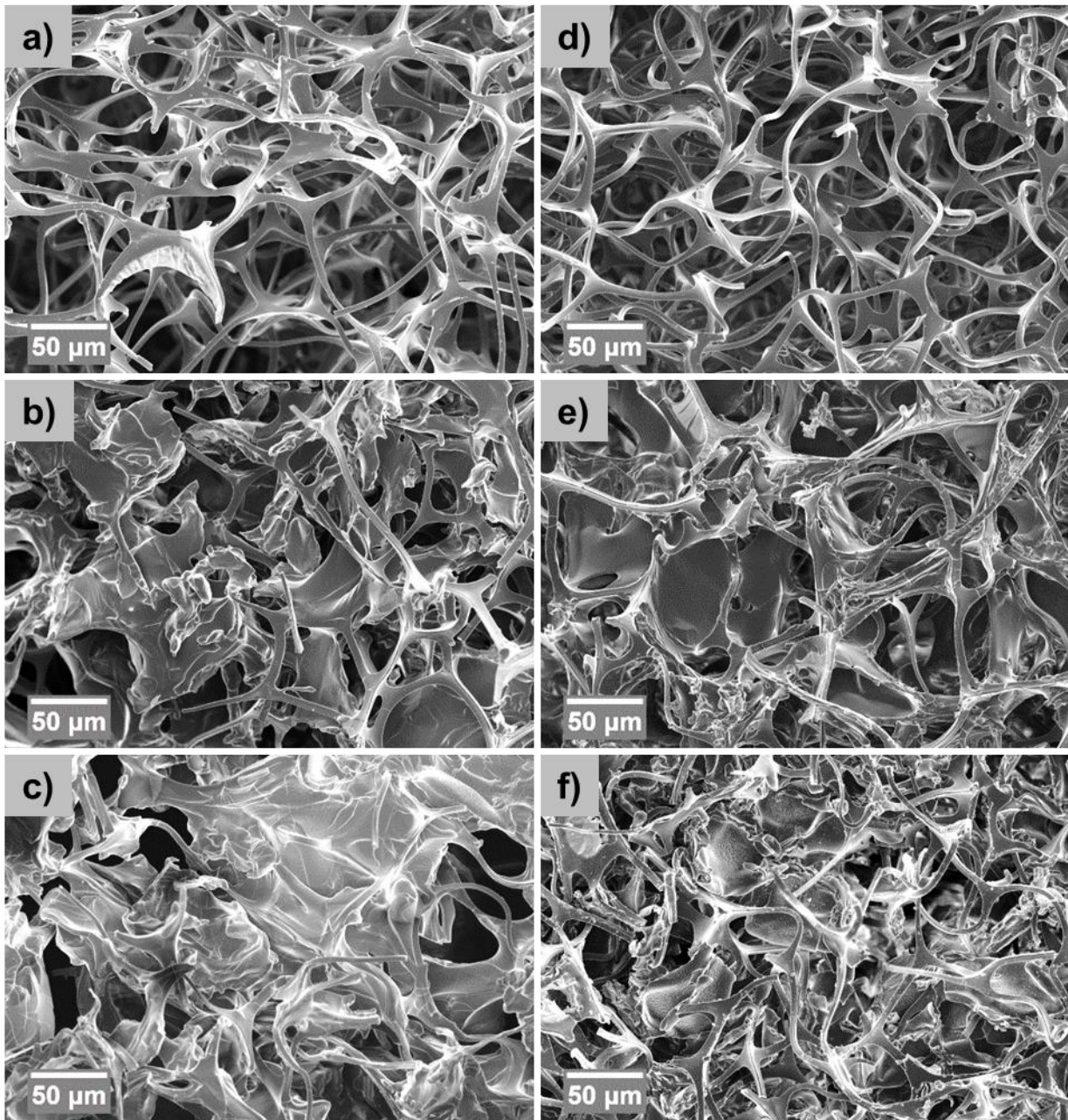
Figure 29. SEM images of SAP-Basotect® composites after swelling in demineralized water and lyophilization (a–c) or solvent exchange with DMSO and drying with super-critical CO_2 (d–f) at 800x magnification. The hydrogels were synthesized with 10 mol% PEGda and 0.5 mol/L (a, d), 0.7 mol/L (b, e) or 0.9 mol/L (c, f) acrylic acid in the initial monomer solution.

SEM images of the surface of the composites at higher magnification showed that the SAP was firmly bound to the Basotect® surface and filled the gaps between its web structure at higher amounts of SAP (Figure 30). The SAP chunks exhibited a rough surface in comparison to the smooth Basotect® surface. Small spherical SAP particles could be found on the SAP chunks for some samples (Figure 30f). These spheres may have been formed from collapsed

PAA during the solvent exchange or supercritical drying, since no spherical particles could be found in composites dried by lyophilization.
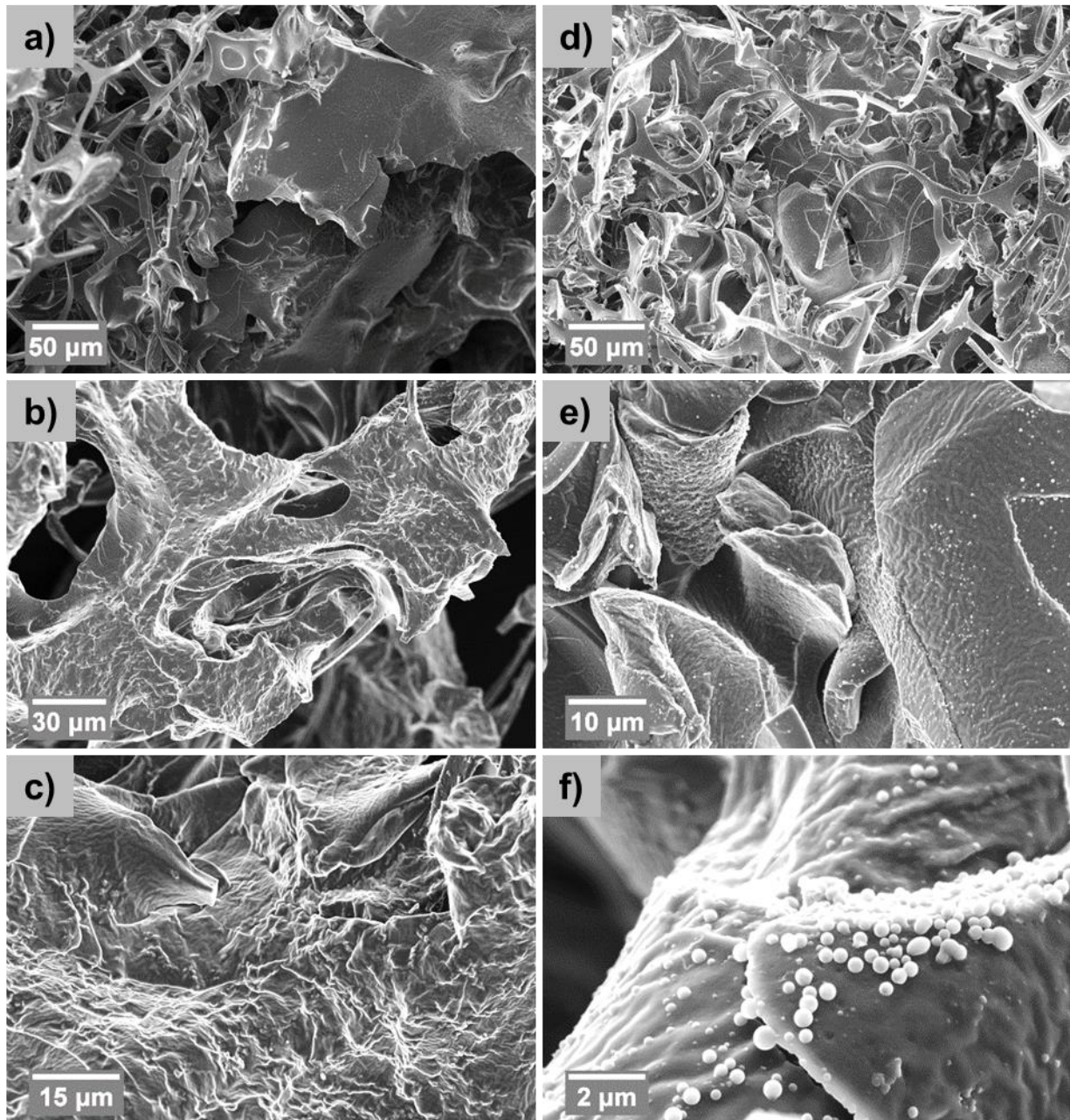
Figure 30. SEM images of SAP-Basotect® composites synthesized from a monomer solution with 0.9 mol/L acrylic acid and 15 mol% PEGda after swelling in demineralized water and lyophilization (a–c) or composites synthesized from a monomer solution with 0.9 mol/L acrylic acid and 10 mol% PEGda after solvent exchange with DMSO and drying with supercritical CO_2 (d–f) at a) 700x, b) 1300x, c) 3000x, d) 800x, e) 4000x and f) 20000x magnification.

4.3 Swelling Behavior of the SAP-Basotect® Composites

The swelling behavior, especially the total amount of water absorption and the swelling kinetics, are important for application of SAPs in hygiene products like diapers or sanitary napkins and wound dressings. Often, a high swelling capacity is correlated with slow swelling progress, whereas a low swelling degree is accompanied by fast swelling kinetics.[100]
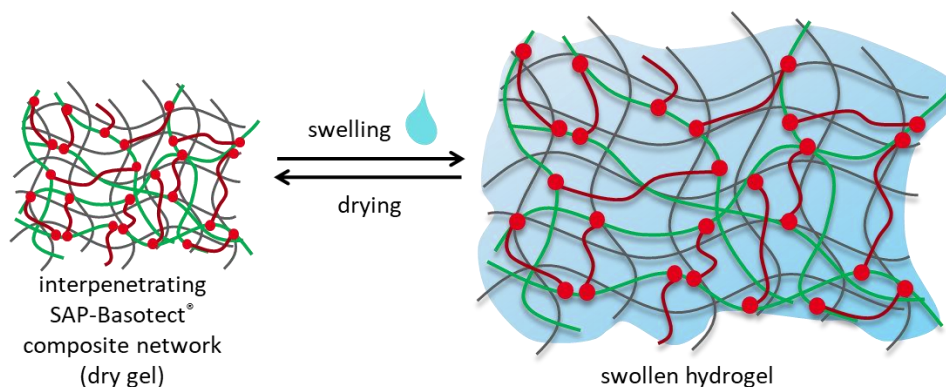
Figure 31. Schematic presentation of swelling experiments with SAP composites.

It was found for the SAP-Basotect® composites that the combination of monomer content, amount of crosslinking agent and the thickness of the matrix have a big influence on the swelling and its kinetics. The hydrogel content and swelling increased with increasing concentration of acrylic acid in the initial monomer solution, but decreased with increasing degree of crosslinking. A decrease of both crosslinking agent and acrylic acid led to an increase of washout effects and to slippery gels. The hydrogel network was destroyed causing the SAP composite sample to fall apart when high swelling occurred. The composites with large swelling capability should be wrapped in fabric to prevent breaking of the samples and entry of impurities into wounds or crumbled parts in diapers.

The influence of the matrix thickness occurred on account of hindered diffusion in thicker samples and lower crosslinking in thin samples with large surface to volume ratios.

Swelling in salt solutions led to decreased swelling relative to swelling in demineralized water. The concentration of the initiator, degree of neutralization and the temperature were kept constant.

The gel-like character increased with increasing concentration of acrylic acid and PEGda in the monomer solution. If small amounts of monomer and crosslinking agent were used, the samples appeared like wet foams instead of gels. The foams got harder and more brittle with increasing amount of acrylic acid and PEGda. The volume of the composites decreased in comparison to the initial volume of Basotect®. These materials showed a large volume expansion during the swelling process.

The SAP was washed out, especially at small initial concentration, or the foam matrix was destroyed by the volume expansion of the SAP composite at high initial monomer concentrations depending on the monomer content used (Table 6).

Low monomer concentrations in the polymerization led to small crosslink densities and short chain lengths of the SAP inside the foam matrix. This correlated with washout effects. Samples should have a high swelling degree and no washing out of the SAP for application of the composites in hygiene products or wound dressings. The hydrogels should preferably not disintegrate. The disadvantages of crumbled hydrogels can be counteracted by covering the SAP composite. Therefore, higher amounts of both acrylic acid and crosslinking agent are favorable.

The synthesized composites can be classified into five types:

I.   The monomer concentration was small; almost all hydrogel is washed out instantly. The properties including water-uptake do not differ from Basotect®.

II. The polymer chains are short and slightly crosslinked. This leads to slippery gels that lose weight during the swelling procedure.

III. The SAP was crosslinked in the Basotect® matrix; there is no visible out-washing in the beginning. The volume stress while swelling tears the matrix and the SAP apart. This can be accompanied by out-washing of short or insufficiently crosslinked SAP chains. Usually, these samples disintegrate into layers before they completely fall apart.

IV. The SAP was firmly crosslinked in the Basotect® matrix; there was no visible washing out. Both the foam matrix and the SAP remain stable despite the volume expansion on swelling.

V.   The SAP was firmly crosslinked in the Basotect® matrix; there was no visible washing out. The foam matrix and the SAP get brittle by the volume stress on swelling. Usually, these samples break in the middle.

Table 6. Appearance and swelling properties of the synthesized SAP-Basotect® composites for various amounts of acrylic acid and PEGda in the monomer solution. Thickness of the Basotect® foam: d = 0.5 cm. The swelling measurements were implemented in demineralized water.

		Acrylic acid concentration [mol/L]				
		0.5	**0.6**	**0.7**	**0.8**	**0.9**
PEGda concentration [mol%]	**5**	Like unmodified Basotect®, no hydrogel (Type I)	Like unmodified Basotect®, no hydrogel (Type I)	Like unmodified Basotect®, no hydrogel (Type I)	Slippery hydrogel, out-washing (Type II)	Slippery hydrogel, out-washing (Type II)
	10	Almost like Basotect®, slippery, out-washing (Type I/II)	Slippery hydrogel (Type II/III)	Hydrogel, disintegrated (Type III)	Hydrogel, disintegrated (Type III)	Hydrogel, crumbled (Type V)
	15	Hydrogel (Type IV)	Hydrogel (Type IV)	Hydrogel, crumbled (Type V)	Hydrogel, crumbled (Type V)	Hydrogel, crumbled (Type V)

Type I composites were obtained at small concentrations of acrylic acid and PEGda in the initial monomer solution. Type II composites were synthesized with an increased concentration of acrylic acid. A further increase of the acrylic acid concentration led to Type III composites, and Type IV and Type V composites were obtained by increased crosslinking (increased concentration of PEGda).

4.3.1 Characterization of the SAP-Basotect® Composites

The swelling degree Q_{real} is defined as ratio of the swollen gel m_{gel} and the dry mass of the gel $m_{gel,dry}$ (Equation 16).[103] The weight of the gel is the sum of the mass of the original dry Basotect® sample m_{Bas}, the dry mass of the superabsorbent polymer m_{SAP} and the mass of absorbed solvent $m_{s,gel}$ upon swelling SAP-Basotect® composites.

$$Q_{real} = \frac{m_{gel}}{m_{gel,dry}} = \frac{m_{Bas} + m_{SAP} + m_{s,gel}}{m_{Bas} + m_{SAP}} \tag{16}$$

Usually, it is challenging to measure Q_{real} because solvent is also trapped in the interstitial volume between the swollen gel particles and in the pores of the Basotect® matrix. The interstitial solvent is taken into account in Equation 17 with its mass $m_{s,int}$. Q therefore overestimates the real swelling degree Q_{real}.[103]

$$Q = \frac{m_{gel} + m_{s,int.}}{m_{gel,dry}} = \frac{m_{Bas} + m_{SAP} + m_{s,gel} + m_{s,int}}{m_{Bas} + m_{SAP}} \tag{17}$$

The solvent from the interstitial volume can be removed by applying vacuum to the swollen composite. It is difficult to identify whether Q_{vac} is corresponding to Q_{real}, because it is possible to remove solvent bound to the gel during the vacuum treatment, or not to remove the whole interstitial solvent (Equation 18). The weight of the swollen gel after vacuum treatment $m_{gel,vac}$ is the sum of the weight of the dry SAP-Basotect® composite and the remaining solvent m_{s^*}.

$$Q_{vac} = \frac{m_{gel,vac}}{m_{gel,dry}} = \frac{m_{Bas} + m_{SAP} + m_{s^*}}{m_{Bas} + m_{SAP}} \tag{18}$$

The ratio g of the swelling degree after and before the vacuum treatment is an indication for the water bound to the hydrogel (Equation 19). The larger g is the higher is the gel content.

$$g = \frac{Q_{vac}}{Q} \tag{19}$$

The product P of the swelling degree Q with the gain in weight G_w (cf. Chapter 4.1.3, Equation 13) is a measure for the swelling and modification with hydrogel of the original Basotect® sample (Equation 20). It describes the swelling of the composite relative to the original Basotect® sample. This is an important parameter since the volume in which the superabsorbent polymer can be formed is given by the mass of the Basotect® sample used. P normalizes the swelling on the initial volume filled with monomer solution.

$$P = Q \cdot G_w = \frac{m_{Bas} + m_{SAP} + m_{s,gel} + m_{s,int.}}{m_{Bas}} \tag{20}$$

4.3.2 Influences of the Concentrations of Acrylic Acid and Crosslinking Agent on the Swelling

The swelling of the SAP-Basotect® composites generally increased with increasing amount of acrylic acid in the monomer solution (Table 6). However, this could not be observed if the swelling degree Q as ratio of wet and dry composite mass was analyzed (Figure 32).
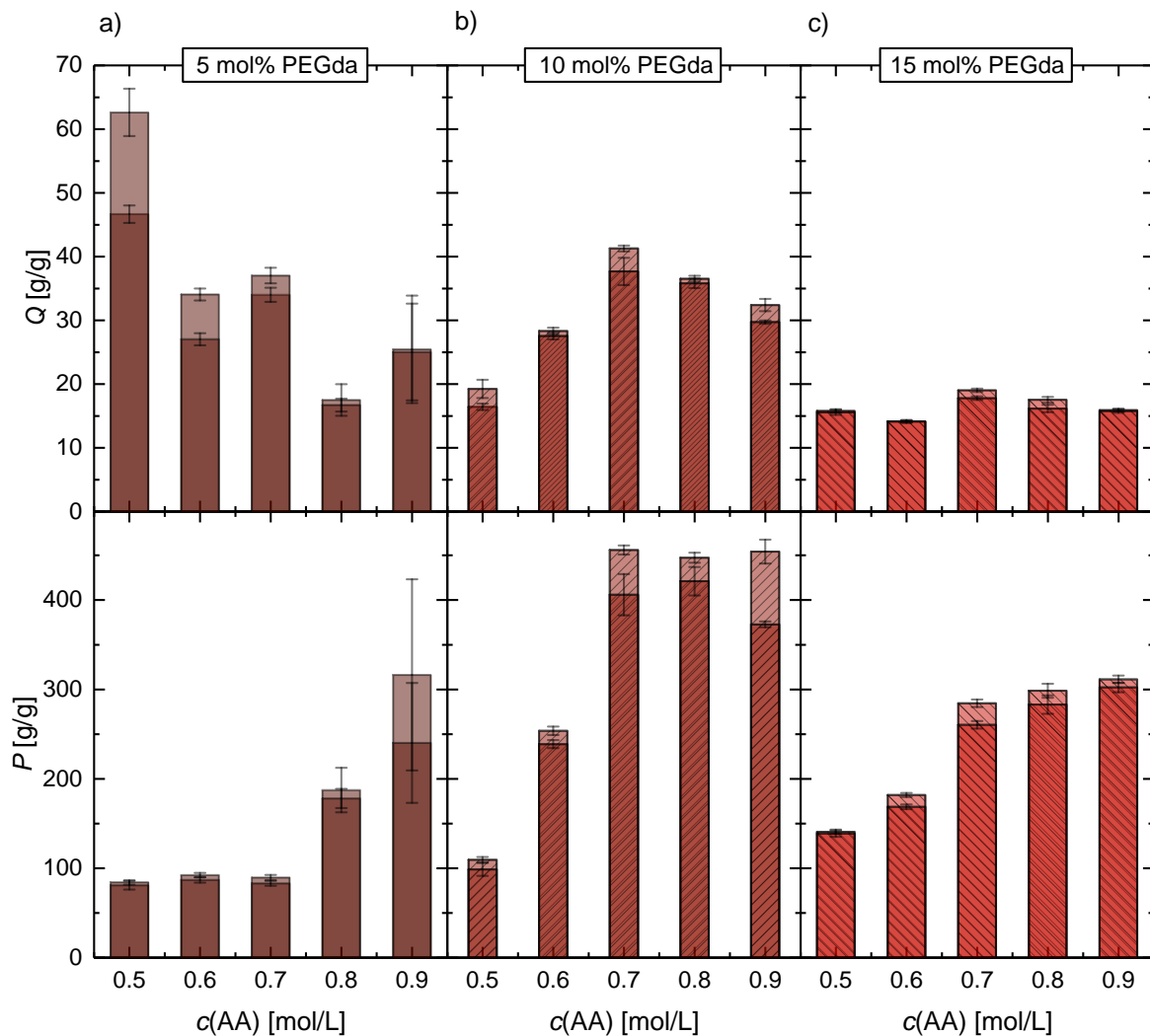
Figure 32. *Q* and *P* for 5, 10 and 15 mol% PEGda in the initial monomer solution at a Basotect® thickness of *d* = 0.5 cm.

The swelling degree *Q* was large at little or no modification of Basotect® at small concentrations of acrylic acid and crosslinking agent in the initial monomer solution (Figure 32a). The reason for this is that unmodified Basotect® has a low density of about 9 g/L[97] and consequently a small mass and a large water uptake on account of its large free volume and hydrophilicity. An increase in the concentration of acrylic acid led to an increased gel content and swelling. The swelling degree *Q* as ratio of wet mass and dry mass decreased because the dry mass of the composite was higher than the dry mass of pure Basotect®. In case of strong swelling with high volume expansion and associated weight gain relative to the dry mass, there was an increase or stagnation of the swelling degree *Q* (Figure 32b–c). Therefore, no uniform swelling behavior *Q* is found.

The gain in weight G_w increased with increasing amount of acrylic acid in the initial monomer solution, which led to a bigger dry mass $m_{gel,dry}$ and to a bigger mass of the swollen composite m_{gel}. The swelling degree *Q* is not a function of the concentration of acrylic acid $f(c(AA))$

because both numerator and denominator of *Q* are linear dependent on the amount of acrylic acid used in the monomer solution (Equation 21).

$$m_{\text{gel}} = f(c(\text{AA})) \atop m_{\text{gel,dry}} = f(c(\text{AA}))} \Rightarrow Q = \frac{m_{\text{gel}}}{m_{\text{gel,dry}}} \neq f(c(\text{AA})) \tag{21}$$

   The swelling of the composite in dependence on the mass of the original Basotect® sample *P* is more suitable to describe the swelling behavior of the gel composites since it is not only a measure of swelling, but also a measure for the amount of hydrogel (Figure 32). An increase of the concentration of acrylic acid in the monomer solution usually led to an increase of *P*. An increase in *P* was not observed for small concentrations of crosslinking agent until a monomer concentration of at least 0.7–0.8 mol/L was reached (Figure 32a). This is because the polymer chains were short and insufficiently crosslinked at low monomer concentrations with a small amount of crosslinking agent. Therefore, high washout effects occurred during washing and swelling experiments. This fits to the observations made during analysis of the gain in weight. The error bars are based on multiple weighing when the swelling equilibrium was reached. The experimental errors were large especially for $c(\text{AA}) = 0.8$ mol/L and 0.9 mol/L with 5 mol% PEGda (Figure 32a). The reason for this is that the composites were slippery and SAP was washed out of the matrix (Table 6). The swelling equilibrium could not be defined but was estimated from an average over a period of time. The deviations were larger at increased concentration of acrylic acid for samples synthesized with 10 mol% PEGda in the initial monomer solution (Figure 32b). These deviations resulted from large swelling accompanied by large volume stress and disintegration of the composites with subsequent out-washing of polymer chains. *P* increased from 0.5 mol/L to 0.7 mol/L acrylic acid and then remained constant if 10 mol% PEGda were used. The reason for this is that the swelling was hindered with increased degree of crosslinking. The number of crosslinks with regard to acrylic acid was constant, but the number of crosslinks with regard to the mass of Basotect® increased with increasing concentration of acrylic acid in the initial monomer solution (Figure 33). The stability of the gel increased, which hindered the volume expansion of the composite and thus the swelling of the gel.
   Samples synthesized with 15 mol% PEGda exhibited an increased swelling degree with increasing amount of acrylic acid in the initial monomer solution (Figure 32c, Figure 33). The larger crosslink density resulted in an increased stability of the sample shape. This led to small experimental errors and a higher reproducibility. Even samples that broke during the swelling measurements showed no visible washout effects. *P* increased with increasing concentration of acrylic acid for all samples synthesized with 15 mol% PEGda. The differences were larger at smaller acrylic acid concentrations in the initial monomer solution. Again, the reason for this swelling behavior is the increased swelling with increased amount of SAP accompanied with stronger crosslinking and deductive decreased swelling. Therefore, the effect of increased concentration of acrylic acid outweighed the effect of the increased crosslink density at 15 mol% PEGda in the considered range of concentrations.

Composites synthesized from 5 mol% of PEGda exhibited a low swelling relative to the samples with higher amounts of crosslinking agent. This resulted from washing out of the polymer. The highest swelling was reached with 10 mol% PEGda. The SAP was crosslinked strongly enough to prevent washing out, and not too strongly crosslinked to hinder the swelling. The latter is the case when 15 mol% PEGda were used.
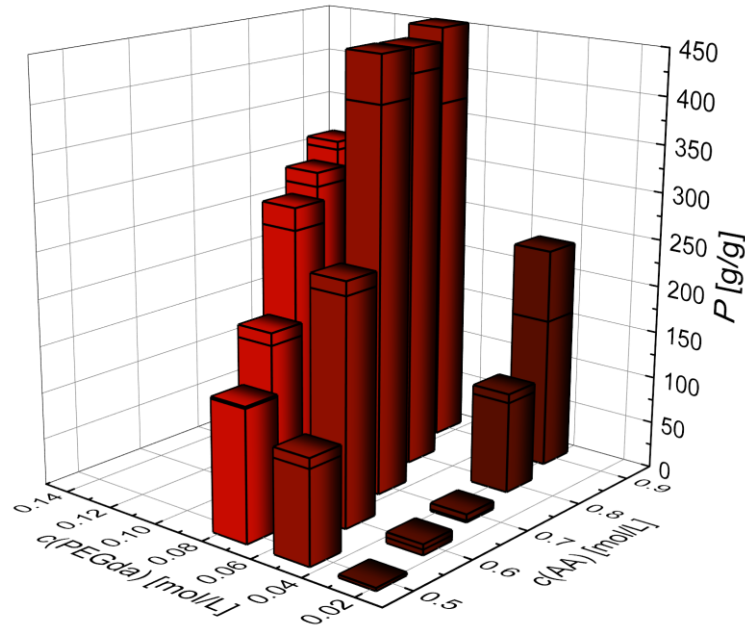
Figure 33. *P* in dependence on the concentrations of acrylic acid and PEGda for a Basotect® thickness of *d* = 0.5 cm.

The ratio *g* of the weight of the swollen composite materials after vacuum treatment and before vacuum treatment was small for samples with a swelling behavior similar to Basotect® and approximately 1 for composites with high gel content (Figure 34). It increased with increasing amount of acrylic acid.
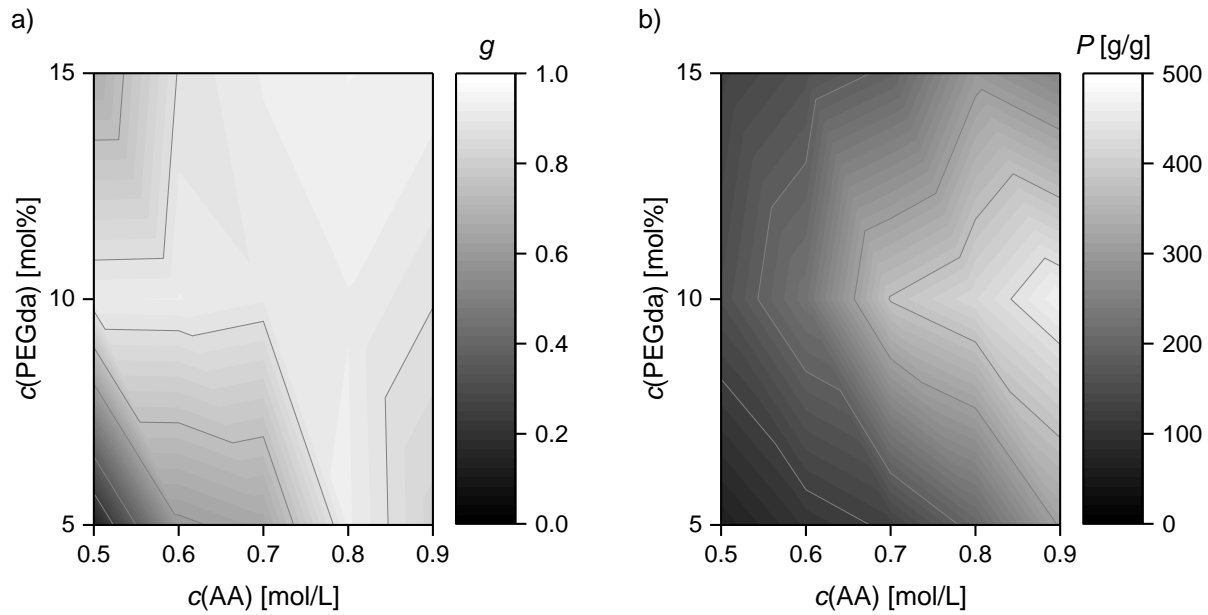
Figure 34. a) Ratio *g*, amount of acrylic acid and PEGda for a Basotect® thickness of *d* = 1 cm. The contour plot b) of the swelling *P* in dependence on the concentrations of acrylic acid and PEGda is shown for comparison.

4.3.3 Influence of the Thickness of the Basotect® Samples on Swelling

The Basotect® matrix was cut by hand; therefore, a certain variation in the size of the foam was unavoidable. The relative differences were large for small samples. SAPs made from samples with a thickness from 0.2 cm to 0.5 cm were having a large spread of properties. The thickness of the sample then had a large impact on the swelling behavior. Samples with low thicknesses, synthesized under same reaction conditions, swelled with volume extension and shrank while drying, or did not change their volume at all.

The main reasons for the dependence of the swelling behavior on the sample thickness are surface effects. The physical interpenetrating network of Basotect® and the SAP can be formed more easily if there is more Basotect® (higher inner surface) to interact with. The inner Basotect® surface increases with increasing density and thickness. A thicker sample can hold the monomer solution better before the polymerization because of the increased number of Basotect® filaments. At constant density, thicker samples offer the opportunity for stronger crosslinking of the SAP in the matrix and less washout effects. The Basotect® filaments on the inside of the foam are more suitable for strong crosslinking than the filaments on the outer surface since they have no or less free ends. The ratio of surface and volume changes by changing the sample thickness. The Basotect® samples are cuboids with a square base area with the constant edge length *a* and the thickness *d*. The volume *V* and the surface area *A* of these samples are given in Equation 22–23.

$$V = a^2 \cdot d \tag{22}$$

$$A = 2 \cdot (a^2 + 2 \cdot a \cdot d) \tag{23}$$

The variation of the thickness d by a factor x (Equation 24–25) changes the volume of the sample by the factor x, whereas the change of the surface area depends on x, on the length and width a and the thickness d (Equation 26–27).

$$V_x = a^2 \cdot d \cdot x \tag{24}$$

$$A_x = 2 \cdot (a^2 + 2 \cdot a \cdot d \cdot x) \tag{25}$$

$$\frac{V_x}{V} = x \tag{26}$$

$$\frac{A_x}{A} = \frac{a + 2 \cdot d \cdot x}{a + 2 \cdot d} \tag{27}$$

The maximum increase x of the surface area is achieved if d is large relative to a. If d is much smaller than a, there is (almost) no increase of the surface (Equation 28).

$$\lim_{d \gg a} \frac{A_x}{A} = \frac{2 \cdot d \cdot x}{2 \cdot d} = x; \quad \lim_{d \ll a} \frac{A_x}{A} = 1 \tag{28}$$

The edge length is larger than the thickness in the Basotect® samples. Consequently, the increase of the surface area with increasing thickness is smaller than the increase of the volume. The ratio of surface and volume decreases with increasing factor x (Equation 29).

$$\frac{A_x}{A} \bigg/ \frac{V_x}{V} = \frac{a + 2 \cdot d \cdot x}{(a + 2 \cdot d) \cdot x} \tag{29}$$

As a result, a small change in the thickness of the matrix sample may have a large impact on the ratio of surface and volume. It is difficult to bind the monomer solution inside the matrix before the polymerization and surface effects like washing out of the SAP during swelling have a big influence for composites with large surface relative to their volume (low thickness). These effects become less important for thicker samples (smaller difference between a and d) on account of their larger volume and corresponding mass. In addition, the density distribution of Basotect® is not homogenous in micrometer range. Therefore, small changes in density can lead to large differences in the number of filaments for solvent stabilization and consequently in the number and quality of physical crosslinks of the SAP in the matrix at a low sample thickness. Results for small thickness show a large scattering.

The sample thickness affected the rate of sample impregnation with the monomer solution, the swelling kinetics and the stability of the matrix. The thicker the sample was, the longer it took a fluid to fully wet the foam. It was more difficult for the swelling medium during swelling experiments to get inside the composite since the diffusion was hindered by the hydrogel. The time for reaching the swelling equilibrium was longer. The SAP was fixed inside the matrix and caused a volume expansion while the matrix and the crosslinking agent counteracted

this. Depending on the "strength" of the interpenetration network (thickness, amount of crosslinking agent and SAP), the matrix was either stretched or filaments broke. The strength of the network usually prevailed over the volume expansion for thick samples. Therefore, like washing-out, disintegration was a surface effect. The surface area grew with increasing disintegration at the surface, which led to disintegration of the inner areas as well.

There was almost no increase of the swelling P with increasing amount of acrylic acid in the initial monomer solution for small thicknesses ($d < 0.5$ cm; Figure 35a). P was small relative to the swelling of thicker samples because of to the effects described above. The scattering between the different composites synthesized under the same reaction conditions was large. The proportion of SAP fixed in the matrix varied for all samples. This resulted in various values for P. The swelling was increased and depended on the amounts of acrylic acid in the initial monomer solution and crosslink density for thicker matrices. Surface effects became less important. This trend applied not for all samples since sometimes the volume expansion associated with the swelling predominated over the stability of the network (Figure 35b). This led to disintegration of the composites and was often accompanied by an increased P because the additional space allowed the hydrogel to swell more. The swelling and impregnation with the monomer solution during the synthesis was hindered by decreased diffusion inside the sample if matrices of 3 cm thickness were used. This led to larger variations between the swelling behaviors of the composites. This effect was already shown by investigation of the gain in weight G_w (Chapter 4.1.3, Figure 24).
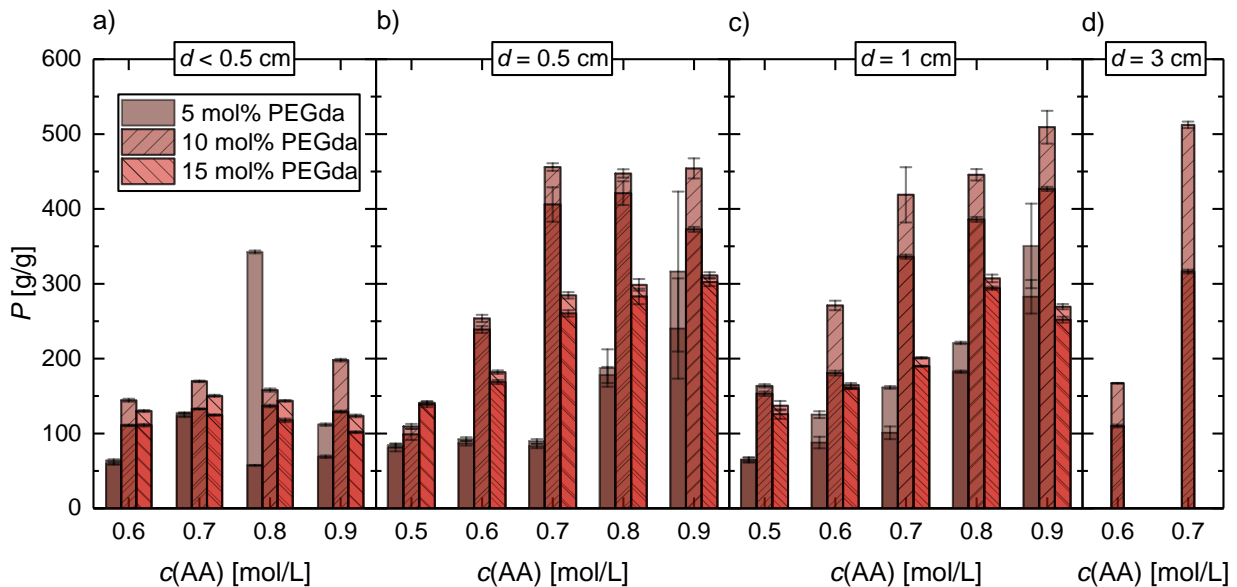
Figure 35. *P* in dependence on the thickness *d* of the Basotect® sample and the concentration of acrylic acid *c*(AA) in the initial monomer solution for different amounts of PEGda as crosslinking agent. a) *d* < 0.5 cm; b) *d* = 0.5 cm, c) *d* = 1 cm and d) *d* = 3 cm. Average of two determinations.

The thickness-dependent swelling of the SAP-Basotect® composites synthesized with 5–15 mol% PEGda and a matrix thickness between $d < 0.5$ cm and $d = 1$ cm are shown as contour plot in Figure 36. This allows assessing the overall behavior.
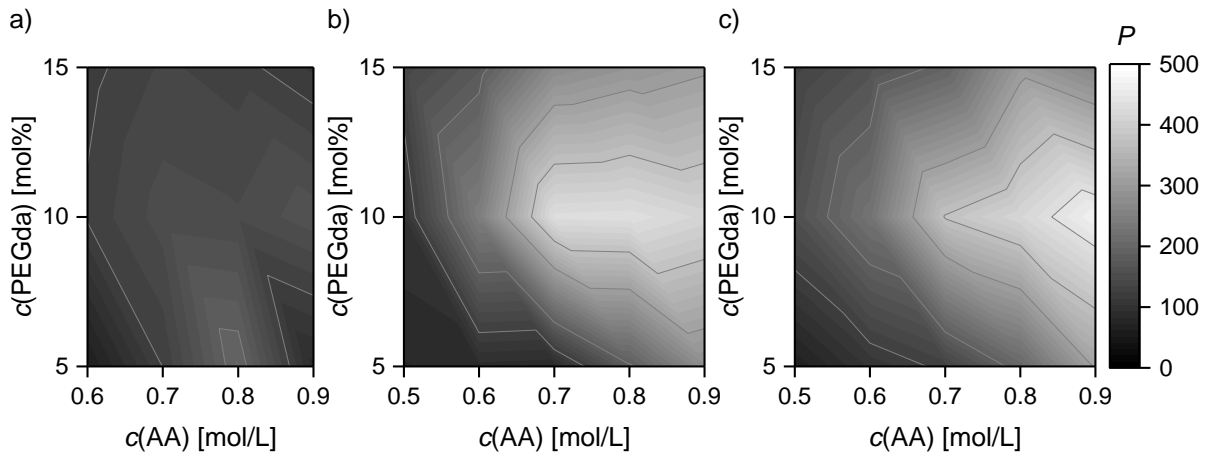
Figure 36. Contour plots of the swelling P of composites with a matrix thickness of a) $d < 0.5$ cm, b) $d = 0.5$ cm and c) $d = 1$ cm in dependence on the concentrations of acrylic acid and crosslinking agent PEGda in the initial monomer solution.

4.3.4 Influence of the Salt Concentration on the Swelling Behavior

The influence of salts on the swelling behavior of the SAP-Basotect® composite gels was investigated by swelling in differently concentrated aqueous sodium chloride solutions. An increase of sodium chloride in the swelling solution led to decreased swelling (Figure 37). A concentration of $1 \cdot 10^{-4}$ mol/L sodium chloride leads to a decrease of the water uptake in comparison to swelling in demineralized water. As with swelling in demineralized water, the swelling in saline solution of the composites made from 0.9 mol/L acrylic acid in the monomer solution was higher than the swelling of the composites made from 0.6 mol/L acrylic acid. The swelling P of samples made from 0.6 mol/L acrylic acid was about 60 % of the value of the 0.9 mol/L acrylic acid composites for all salt concentrations. The factor for ionic sensitivity f (cf. Chapter 1.2.2, Equation 1) increased with increasing salt concentration. The factor f was smaller at low salt concentrations for hydrogels synthesized with an acrylic acid concentration of 0.6 mol/L than for composites made with 0.9 mol/L acrylic acid. The values of f converged for both acrylic acid concentrations at higher salt concentrations.

The reason for the decreased swelling in saline solution and increased factor for ionic sensitivity f is the osmotic pressure of the SAP gel, which is the main driving force of the swelling. The osmotic pressure caused by the large concentration of ions in the dry gel is decreased by swelling in water. The ion concentration in the gel was less reduced by swelling in saline solution, and therefore the swelling decreased.[78] The sodium chloride ions shield the charges in the SAP so that less swelling was needed to compensate the large ion concentration.
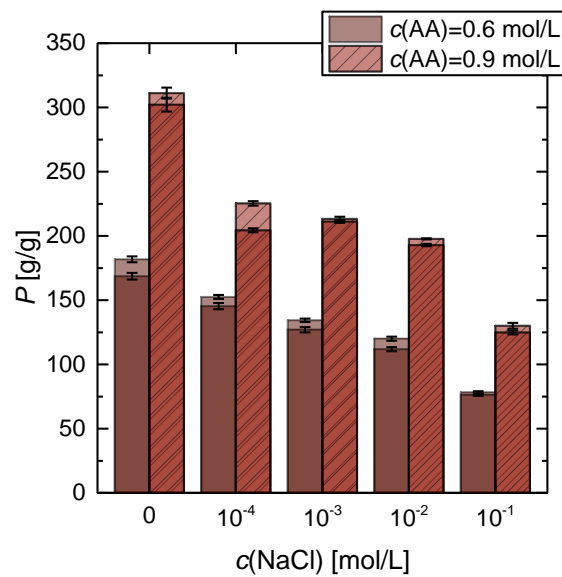
Figure 37. *P* in dependence on the salt concentration in the swelling solution for composites synthesized with 0.6 mol/L and 0.9 mol/L acrylic acid in the initial monomer solution. The amount of crosslinking agent was 15 mol% PEGda with regards to the acrylic acid concentration, the neutralization degree was 80 % and the Basotect® thickness was *d* = 0.5 cm. Average of two determinations.
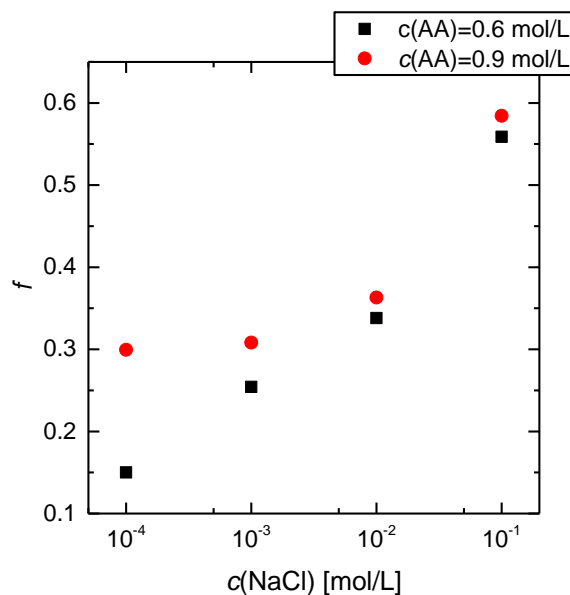
Figure 38. Factor for ionic sensitivity *f* in dependence on the salt concentration in the swelling solution for composites synthesized with 0.6 mol/L and 0.9 mol/L acrylic acid in the initial monomer solution. The amount of crosslinking agent was 15 mol% PEGda with regards to the acrylic acid concentration, the neutralization degree was 80 % and the Basotect® thickness was *d* = 0.5 cm.

Many applications for SAPs like sanitary napkins, diapers or wound dressings involve the absorption of water containing salts. For these applications, the hydrogel content in the Basotect® composites should be increased to ensure a high absorption. A larger amount of acrylic

acid and a larger degree of neutralization could be used in the monomer solution for an adequate absorption of salt-containing liquids.

4.3.5 Repetition of Swelling Measurements

The swelling measurements in demineralized water were repeated for some samples to investigate the influence of the swelling and drying procedures. The second cycle differed from the first run (Figure 39). The structure of the sample used in the second run differed from the structure at the start of the first swelling. The samples used for the repetition experiments had an original thickness of 0.5 cm. The concentration of acrylic acid in the monomer solution was either 0.5 mol/L or 0.9 mol/L and the amount of crosslinking agent was either 5 mol% or 15 mol% to cover a large range. During the first swelling cycle, the highest swelling *P* was obtained with 0.9 mol/L acrylic acid and 5 mol% PEGda, but the gel was washed out with increasing swelling time (Figure 39, cycle 1). The highest constant swelling was achieved with the samples with the largest monomer concentrations (0.9 mol/L acrylic acid and 15 mol% PEGda). No gels were obtained for samples with 0.5 mol/L acrylic acid and 5 mol% PEGda in the initial monomer solution. The swelling behavior was similar to pure Basotect®. The swelling behavior of a hydrogel was present but not strong in samples synthesized with 0.5 mol/L acrylic acid and 15 mol% PEGda in the initial monomer solution.

In the second swelling cycle, the samples made from 0.9 mol/L acrylic acid and 15 mol% PEGda reached the equilibrium swelling faster than in the first run (5 h compared to more than 3 days). The reason for this was the disintegration of the composites during the first swelling. It was easier for the swelling medium to wet the SAP in the second run. The swelling degree was in the same range for both the second and the first swelling cycle, which indicated scarcely any loss of the SAP. In fact, there was a mass loss of 21 % after the first swelling, but this loss in mass seemed to be insignificant for the swelling degree. The swelling *P* in the second cycle is 22 % lower than in the first run for the samples made with 0.5 mol/L acrylic acid and 15 mol% PEGda in the initial monomer solution. This is because SAP was washed out during the first swelling measurement resulting in a decrease of its dry weight. Again, the loss in weight of 45 % was larger than the decrease of the swelling *P*.

High washout effects occurred for samples made from 0.9 mol/L acrylic acid and 5 mol% PEGda in the initial monomer solution. This was not surprising since they could be observed during the first swelling measurement. The loss in weight after the first swelling cycle was about 86 %, so that almost pure Basotect® remained. The swelling fell to its minimum.

In the third swelling cycle, there was no weight loss of the samples in comparison to the weight after the second swelling cycle except for the most concentrated sample (34 % loss compared to the first run, 17 % loss compared to the second run). This loss in weight is not surprising since the samples were fully disintegrated so that some gel was lost. The swelling *P* was identical to that of the second run.
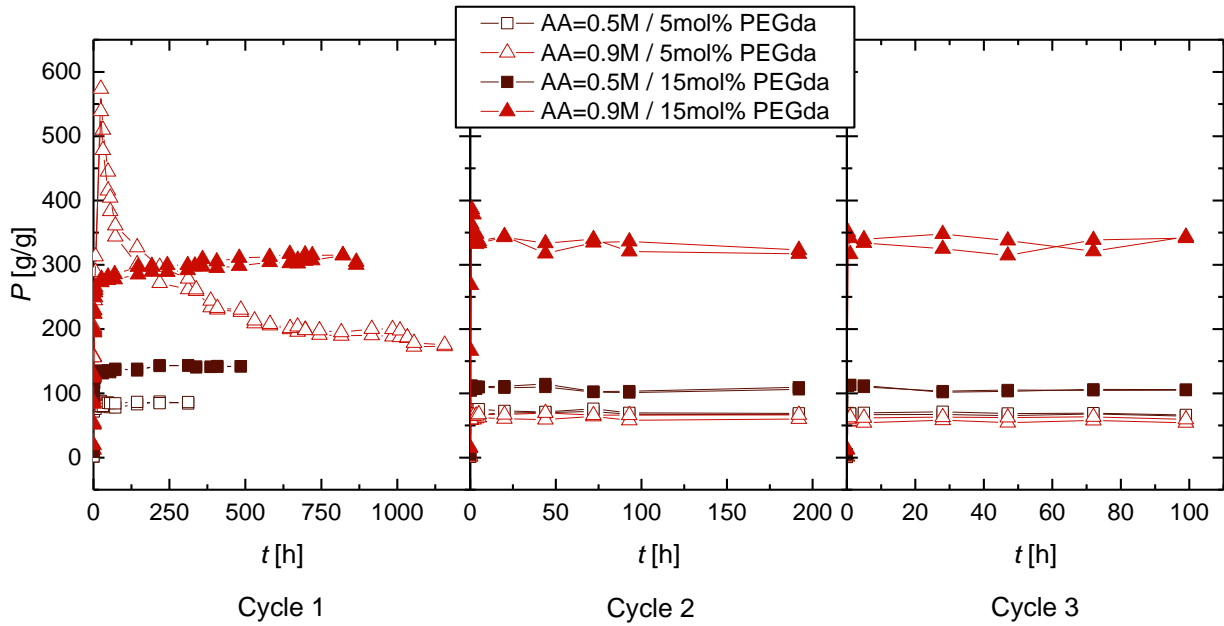
Figure 39. Swelling *P* in dependence on the swelling time for the first three swelling cycles. The original matrix thickness was *d* = 0.5 cm. The lines are used for reasons of clarity only.

4.3.6 Sol and Gel Fraction

The sol content of the hydrogel can be extracted by swelling of the polymer composite in a swelling medium. Only the SAP gel can be affected by washing out of polymer. Therefore, the amount of sol content w_{sol} can be defined as ratio of the SAP dry mass difference before and after swelling ($m_{SAP,bs}-m_{SAP,as}$) and the SAP dry mass before the swelling $m_{SAP,bs}$ (Equation 30).

The gel content w_{gel} of the polymer composites contains the crosslinked polymer chains tightly bound in the interpenetrating network. The sol content w_{sol} and the gel content w_{gel} add up to 100 %. High gel content and small sol content are preferred since washing out has negative effects on the composite properties for many applications.

$$w_{sol} = \frac{m_{SAP,bs} - m_{SAP,as}}{m_{SAP,bs}} = 1 - \frac{m_{SAP,as}}{m_{SAP,bs}} = 1 - w_{gel} \tag{30}$$

Low sol content is crucial for applications with permanent skin contact since polymer chains that are insufficiently crosslinked must not remain on the skin or in an open wound. The sol content decreased with increasing monomer concentration (Figure 40). The degree of cross-linking had a large influence on the sol content (Figure 40a). The sol content was almost 100 % at low amounts of crosslinking agent in the initial monomer solution with small and large concentrations of acrylic. The thickness of the Basotect® matrix seemed to have less influence on the sol and gel content (Figure 40b).
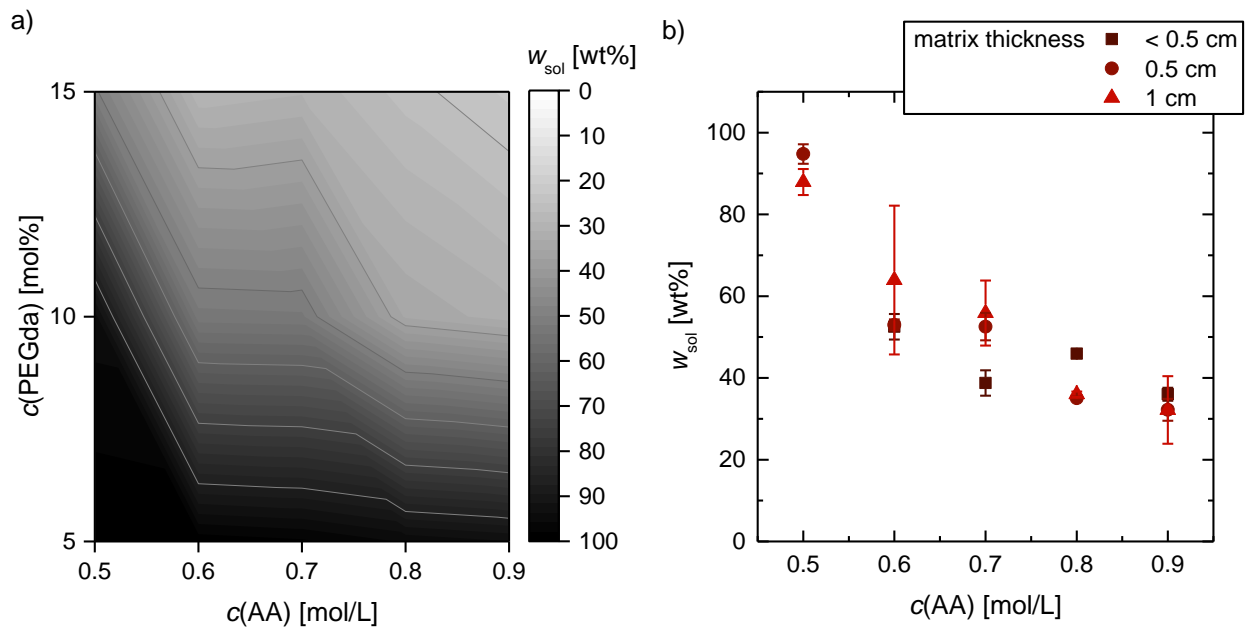
Figure 40. Sol fraction w_{sol} in dependence on the concentration of acrylic acid in the initial monomer solution and a) the amount of crosslinking agent PEGda at a thickness of 0.5 cm or b) the thickness of the matrix with 10 mol% PEGda.

The sol content decreased with increasing modification and consequently with increasing gain in weight G_w (Figure 41). As described above, the sol content of composites slightly cross-linked (5 mol% PEGda) was large in comparison to strongly crosslinked samples at the same gain in weight since short and linear polymer chains were more easily removed from the matrix than crosslinked polymers.
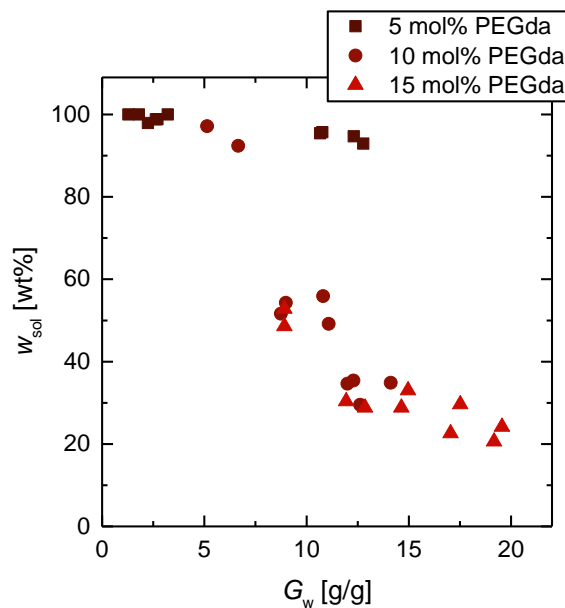
Figure 41. Sol fraction w_{sol} in dependence on the gain in weight G_w for composites synthesized with 5, 10 or 15 mol% PEGda and a concentration of acrylic acid between 0.5 mol/L and 0.9 mol/L at a matrix thickness of d = 0.5 cm.

Composites with high gel content were obtained from large concentrations of monomer and crosslinking agent in the initial monomer solution.

4.3.7 Kinetics of the Swelling Measurements

The swelling kinetics were investigated by applying the combined diffusion-relaxation model.[99] This model takes the Fickian diffusion of the water molecules into the SAP as well as the non-Fickian relaxation of the hydrated polymer chains into account. In this work, the swelling measurements were carried out under ambient and varying conditions of the lab. The temperature can have an influence on the swelling. The deviations caused by the weighing process were considered to be larger than the temperature-induced errors.

The water was exchanged after measuring the weight regardless of the time passed since the last exchange. The swelling of the SAP-Basotect® composites is a complex process, since both swelling of the superabsorbent polymer and trapping of water in the interstitial volume of the Basotect® matrix must be considered. In the following, it is assumed that the composite is a material with a swelling behavior solely controlled by diffusion and relaxation so that the combined diffusion-relaxation model can be applied. Furthermore, it must be considered that the diffusion-relaxation model was investigated for spherical particles[105] and not for IPNs of undefined shape. This was also neglected.

The kinetic fitting is possible for samples that show increased swelling at increasing swelling time and reach a maximum equilibrium swelling. Fitting with the combined diffusion-relaxation model is not possible for composites if washout effects have a major impact on the swelling. Large washing out effects occurred at low concentrations of crosslinking agent (Figure 42a). Furthermore, there has to be enough data in the fitting area for proper modelling. It took days or weeks for more crosslinked samples to reach the maximum (equilibrium) swelling depending on the monomer concentration (Figure 42b–c). The obtained time-dependent swelling curves were more suitable for investigation of the swelling kinetics. The influence of increased amount of PEGda with regard to Basotect® led to decreased swelling at larger concentrations of acrylic acid in the initial monomer solution for composites synthesized with 10 mol% PEGda (cf. Chapter 4.3.2). Therefore, the combined diffusion-relaxation model was applied to the samples synthesized with 15 mol% PEGda.
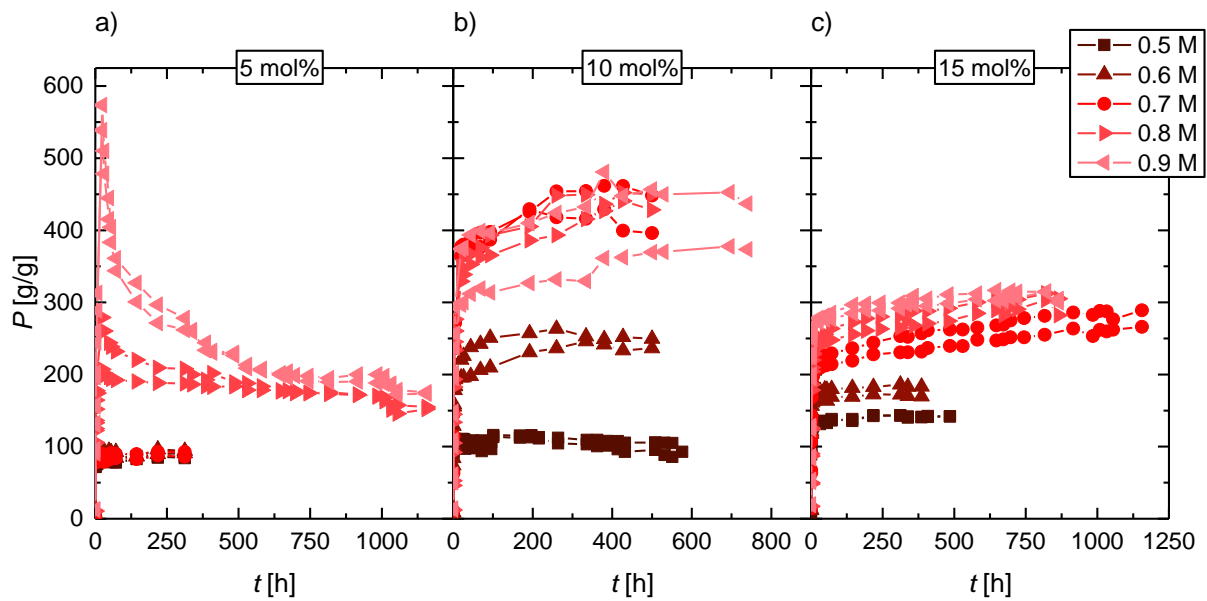
Figure 42. Time-dependent swelling *P* in dependence on the concentrations of acrylic acid for a) 5 mol% PEGda, b) 10 mol% PEGda and c) 15 mol% PEGda in the initial monomer solution and a Basotect® thickness of *d* = 0.5 cm.

The experimental data was fitted along Equation 9 (cf. Chapter 1.2.4, *Kinetics of Swelling Processes*) as NLFit in *OriginPro 2016.* The summation was carried out from *n* = 1 till *n* = 100 for all calculations.

The diffusion controlled processes *x* and relaxation controlled processes (1–*x*) as well as the rate constants k_D for diffusion processes and k_R for relaxation controlled processes changed when varying the number of summations *n* depending on the experimental data. It was found that there was one solution of the equation with a coefficient of Fickian diffusion *x* ≤ 0.5 and one solution with *x* ≥ 0.5 for each experimental data set. The model was split into one model limited to 0 ≤ *x* ≤ 0.5 and one model limited to 0.5 ≤ *x* ≤1. The quality of the reduced χ^2 and the coefficient of determination R^2 were in the same range for both models.

The model and experimental data are shown in an exemplary way for a sample with a thickness of 0.5 cm synthesized with 0.6 mol/L acrylic acid and 15 mol% PEGda (Figure 43, Table 7). The normalized mass increase M_t/M_∞ is plotted against the square root of the swelling time. It is shown that both models are suitable for fitting the experimental data.
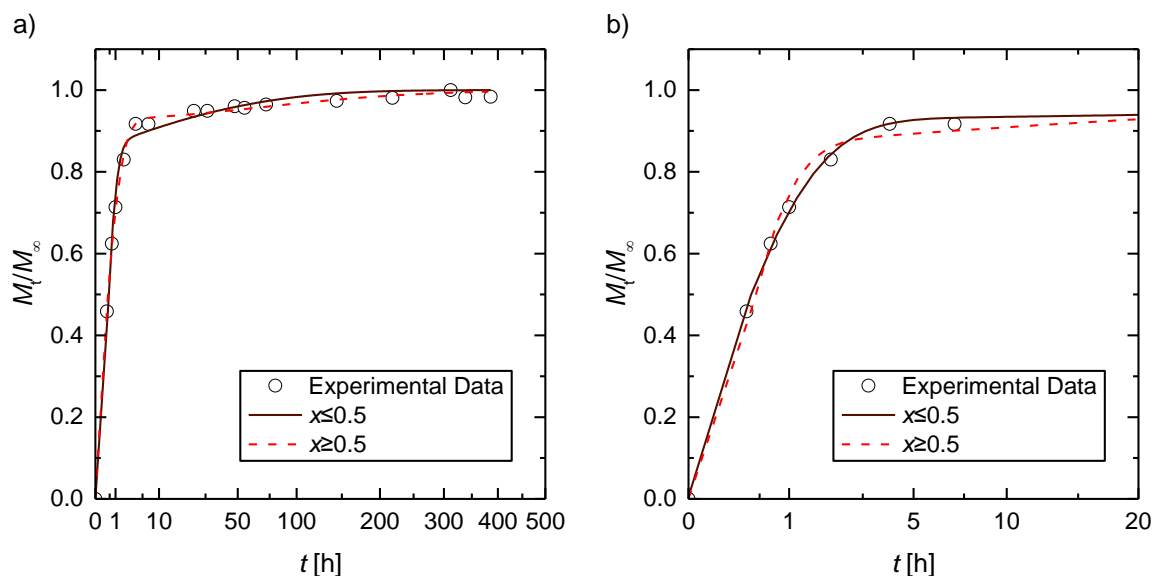
Figure 43. Normalized time-dependent swelling M_t/M_∞ with fit curves for $x \leq 0.5$ and $x \geq 0.5$. The experimental data was obtained from a sample with a thickness of 0.5 cm synthesized with 0.6 mol/L acrylic acid and 15 mol% PEGda. The X-axis is shown as square root of swelling time to obtain better overview in the range of short times. a) Full swelling curve. b) Initial area.

Table 7. Coefficient of Fickian diffusion x and rate constants k_D and k_R with reduced χ^2 and coefficient of determination R^2 obtained by fitting the experimental data from a sample with a thickness of 0.5 cm synthesized with 0.6 mol/L acrylic acid and 15 mol% PEGda with the combined diffusion-relaxation model.

Model	x	k_D [h^{-1}]	k_R [h^{-1}]	Reduced χ^2	R^2	Adjusted R^2
$x \geq 0.5$	0.9293 ± 0.006403	0.9310 ± 0.03163	0.007671 ± 0.001802	9.843·10^{-05}	0.9987	0.9986
$x \leq 0.5$	0.1492 ± 0.02287	0.01674 ± 0.006354	1.930 ± 0.1205	4.742·10^{-04}	0.9939	0.9931

A high value for x indicates a system controlled by a Fickian diffusion step. The solvent mobility of the system is low relative to the relaxation rate of the polymer chains. Diffusion and relaxation rate may be comparable when x is small.[99] A linear increase in the initial area of the swelling curves indicates the predominance of diffusion controlled processes when plotting the normalized mass increase against the square root of the time. A sigmoidal curve in the initial area indicates a high proportion of relaxation processes.[99]

The swelling equilibrium was reached fast for composites synthesized with 0.5 or 0.6 mol/L acrylic acid in the monomer solution (Figure 44a–d). Consequently, there are few experimental data points in the initial area and it is difficult to estimate the quality of the fitting curves. A sigmoidal form could not be fitted to the data with an acceptable accuracy.

Sigmoidal shapes of the experimental data in the initial range are recognizable for composites synthesized with acrylic concentrations of 0.7–0.9 mol/L (Figure 44e–j). This indicates a

relaxation controlled swelling mechanism with a small value of diffusion controlled processes x. Therefore, the following evaluation is based on the solution of the fit model with a coefficient of Fickian diffusion $x \leq 0.5$.
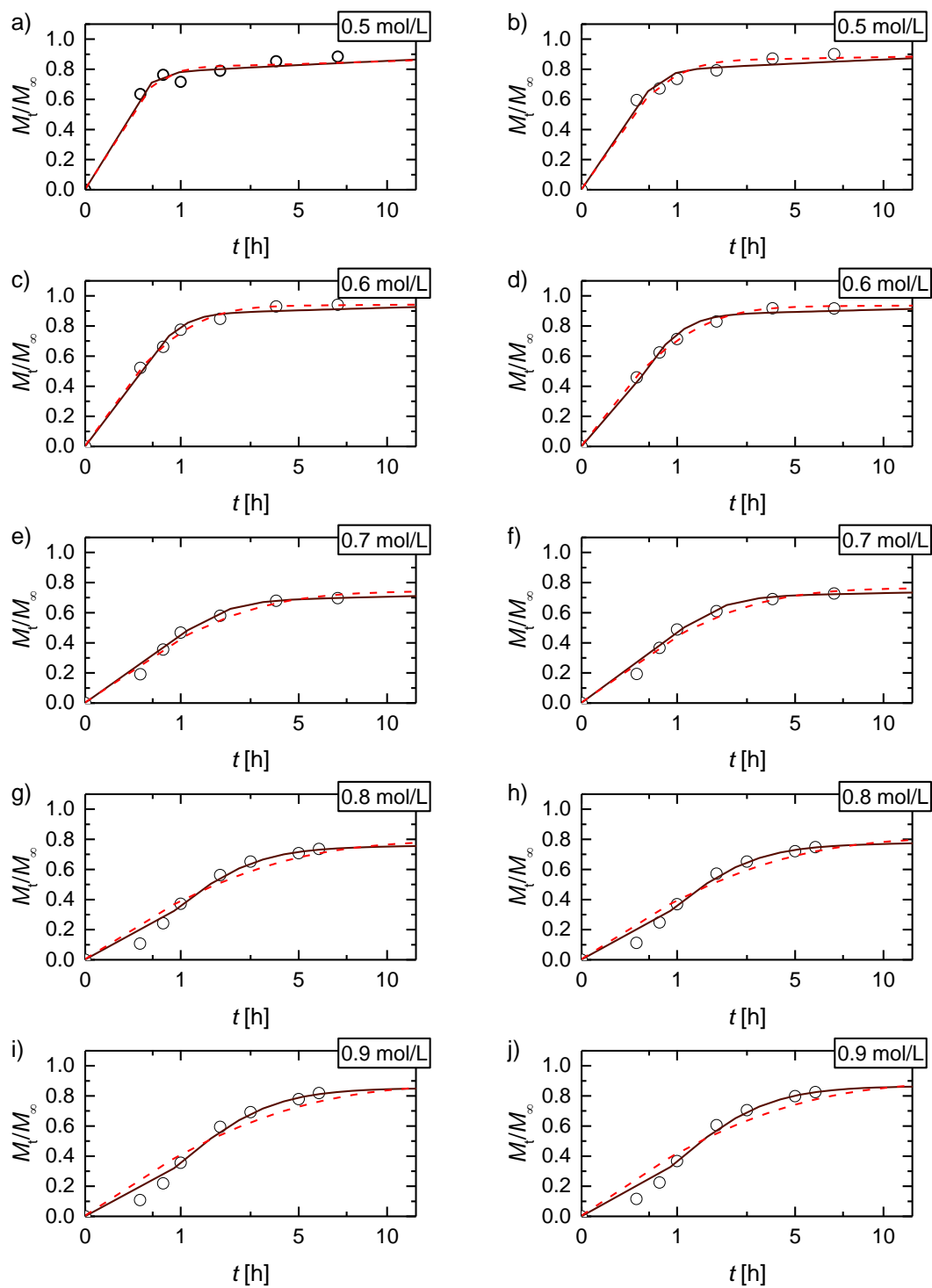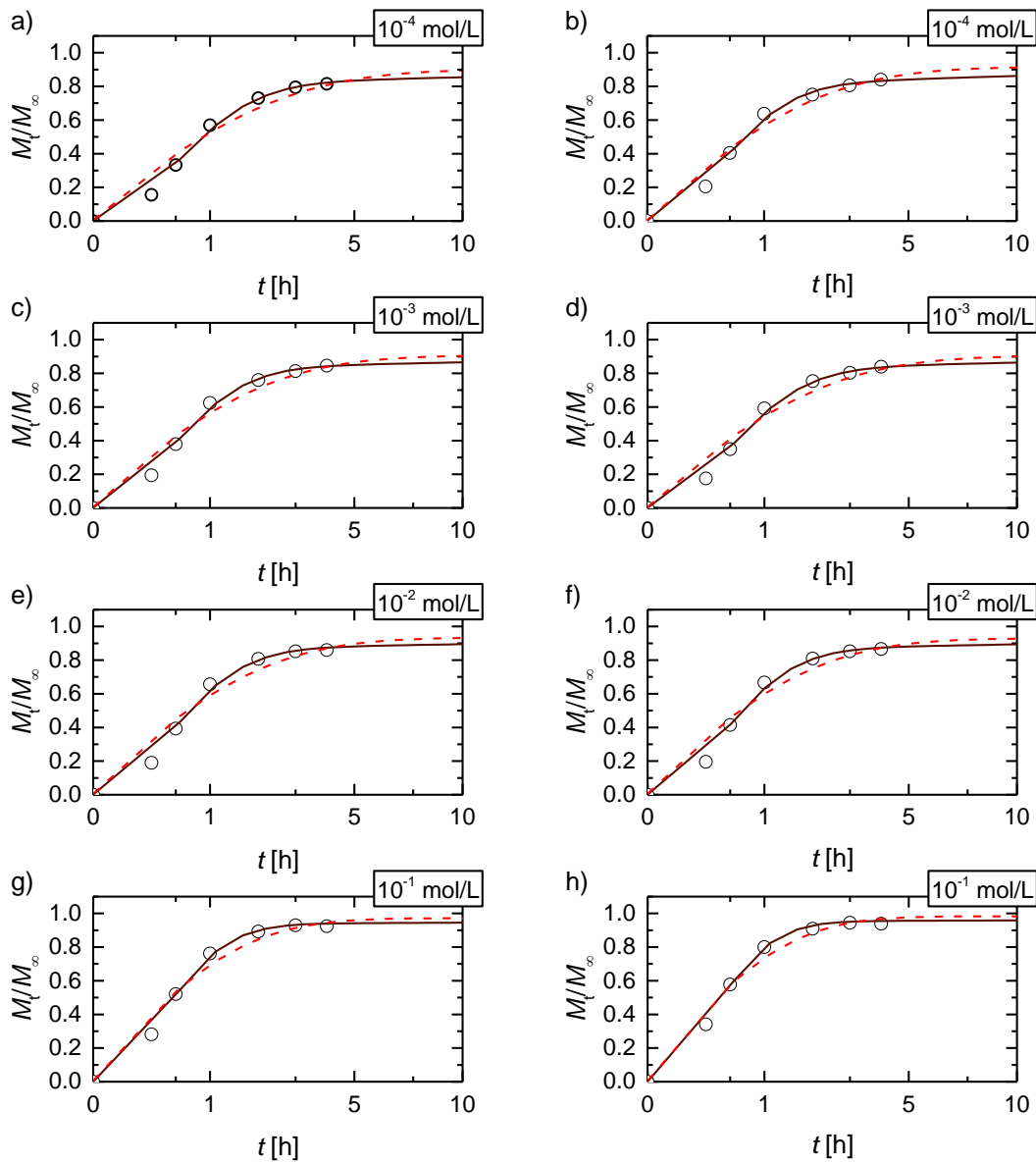
Figure 44. Normalized swelling M_t/M_∞ (○) in dependence on the square root of time with fit curves for $x \leq 0.5$ (solid line) and $x \geq 0.5$ (dashed line). The experimental data was obtained from samples synthesized with a+b) 0.5 mol/L, c+d) 0.6 mol/L, e+f) 0.7 mol/L, g+h) 0.8 mol/L and i+j) 0.9 mol/L acrylic acid and 15 mol% PEGda at a thickness of 0.5 cm.

The weighting coefficient of Fickian diffusion x decreased with increasing amount of acrylic acid in the initial monomer solution (Figure 45a). The relaxation process increasingly controlled the swelling mechanism, and the influence of diffusion decreased with increasing hydrogel content. The water uptake of the samples was hindered and depends more and more on the relaxation processes of the polymer because of the higher amount of superabsorbent polymer in the composite at larger concentrations of acrylic acid in the initial monomer solution. The rate constant for diffusion processes k_D was low and remained in the same order of magnitude when changing the acrylic acid concentration (Figure 45b). The rate constant for relaxation processes k_R was larger than k_D (Figure 45c). The rate constant k_R decreased with increasing monomer concentration. The relaxation of the hydrogel chains and consequently the swelling was slower because of the larger amount of SAP and stronger crosslinking within the Basotect® matrix.
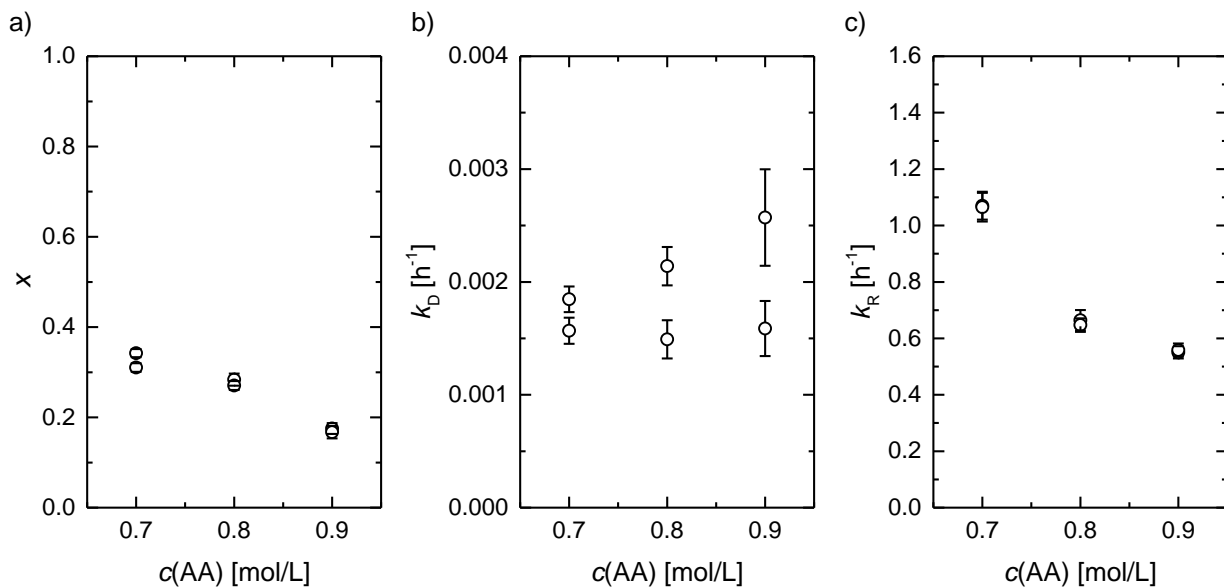
Figure 45. a) Weighting coefficient of Fickian diffusion x and rate constants b) k_D and c) k_R in dependence on the concentration of acrylic acid in the initial monomer solution. The thickness was 0.5 cm and the amount of crosslinking agent PEGda was 15 mol%.

A precise analysis of the initial area of the kinetic fits was possible for 0.8 mol/L and 0.9 mol/L acrylic acid in the initial monomer solution for composites with a sample thickness of 1 cm (Figure 46). The sigmoidal initial shape of the curves indicates a relaxation controlled mechanism with a weighting coefficient of Fickian diffusion $x \leq 0.5$.
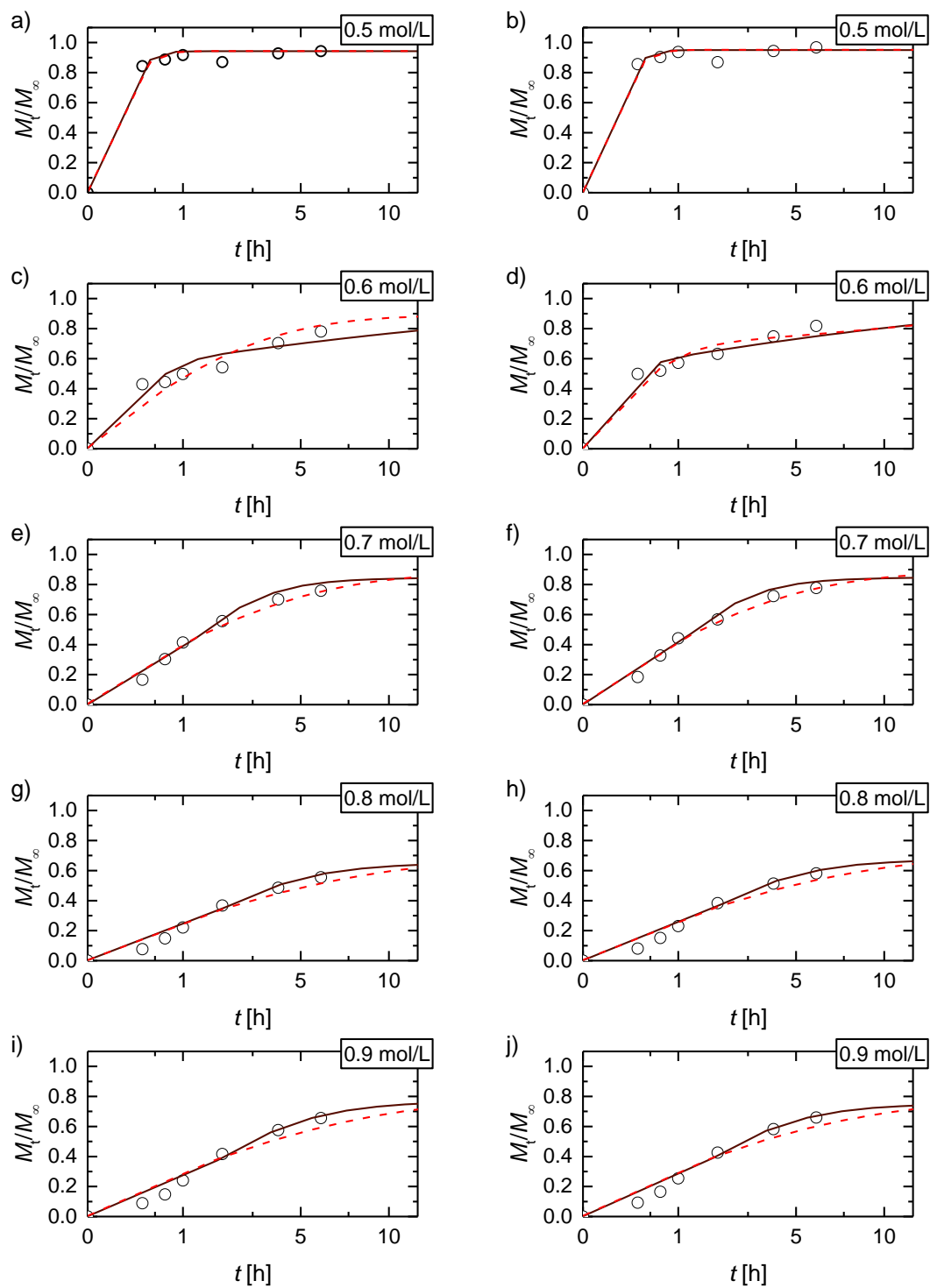
Figure 46. Normalized swelling degree M_t/M_∞ ($\circ$) in dependence on the square root of time with fit curves for $x \leq 0.5$ (solid line) and $x \geq 0.5$ (dashed line). The experimental data was obtained from samples synthesized with a+b) 0.5 mol/L, c+d) 0.6 mol/L, e+f) 0.7 mol/L, g+h) 0.8 mol/L and i+j) 0.9 mol/L acrylic acid and 15 mol% PEGda at a thickness of 1 cm.

The impact of diffusion processes x is larger for thicker ($d = 1$ cm) than thinner ($d = 0.5$ cm) composites (Figure 47a). Diffusion is faster in thin samples. Consequently, diffusion is more rate-determining in thicker samples. The swelling constants k_D and k_R were lower for thicker samples in comparison to thinner composites on account of their larger network expansion (Figure 47b–c).
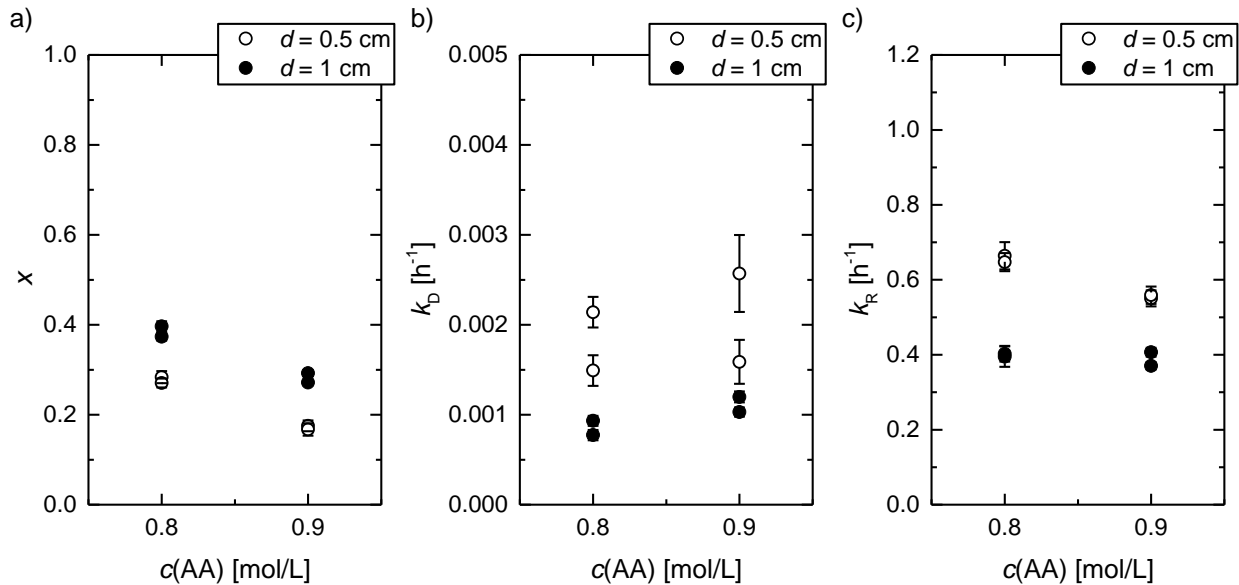
Figure 47. a) Weighting coefficient of Fickian diffusion x and the rate constants b) k_D and c) k_R in dependence on the concentration of acrylic acid in the monomer solution for samples with a thickness of 0.5 cm or 1 cm. The amount of crosslinking agent PEGda was 15 mol%.

The normalized swelling curves of samples synthesized with 0.9 mol/L acrylic acid, 15 mol% PEGda and a thickness of 0.5 cm in aqueous sodium chloride solution with various concentrations ($1 \cdot 10^{-4}$ mol/L, $1 \cdot 10^{-3}$ mol/L, $1 \cdot 10^{-2}$ mol/L and $1 \cdot 10^{-1}$ mol/L) exhibited a sigmoidal initial area and consequently a small value for x (Figure 48).

Figure 48. Normalized swelling degree M_t/M_∞ (○) in dependence on the square root of time with fit curves for $x \leq 0.5$ (solid line) and $x \geq 0.5$ (dashed line). The experimental data was obtained from samples synthesized with 0.9 mol/L acrylic acid and 15 mol% PEGda at a thickness of 0.5 cm. The swelling measurements were carried out in aqueous sodium chloride solutions with a concentration of a+b) $1 \cdot 10^{-4}$ mol/L, c+d) $1 \cdot 10^{-3}$ mol/L, e+f) $1 \cdot 10^{-2}$ mol/L and g+h) $1 \cdot 10^{-1}$ mol/L sodium chloride.

The values for the weighting coefficient of Fickian diffusion decreased with increasing salt concentration (Figure 49a). The reason for this behavior is that the swelling of the composites was lower at larger salt concentrations. The polymer density of the composites was larger than for samples with a higher swelling degree, which increased the influences of the polymer chain relaxation processes. The rate constant for diffusion controlled processes stayed at the same low level, while the relaxation rate constant increased with increasing salt concentra-

tion. The reason for this is the decreased time to reach the equilibrium swelling because the swelling at larger salt concentrations was reduced.
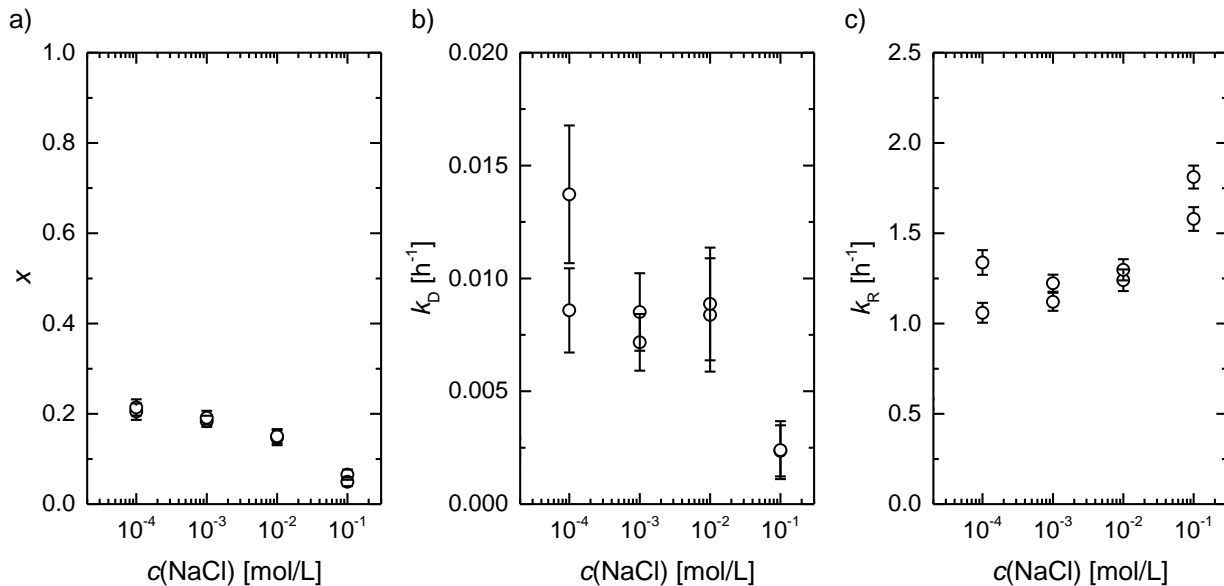
Figure 49. a) Weighting coefficient of Fickian diffusion x and rate constants b) k_D and c) k_R of samples with a thickness of 0.5 cm synthesized with 0.9 mol/L acrylic acid and 15 mol% PEGda in dependence on the concentration of sodium chloride in the swelling solution.

The combined diffusion-relaxation model[99] could successfully be applied to the SAP-Basotect® composites with a large hydrogel content even though it was investigated for spherical particles under constant swelling conditions. It was shown that the swelling mechanism was highly dependent on relaxation processes, whereby the proportion of diffusion-controlled processes was larger for thick samples than for thin ones and swelling rates were higher in thinner samples.

Diffusion controlled processes decreased with increasing concentrations of salts in the swelling medium while the relaxation rate constant increased because of the decreased absorption of saline solution.

4.4 Rheological Characterization

The rheological characterization of the SAP-Basotect® composites was performed on samples that were allowed to swell until the equilibrium swelling degree was reached. The samples showed the typical behavior of crosslinked gels (Figure 50). The storage modulus G' and the loss modulus G'' were almost constant in the examined frequency range. The logarithmic complex viscosity $|\eta^*|$ decreased with a slope of -1 with logarithmic angular frequency ω.[55,138,139]
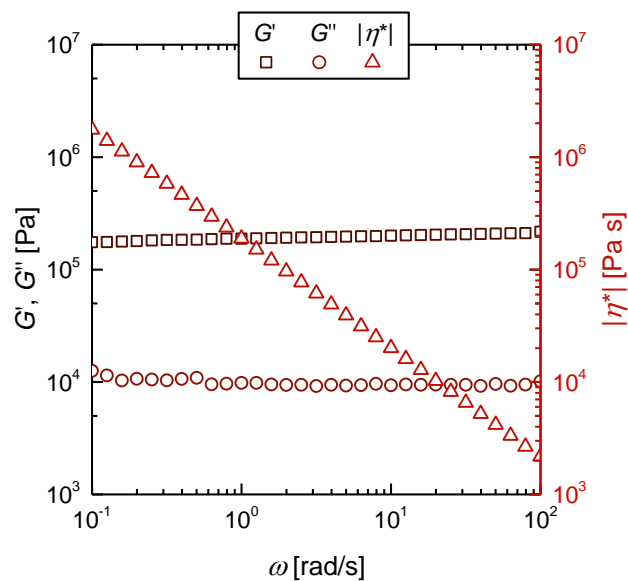
Figure 50. Storage modulus G', loss modulus G'' and complex viscosity $|\eta^*|$ of a SAP-Basotect® composite after swelling to equilibrium in dependence on the angular frequency ω at an axial force of 10 N.

The storage and loss moduli of gels synthesized with 0.6 mol/L or 0.9 mol/L acrylic acid in the initial monomer solution were almost constant at adjusted axial forces in the range between 5 N and 15 N (Figure 51). Consequently, it was not to be expected that a small deviation from the adjusted normal force leads to large errors.
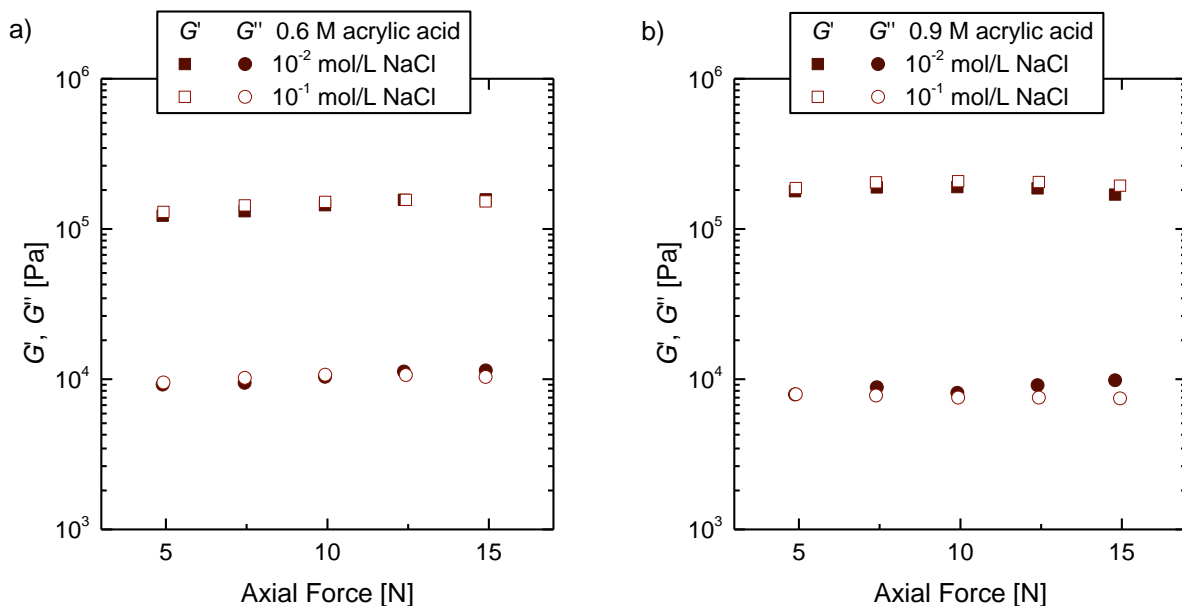
Figure 51. Storage modulus G' and loss modulus G'' in dependence on the axial force for composites synthesized with a) 0.6 mol/L or b) 0.9 mol/L acrylic acid and 15 mol% PEGda in the initial monomer solution after swelling to equilibrium in aqueous sodium chloride solution.

An influence of the concentration of acrylic acid in the initial monomer solution (0.6 mol/L or 0.9 mol/L) on the storage and loss moduli could not be observed (Figure 52). In addition, a variation of the concentration of sodium chloride ions in the swelling medium in the range between $1 \cdot 10^{-4}$ mol/L and $1 \cdot 10^{-1}$ mol/L did not influence the storage and loss moduli. The measured samples were only slightly swollen (cf. Chapter 4.3.4). Therefore, it was assumed that the viscoelastic properties of the gels were too similar to distinguish between the samples because the differences were in the range of the experimental accuracy.
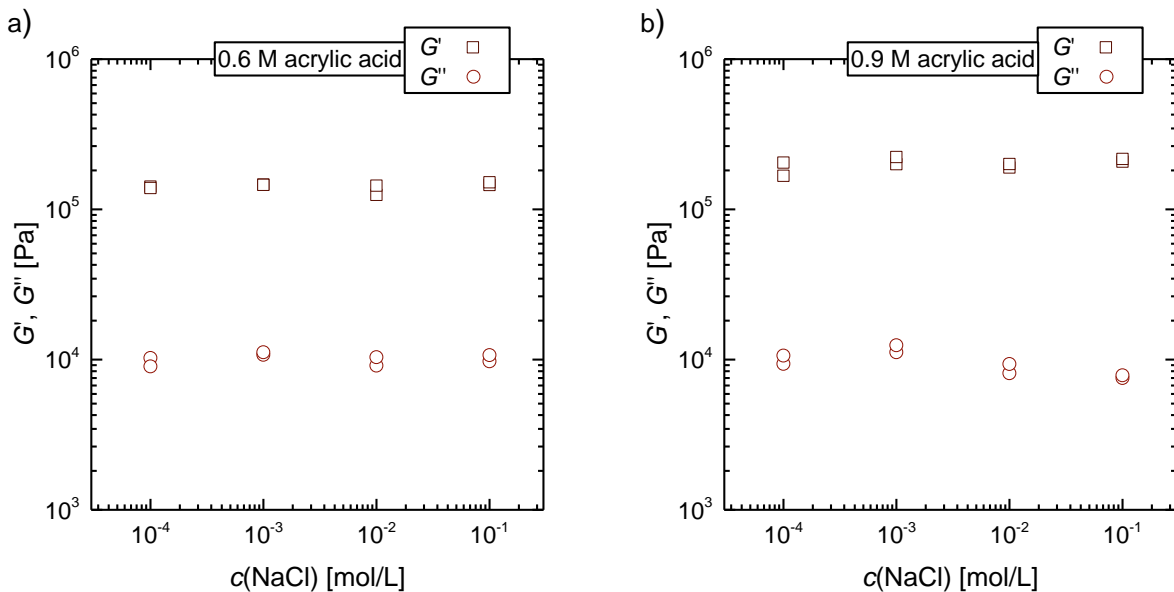
Figure 52. Storage modulus G' and loss modulus G'' in dependence on the concentration of sodium chloride in the swelling solution for composites synthesized with a) 0.6 mol/L or b) 0.9 mol/L acrylic acid and 15 mol% PEGda in the initial monomer solution.

Additionally, SAP-Basotect® composites with strongly different swelling properties were analyzed. Samples were selected that were synthesized with 0.6 mol/L acrylic acid and 5–15 mol% PEGda as crosslinking agent in the monomer solution (Figure 53a). The highest values for the storage and loss moduli were obtained with 5 mol% crosslinking agent. The values for G' and G'' at 10 mol% PEGda were about half a decade lower. The moduli of the 15 mol% PEGda gels were increased by a quarter of a decade relative to the 10 mol% PEGda samples. This could be explained by the swelling properties of the different gels (cf. Chapter 4.3, Table 6). The composites synthesized with 5 mol% PEGda appeared like unmodified Basotect® since (almost) all SAP was washed out during the swelling experiments. Without modification of the sample with SAP it did not swell in water. This ensured the high crosslink density given by the Basotect® structure and consequently led to large storage moduli.

The 10 mol% PEGda samples appear as slippery, flexible hydrogels with high swelling power. The high swelling degree led to expansion of the network and consequently to a low crosslink density of the composites resulting in a decrease of storage and loss moduli.

The 15 mol% PEGda composites were firmly crosslinked, brittle hydrogels. These composites swelled less than 10 mol% PEGda samples and stronger than 5 mol% PEGda samples. Consequently, the values of crosslink density and netpoint distance as well as storage and loss moduli ranged between the values of the samples synthesized with 5 mol% and 10 mol% PEGda. The storage and loss moduli decreased with increasing swelling *P* and netpoint distance (Figure 53b).
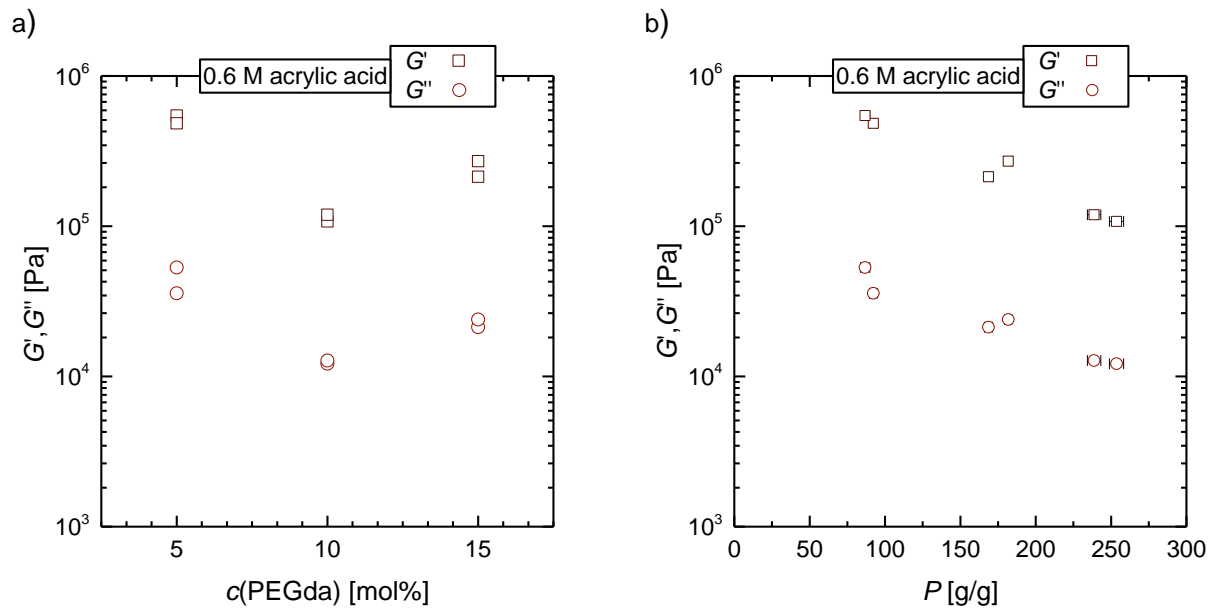
Figure 53. Storage modulus *G'* and loss modulus *G''* in dependence on a) the amount of PEGda in the initial monomer solution and b) the swelling *P* for composites synthesized with 0.6 mol/L acrylic acid at a normal force of 7.5 N.

5. Summary

Studies on the synthesis of bio-based sugar-containing RAFT agents and their application as chain transfer agents in RAFT polymerizations were carried out in the beginning of this work. Specific attention was paid to the reaction kinetics, the control of the polymerization and the molecular weight distribution of the resulting polymers. The RAFT agents MMPX, MMBX and MGluBX were synthesized in high purity, but low yields (MMBX: 25 %, MMPX: 15 % and MGluPX: 43 %). However, it is possible to regain the starting materials to further increase the yield. Methyl-α-D-mannopyranoside and methyl-α-D-glucopyranoside are simply transformed into the corresponding xanthate at position 6 of the sugar. No costly introduction of protecting groups was necessary.

PNIPAm and PVP were synthesized with MMPX (PNIPAm, PVP), MMBX (PNIPAm) and MGluBX (PNIPAm) by RAFT/MADIX polymerization with tailor-made functionalities at the chain ends. The molecular weight distributions were broad in comparison to other reported RAFT polymerizations. The PDIs were in the range of 1.5 to 1.8 depending on the reaction conditions. Nonetheless, the polymerization of NIPAm and NVP as RAFT/MADIX polymerization with MMPX, MMBX or MGluBX as CTA is an easy route to obtain polymers with mannose or glucose end groups.

The RAFT/MADIX polymerization of NVP with MMPX as CTA is more than twice as slow as the conventional free radical polymerization without CTA. This might be caused by the reduction of the gel effect. Almost full conversion of the monomer was reached within 3 hours for the RAFT progress.

The RAFT/MADIX polymerization of NIPAm with the sugar-based RAFT agents MMBX, MMPX and MGluBX was almost as fast as the conventional free radical polymerization at a ratio of monomer, CTA and initiator of 100:1:0.2. The rate constants decreased with increasing concentration of the CTA and decreasing reaction temperature. The application of MMPX as CTA led to the highest rate of RAFT polymerization and provided the highest control over the polymerization compared to the other sugar-containing CTAs. The control over the polymerization of NIPAm using MMBX as CTA was increased by lowering the temperature and, consequently, by decreasing the reaction rate. A change in the ratio of the CTA and initiator did not affect the molecular weight distribution of the resulting PNIPAm but the polymerization rate. An inhibition phase occurred if the ratio of CTA and initiator was significantly increased.

It was assumed that a part of the polymers had no tailor-made functional groups at the chain ends since the control of the RAFT agents over the polymerization was not perfect. These polymers are referred to as dead polymer, because they cannot act as macro CTA. The amount of dead polymer was determined by synthesis of poly(NIPAm-*co*-NIPAm) diblock copolymers by running two RAFT polymerization cycles and analysis of the molecular weight distribution by SEC. The content of dead polymer was 19.25 % for MMPX as CTA and 36.27 % for MMBX as CTA in the polymerization of NIPAm. This confirmed that the control over the RAFT process was higher with MMPX than with MMBX.

The qualitative proof of the presence of the R and Z group at the chain ends of PNIPAm was given by ^{13}C NMR spectroscopy to show the benzyl group of MMBX-modified PNIPAm, by staining with ethanol/sulfuric acid to show the sugar functionalities and by reaction of the carboxyl group of MMPX-modified PNIPAm with furfurylamine and subsequent detection by ^{1}H NMR spectroscopy.

In spite of the relatively large PDIs, there is big interest in biocompatible polymers with tailor-made end groups including sugar moieties, especially if they are stimuli-responsive like PNIPAm. The sugar functionalities can be used to selectively bind enzymes, whereas carboxyl groups can be used for further post modifications.

The second part of this thesis dealt with polymer hydrogels for use as wound dressings or application in hygiene products. The general approach for these materials was the synthesis of superabsorbent composite materials containing an interpenetrating network of the melamine/formaldehyde foam Basotect® as carrier material and a superabsorbent hydrogel. The composite foams should be different from unmodified Basotect®, washing out effects should not occur and the composite should not disintegrate for use as wound dressings. Disintegration was considered the least disadvantageous property since it is possible to hold the composite together by covering it with a fabric.

Basotect® was chosen since it is a web foam, has a high flexibility, an open-pore structure and high hydrophilicity. Partially neutralized poly(acrylic acid) was used as superabsorbent hydrogel. The introduction of the poly(acrylic acid) and sodium polyacrylate into the Basotect® carrier material was carried out by *in situ* polymerization of partially neutralized acrylic acid in the Basotect® matrix. The free radical polymerization using thermal initiators was a suitable synthesis path to achieve this. Composites with different properties could be obtained by variation of the reaction parameters like the concentrations of acrylic acid, sodium acrylate, crosslinking agent and matrix thickness.

Composites of Basotect® and partially neutralized poly(acrylic acid) crosslinked with PEGda were easily accessible by free radical polymerization after impregnation of the foam with the degassed monomer solution and subsequent thermal initiation. No monomer signals could be detected by FT-IR spectroscopy after 6–22 h even at low monomer concentrations at a reaction temperature of 80 °C and with an initiator concentration of 1 mol% KPS with regard to acrylic acid. The size of matrix surface and volume changed during the synthesis by evaporation of water. The increase of the ratio of surface and volume after synthesis depended on the monomer concentration since the monomer concentration had an influence on the resulting hydrogel and its ability to bind water. An increase in the monomer concentration led to a smaller increase in the surface/volume ratio and it had an increasing effect on the gain in weight of the composite in comparison to the unmodified matrix before the synthesis.

Swelling measurements in water and subsequent solvent exchange to DMSO and ethanol showed a high volume decrease for composites with large hydrogel content. This decrease was high for a change to ethanol since the compatibility of poly(acrylic acid) and sodium polyacrylate was higher to water and DMSO than to ethanol.

The SEM images of the SAP-Basotect® composites synthesized by the methods described above and dried with supercritical carbon dioxide or by lyophilization showed the inhomogeneity of the composites. Samples had areas with a high load next to areas with a low load of SAP. This is tentatively the result of the synthesis conditions. The monomer solution in the impregnated matrix moved downwards by gravity so that a higher SAP concentration was formed at the bottom of the sample. This may be counteracted by a higher polymerization rate, e. g. by applying higher temperatures or application of a redox initiator pair, or by selectively spraying the dry Basotect® with a more concentrated monomer solution.

The new parameter *P* as measure for swelling and modification with hydrogel was introduced for the characterization of the swelling behavior of the portrayed composites of SAP and Basotect®. *P* was more suitable for the description of the swelling behavior of these SAP-Basotect® composites than the commonly used swelling degree *Q*. The hydrogel character and swelling behavior of the composites depended on the amount of acrylic acid and sodium acrylate used in the monomer solution. An increased amount of acrylic acid usually led to higher gel content and higher swelling. The crosslinking agent also had a big influence. Small degrees of crosslinking led to high washing out and low swelling. A large degree of crosslinks hindered the swelling by restraining the polymer segments. The highest swelling was obtained with moderate crosslink density at large concentrations of acrylic acid and sodium acrylate. The thickness of the Basotect® matrix had an influence on the swelling inflicted by the change of surface and volume ratio. Thin samples did not bind the monomer solution during transfer from impregnation to the polymerization dish strong enough to obtain high degrees of modification. Diffusion was hindered for thick samples.

Swelling in saline solution led to decreased swelling compared to swelling in demineralized water since the salt ions shielded the ions in the gel better so that less swelling was required to lower the elastic potential.

Kinetic models of the swelling suggest a large amount of relaxation controlled swelling processes that increase with increasing amount of poly(acrylic acid) and sodium polyacrylate as the swelling rate decreased. This was because the water uptake of the composite was more hindered at higher hydrogel content and consequently, water absorption depends more on the relaxation processes of the polymer chains. Diffusion controlled processes had a bigger influence in thick samples.

Rheological measurements of the swollen composites showed the typical behavior of crosslinked gels. The storage and loss moduli depend on the swelling behavior of the superabsorbent composites and decreased with increasing swelling as the network has a lower crosslink density.

The SAP-Basotect® composite materials show potential for application as superabsorbent wound dressings or sanitary napkins because of their increased form stability and easily adjustable size by simply cutting the composites. The swelling degree can be adjusted by increasing the sodium acrylate content for the absorption of saline solutions such as blood or urine. The composite should be wrapped in a fabric so that no superabsorbent polymer can enter wounds or spread on the body if fracture occurs. Another precaution could be post-

crosslinking of the composite surface to increase the surface stability and decrease the sol content.

6. Experimental Part

6.1 Materials and Characterization

6.1.1 Materials

RAFT Agents and Polymers

Acetic acid (*VWR*, ≥ 99.7 %), aluminum oxide (*Merck*, aluminum oxide 90 active basic, 0.063–0.200 mm), benzyl bromide (*Merck*, ≥ 98 %), 1,2-bis(2-(4,5-dihydro-1H-imidazol-2-yl)-propan-2-yl)diazene dihydro-chloride (VA-044; *WAKO Chemicals*, ≥ 97 %), 3-bromopropionic acid (*Aldrich*, 99 %), carbon disulfide (*Aldrich*, ≥ 99.5 %), chloroform (technical grade), chloroform-*d* (CDCl$_3$; *Deutero*, 99.8 %), dichloromethane (DCM; technical grade), diethyl ether (technical grade), deuterium oxide (D$_2$O; *Deutero*, 99.9 %), dimethylformamide (DMF; *Acros*, 99.8 %), *N*-Ethyl-*N*′-(3-dimethylaminopropyl)carbodiimide hydrochloride (EDC · HCl; *Alfa Aesar*, ≥ 98 %), furfurylamine (*Aldrich*, ≥ 99 %), hydrochloric acid (HCl; *VWR*, 37 %), *N*-isopropylacrylamide (NIPAm; *Aldrich*, 97 %), methyl α-D-glucopyranoside (*Aldrich*, ≥ 99 %), methyl α-D-mannopyranoside (*Aldrich*, ≥ 99 %), magnesium sulfate (*R. d. H.*, ≥ 99 %), petroleum ether (technical grade), silica gel (*Merck*, 70–230 mesh, 60 Å), sodium acetate (*Aldrich*, ≥ 99 %), sodium chloride (NaCl; *VWR*, 99 %) and sodium hydroxide (NaOH; *Merck*, ≥ 99 %) were used as obtained.

Azobisisobutyronitrile (AIBN; *Aldrich*, 98 %) was purified by recrystallization from methanol. *N*-Vinylpyrrolidone (NVP; *Aldrich*, ≥ 99 %) was filtered through basic alumina immediately before the polymerization to remove the stabilizer Kerobit®. 1,4-Dioxane (*Aldrich*, 99.8 %) was dried with activated 4 Å molecular sieves prior to use and stored under argon atmosphere. Dichloromethane and methanol were distilled prior to column chromatography. Acetate buffer (pH = 5.2) was made from acetic acid and sodium acetate.

SAP-Basotect® Composites

Acrylic acid (AA; *Aldrich*, 99 %, containing 180–200 ppm 4-methoxyphenol as stabilizer), dimethyl sulfoxide (DMSO; *Honeywell*, 99.9 %), ethanol (*Aldrich*, ≥ 99.9 %), poly(ethylene glycol) diacrylate (PEGda; *Aldrich*, M_n ≈ 575 g/mol), potassium persulfate (KPS; *Fluka*, ≥ 99 %), sodium chloride (NaCl; *VWR*, 99 %) and sodium hydroxide (NaOH; *Merck*, ≥ 99 %) were used as obtained.

Basotect® (melamine/formaldehyde foam; *B6 Akustik A/S*) was cut into the desired shape and was washed for 3 days at 80 °C in demineralized water to remove amine-containing residues.

6.1.2 Characterization and Methods

Column Chromatography

Silica gel 60 (*Merck*, 70–230 mesh, 60 Å) was used for separation processes by column chromatography. Thin layer chromatography was carried out on silica gel F254 panels (*Merck*).

NMR Spectroscopy

NMR spectra (^{1}H, ^{13}C, H,H-COSY, HSQC) were recorded in chloroform-*d* (CDCl$_3$) with tetramethylsilane as internal standard or in deuterium oxide (D$_2$O) with 3-(trimethylsilyl)-propionic acid sodium salt as internal standard using a Bruker AVANCE 400 MHz or a Bruker FOURIER 300 MHz spectrometer. The obtained data was analyzed with *Mestre Nova 9.0.1*.

Size Exclusion Chromatography

SEC was performed in dimethylformamide (DMF) with 0.01 N lithium bromide on a *MZ-Gel SD-plus* 5 μm linear column. The obtained data was analyzed with *Chromatographica V1.0.20*.

IR Spectroscopy

FT-IR spectroscopy was carried out on a *Smart iTR-Nicolet iS10* from *Thermo Scientific* and was analyzed with *Omnic 8.3*.

Scanning Electron Microscopy

SEM images were taken with the field emission scanning electron microscope *LEO 1525 Gemini* at an acceleration voltage of 5 kV with an In-Lens detector. *ImageJ 1.48v* was used to evaluate the obtained SEM images.

Dialysis

Purification of polymeric materials was carried out by dialysis in demineralized water using *Spectra/Por® 1 Dialysis Membranes* with a molecular weight cut-off of 6000–8000 g/mol or pre-wetted *Spectra/Por® 6 Dialysis Membranes* with a molecular weight cut-off of 1000 g/mol depending on the expected molecular weight of the polymer to be purified.

Lyophilization

Water containing samples were frozen in liquid nitrogen or overnight in a fridge at -32 °C. The frozen samples were dried using a *Christ Beta 1-16* lyophilizer.

Rheology

Rheological experiments were carried out with a *TA AR-G2 Magnetic Bearing Rheometer* with a plate-plate system (25 mm ETC steel plate) at 25 °C. In oscillatory measurements, a strain sweep at a fixed frequency of 10 rad/s at constant axial force was performed prior to the frequency sweep to ensure that the selected stress was in the linear viscoelastic region. The frequency sweep was usually carried out between 100–0.1 rad/s. *Trios v3.3.1* and *OriginPro 2016* were used to analyze the obtained data.

Drying with Supercritical Carbon Dioxide

Supercritical drying of DMSO-containing samples was carried out at 160 bar and 60 °C at a continuous CO_2 volume flow rate of 20–50 mL/min using a 250 mL *View Cell*. Drying was carried out until no DMSO could be found in the exiting stream.

Supercritical drying of ethanol-containing samples was carried out in 25 L autoclaves at 120–130 bar and 60 °C. The CO_2 atmosphere was exchanged six times with new CO_2 (approximately 20 h).

Kinetic Modelling

OriginPro 2016 was used for fitting of the experimental data with Equation 9. The code can be found in the appendix (Chapter 9.1).

6.2 RAFT Polymers

6.2.1 Synthesis of MMBX

Methyl α-D-mannopyranoside (15.0 g, 77.2 mmol) was suspended in 15.5 mL demineralized water and slowly treated with carbon disulfide (1.64 mL, 27.1 mmol). After the addition of an aqueous 20 N sodium hydroxide solution (3.93 mL, 78.6 mmol), the solution was stirred at room temperature for 5 hours. The reaction mixture was cooled with an ice-water mixture and neutralized with an aqueous solution of acetic acid. Subsequently, a solution of benzyl bromide (5.00 mL, 42.1 mmol) in dichloromethane (13.1 mL) was added. After 2 hours of stirring, the solution was extracted with chloroform, dried over magnesium sulfate and the solvent was removed under reduced pressure.

The crude product was purified by column chromatography using silica gel and eluted with dichloromethane/methanol (19:1) (R_f 0.43). The product was obtained as a colorless solid (yield 25 % with respect to carbon disulfide) and stored at -30 °C under argon atmosphere.

NMR Spectroscopy

The ^1H NMR spectrum of MMBX is shown in Figure 54.
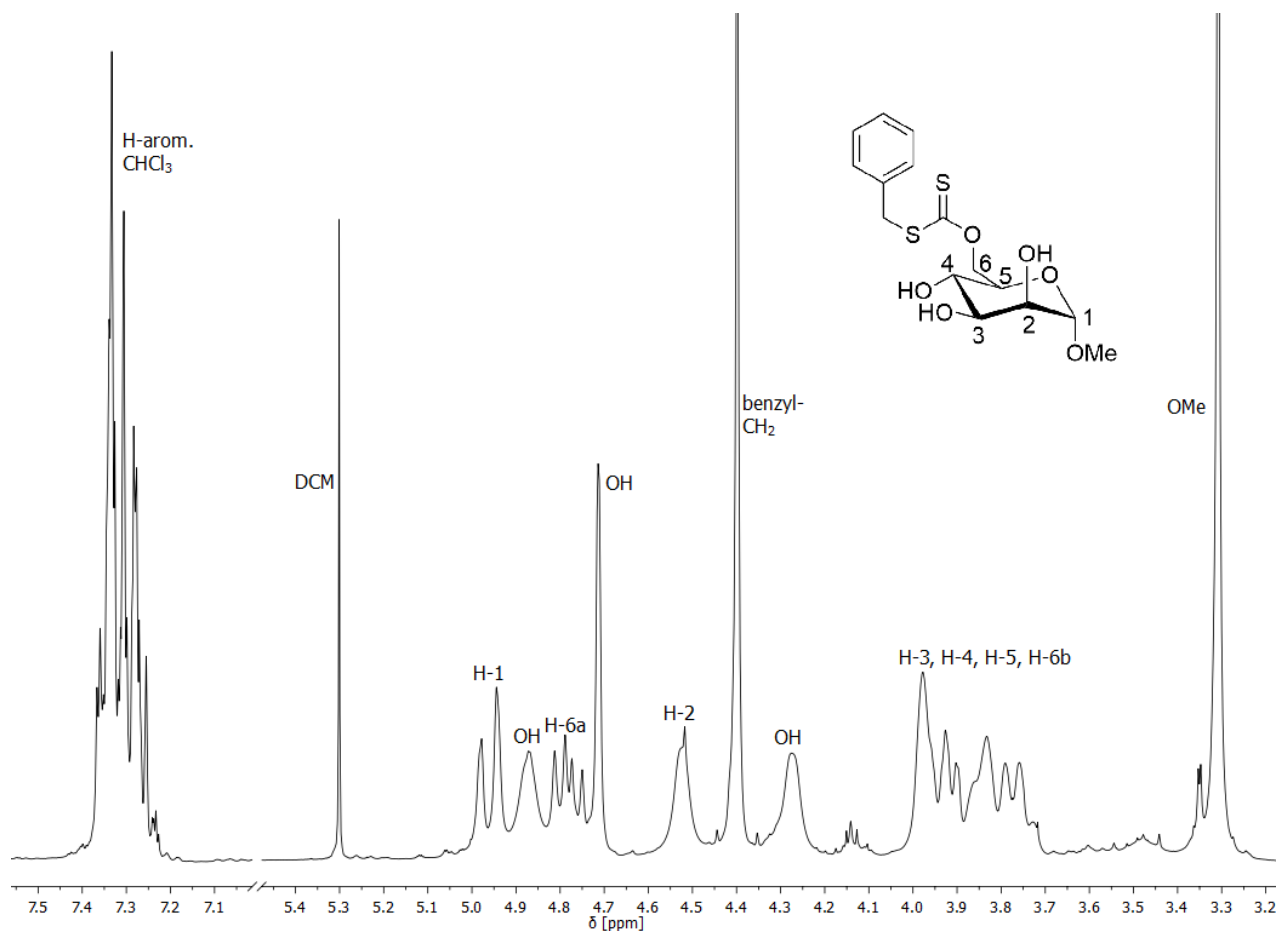
Figure 54. ^{1}H NMR spectrum of methyl α-D-mannopyranoside-6-(*S*-benzyl)xanthate (MMBX) in chloroform-*d*. Residues of dichloromethane are visible at a chemical shift of 5.30 ppm. MMBX was further dried before application as RAFT agent.

^{1}H NMR (300 MHz, CDCl$_3$): δ [ppm] = 7.39–7.23 (m, 5H, H-arom.), 4.96 (d, $^3J(^1H,^1H)$ = 10.2 Hz, 1H, H-1), 4.87 (s, 1H, OH), 4.78 (dd, $^3J(^1H,^1H)$ = 11.6, 7.1 Hz, 1H, H-6), 4.71 (s, 1H, OH), 4.52 (m, 1H, H-2), 4.40 (s, 2H, benzyl-H), 4.27 (s, 1H, OH), 4.00–3.71 (m, 4H, H-3, H-4, H-5, H-6'), 3.31 (s, 3H, OMe).

Mass Spectrometry

ESI-MS: m/z = calculated: 383.0599 [M+Na]$^+$, detected: 383.0593 [M+Na]$^+$.

Elemental analysis

C: calculated: 49.98 %, detected: 51.95 %.
H: calculated: 5.59 %, detected: 5.71 %.
S: calculated: 17.79 %, detected: 15.08 %.
O: calculated: 26.63 %, detected: 26.69 %.

6.2.2 Synthesis of MMPX

Methyl α-D-mannopyranoside (20.0 g, 103 mmol) was suspended in 21.0 mL demineralized water and slowly treated with carbon disulfide (2.20 mL, 36.4 mmol). After the addition of an aqueous 20 N sodium hydroxide solution (5.40 mL, 108 mmol), the solution was stirred at room temperature for 12 hours. The reaction mixture was cooled with an ice-water mixture and neutralized with an aqueous solution of acetic acid.

2-Bromopropionic acid (5.04 mL, 56.0 mmol) was neutralized with diluted sodium hydroxide solution and added dropwise to the reaction mixture. After 4 hours of stirring, the solution was acidified with diluted hydrochloric acid until the pH was pH ≈ 2, extracted with diethyl ether, dried over magnesium sulfate and the solvent removed under reduced pressure.

The crude product was purified by column chromatography using silica gel and eluted with dichloromethane/methanol/acetic acid (180:20:7) (R_f 0.36). The removal of acetic acid was performed by column chromatography with a) dichloromethane and b) methanol as eluent. The product was obtained as a colorless solid (yield 15 % with respect to carbon disulfide) and stored at -30 °C under argon atmosphere. To increase the solubility of the product in organic solvents, the product was dissolved in demineralized water and acidified with hydrochloric acid (pH 1–2), extracted with diethyl ether, dried over magnesium sulfate and the solvent removed under reduced pressure (yield 7 % with respect to carbon disulfide).

NMR Spectroscopy

The ^{1}H NMR spectrum of MMPX is shown in Figure 55.
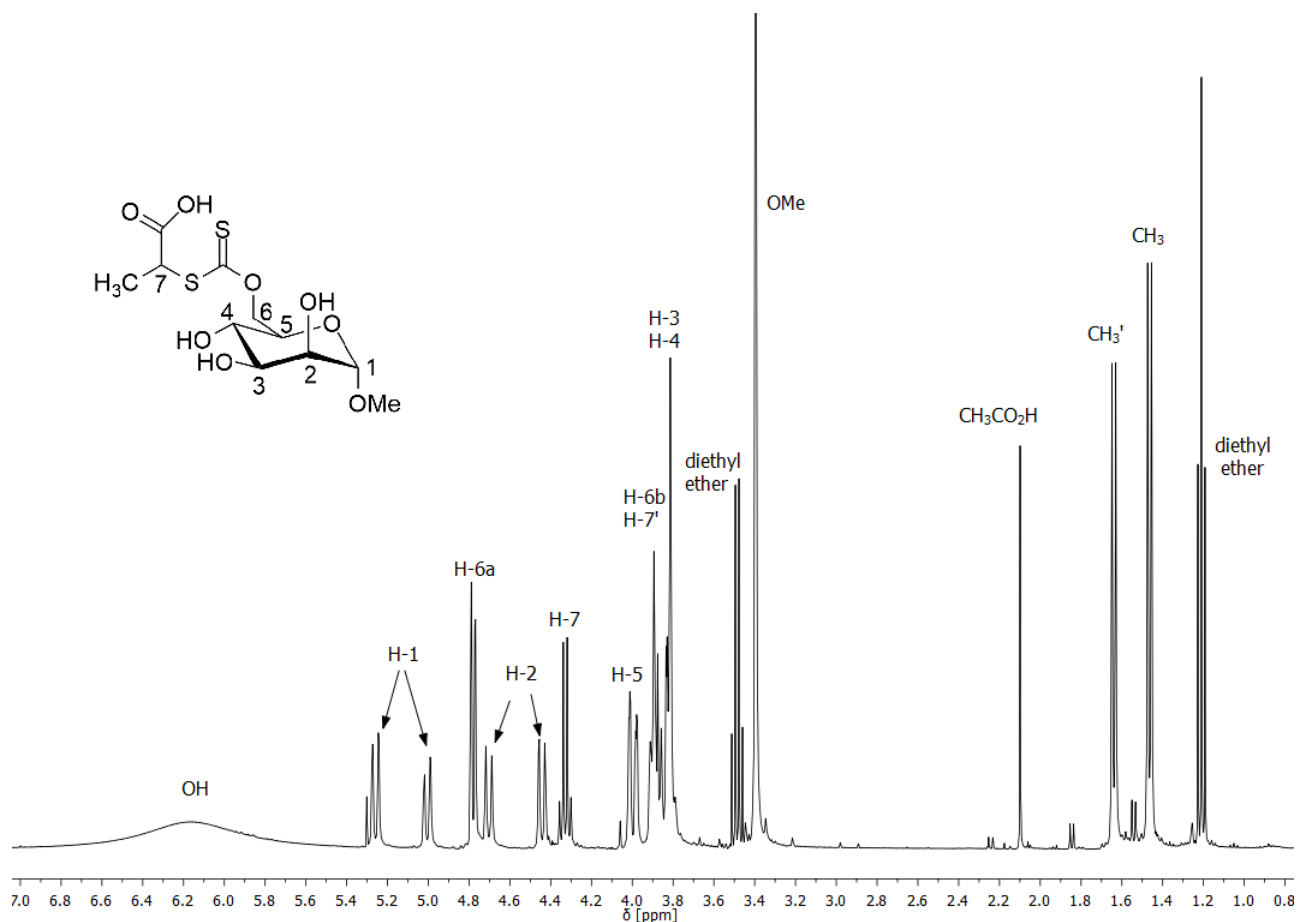
Figure 55. ¹H NMR spectrum of methyl α-D-mannopyranoside-6-(*S*-2-propionic acid)-xanthate (MMPX) in chloroform-*d*. Residues of solvents are visible at 1.21 ppm and 3.48 ppm (diethyl ether) and 2.10 ppm (acetic acid). MMPX was further dried before its application as RAFT agent.

¹H NMR (400 MHz, CDCl₃): δ [ppm] = 6.16 (s, 3H, OH), 5.26 (d, $^3J(^1H,^1H)$ = 11.1 Hz, 0.5H, H-1), 5.00 (d, $^3J(^1H,^1H)$ = 10.9 Hz, 0.5H, H-1), 4.77 (dd, $^3J(^1H,^1H)$ = 9.0, $^2J(^1H,^1H)$ = 4.5 Hz, 1H, H-6a), 4.70 (d, $^3J(^1H,^1H)$ = 1.3 Hz, 0.5H, H-2), 4.44 (d, $^3J(^1H,^1H)$ = 10.8 Hz, 0.5H, H-2), 4.33 (q, $^3J(^1H,^1H)$ = 7.5 Hz, 0.5H, H-7), 4.00 (ddd, $^3J(^1H,^1H)$ = 13.4, 3.1, 1.5 Hz, 1H, H-5), 3.93–3.84 (m, 1.5H, H-6b, H-7), 3.84–3.77 (m, 2H, H-3, H-4), 3.40 (s, 3H, OMe), 1.64 (d, $^3J(^1H,^1H)$ = 7.3 Hz, 0.5H, methyl), 1.46 (d, $^3J(^1H,^1H)$ = 7.5 Hz, 0.5H, methyl).

Mass Spectrometry

ESI-MS: m/z = calculated: 365.0341 [M+Na]⁺, detected: 365.0313 [M+Na]⁺.

Elemental analysis

C: calculated: 38.59 %, detected: 38.48 %.
H: calculated: 5.30 %, detected: 5.63 %.
S: calculated: 18.73 %, detected: 17.35 %.
O: calculated: 37.38 %, detected: 38.54 %.

6.2.3 Synthesis of MGluBX

The synthesis of MGluBX is described in literature.[127] Methyl α-D-glucopyranoside (20.0 g, 103 mmol) was suspended in 21.0 mL demineralized water and slowly treated with carbon disulfide (2.20 mL, 36.4 mmol). After the addition of an aqueous 20 N sodium hydroxide solution (5.25 mL, 105 mmol), the solution was stirred at room temperature for 19 hours. The reaction mixture was cooled with an ice-water mixture and neutralized with an aqueous solution of acetic acid. Subsequently, a solution of benzyl bromide (6.70 mL, 56.4 mmol) in dichloromethane (17.5 mL) was added. After 2 hours of stirring, the solution was extracted with dichloromethane, dried over magnesium sulfate and the solvent was removed under reduced pressure.

The crude product was purified by column chromatography using silica gel and eluted with dichloromethane/methanol (9:1) (R_f 0.39). The product was obtained as a pale yellow solid (yield 43 % with respect to carbon disulfide) and stored at -30 °C under argon atmosphere.

NMR Spectroscopy

The ^{1}H NMR spectrum of MGluBX is shown in Figure 56.
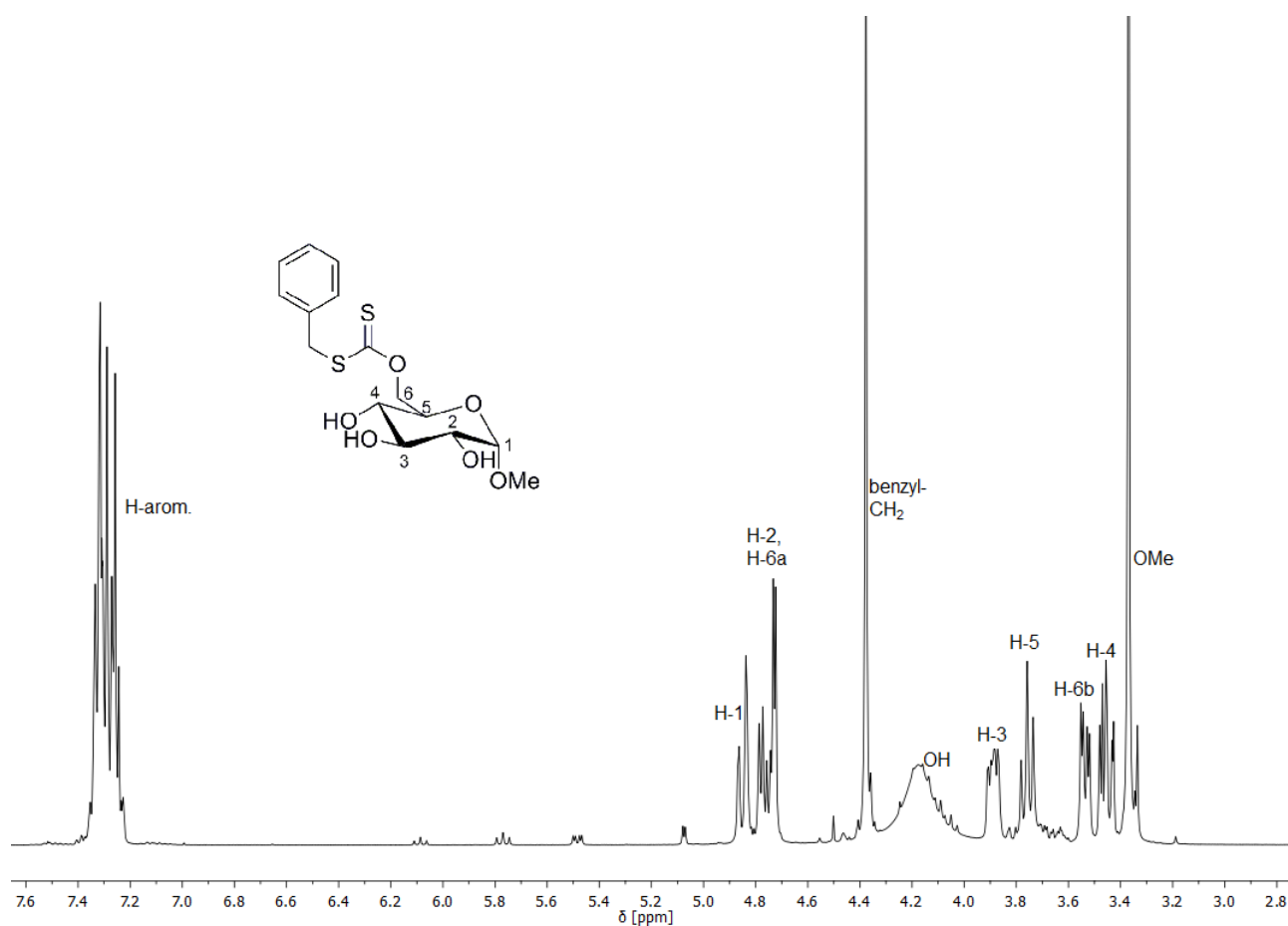
Figure 56. ^{1}H NMR spectra of methyl α-D-glucopyranoside-6-(*S*-benzyl)xanthate (MGluBX) in chloroform-*d*.

^{1}H NMR (400 MHz, CDCl$_3$): δ [ppm] = 7.33–7.21 (m, 5H, H-arom.), 4.85 (dd, ^3J(^{1}H,^{1}H) = 11.8 Hz, ^4J(^{1}H,^{1}H) = 2.0 Hz, 1H, H-1), 4.81–4.69 (m, 2H, H-2, H-6a), 4.38 (s, 2H, ben-zyl-H), 4.17 (s, 3H, OH), 3.89 (ddd, ^3J(^{1}H,^{1}H) = 10.0, ^3J(^{1}H,^{1}H) = 5.6, ^4J(^{1}H,^{1}H) = 2.0 Hz, 1H, H-3), 3.78–3.74 (m, 1H, H-5), 3.54 (dd, ^3J(^{1}H,^{1}H) = 9.7, ^2J(^{1}H,^{1}H) = 3.8 Hz, 1H, H-6b), 3.50–3.41 (m, 1H, H-4), 3.37 (s, 3H, OMe).

Mass Spectrometry

ESI-MS: m/z = calculated: 383.0599 [M+Na]$^+$, detected: 383.0736 [M+Na]$^+$.

Elemental analysis

C: calculated: 49.98 %, detected: 50.00 %.
H: calculated: 5.59 %, detected: 5.62%.
S: calculated: 17.79 %, detected: 17.34 %.
O: calculated: 26.63 %, detected: 27.20 %.

6.2.4 Polymerization of NIPAm

All polymerizations were carried out using standard Schlenk techniques with argon as inert gas. For the polymerization different temperatures (50 or 70 °C) and ratios of monomer, CTA and initiator (M:CTA:I) (usually 100:1:0.2 or 100:1:0.1 or 100:1:0.067) were used.

In a typical experiment, a solution of NIPAm (0.679 g, 6.00 mmol) in 1,4-dioxane (5.00 mL) was added to the RAFT agent (MMBX or MMPX or MGluBX). After degassing the solution, a degassed solution of AIBN in 1,4-dioxane (1.00 mL) was added and a temperature of 70 °C or 50 °C was adjusted. The polymerizations were terminated by quenching the reaction mixture with oxygen and cooling in liquid nitrogen. The polymers were purified either by precipitation in ice-cooled petroleum ether or by dialysis in water for 3 days and subsequent freeze-drying.

Conversions X_i were determined by ^{1}H NMR spectroscopy in chloroform-d by comparison of the integral of H2 (1 H, monomer signal) with the integral of H6 and Hf (6 H, monomer plus polymer signal) (Figure 57, Equation 31).
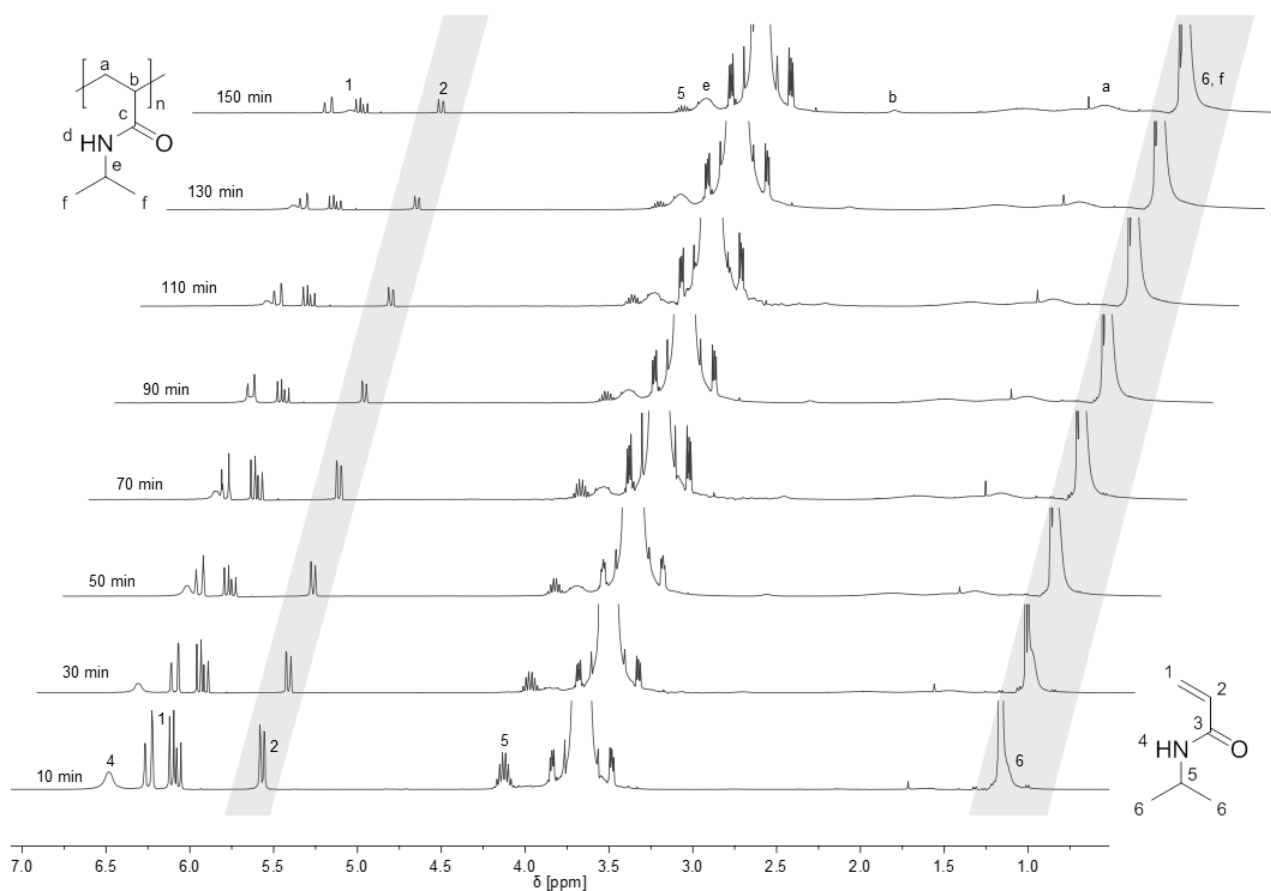
Figure 57. Time-dependent ^{1}H NMR spectra of the polymerization of NIPAm in CDCl$_3$.

$$X_i = 1 - \frac{\int H2}{\frac{1}{6}\left(\int H6 + \int Hf\right)} \tag{31}$$

Evidence of the End Group in Carboxyl Terminated PNIPAm

PNIPAm was coupled with furfurylamine to proof the existence of the carboxyl function at the chain end.

A solution of PNIPAm polymerized in the presence of MMPX (163 mg) and furfurylamine (18.3 µL, 0.202 mmol) in demineralized water (10 mL) was neutralized by addition of diluted hydrochloric acid and sodium hydroxide. After addition of *N*-ethyl-*N'*-(3-dimethylamino-propyl)carbodiimide hydrochloride (EDC · HCl; 80.0 mg, 0.417 mmol) the solution was allowed to react for 24 h at room temperature. Again, EDC · HCl (80.0 mg, 0.417 mmol) was added and the solution stirred for another 24 h. The product was purified by dialysis in demineralized water for 48 h and subsequent freeze-drying.

6.2.5 Polymerization of NVP

All polymerizations were carried out using standard Schlenk techniques with argon as inert gas. For the polymerization different temperatures (30 or 50 °C) and M:CTA:I ratios (usually 100:1:0.2 or 100:1:0.1 or 100:1:0.067) were used.

In a typical experiment, a solution of NVP (0.640 mL, 6.00 mmol) in acetate buffer (4.40 mL, pH = 5.2) was added to the RAFT agent MMPX and degassed. A degassed solution of VA-044 in acetate buffer (1.00 mL, pH = 5.2) was added and a temperature of 50 °C or 30 °C was adjusted. The polymerizations were terminated by quenching the reaction mixture with oxygen and cooling in liquid nitrogen. The polymers were purified by dialysis in water for 3 days and subsequent freeze-drying.

Conversions were determined by ^{1}H NMR spectroscopy in deuterium oxide by comparison of the integral of H2 (1 H, monomer signal) with the integral of He (1 H, polymer signal) (Figure 58, Equation 32).
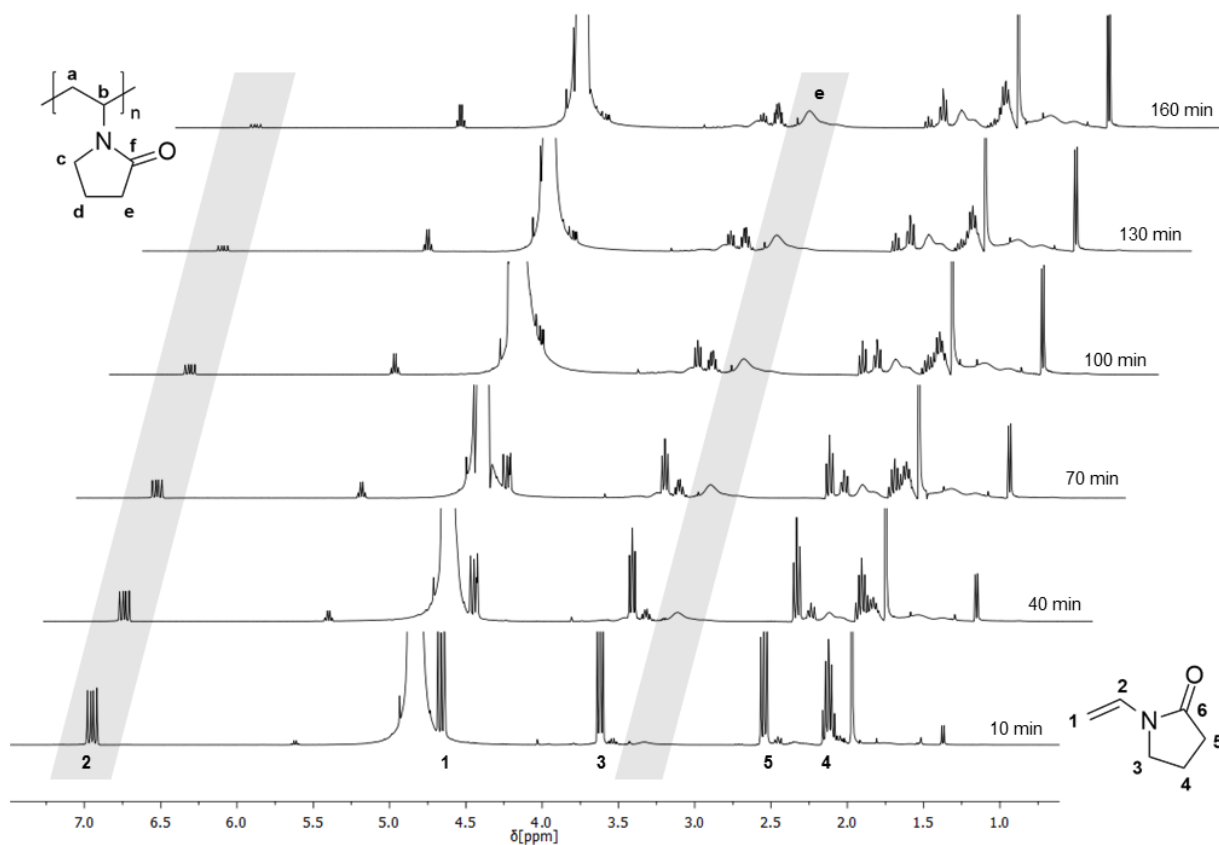
Figure 58. Time-dependent ^{1}H NMR spectra of the polymerization of NVP in D_2O.

$$X_i = \frac{1}{2 \cdot \dfrac{\int H2}{\int He} + 1}$$ (32)

6.3   Hydrogels based on Poly(acrylic acid)

6.3.1   General Synthesis Route

Basotect® was cut into the desired shape (e. g. length x width x thickness: 5.8 x 5.8 x 0.5 cm^3) and washed for 3 days at 80 °C in demineralized water until the amine smell could no longer be noticed. The samples were dried in a vacuum drying oven at 40 °C.

Sodium hydroxide was dissolved in demineralized water and cooled with ice water. Acrylic acid, PEGda and KPS were added stepwise in various proportions, and the monomer solution was degassed with argon or nitrogen for at least 30 min.

The dry, weighted and ruler measured Basotect® samples were transferred into a crystalliz-ing dish in a desiccator, conditioned by applying vacuum and purging with argon or nitrogen and impregnated with the monomer solution. For sufficient impregnation, it was necessary to mechanically press out the air of the foam sample. After 1 h of impregnation under inert gas, the soaked foam was transferred into a clean crystallizing dish in the desiccator and condi-tioned by shortly applying vacuum and purging with argon or nitrogen. The desiccator was transferred into a drying cabinet with a temperature of 80 °C. Usually, the reaction was stopped after 6 h by cooling the composite under air to room temperature, washing with de-mineralized water and drying in a vacuum drying oven at 40 °C. For reaction monitoring, samples were taken after a defined time and freeze-dried to inhibit further polymerization and to remove the solvent.

Typically, concentrations of acrylic acid between 0.5 mol/L and 0.9 mol/L, 5–15 mol% PEGda with regard to acrylic acid, 1 mol% KPS with regard to acrylic acid and a neutralization degree (ND) of 80 % were adjusted.

6.3.2   Swelling Measurements

The dry SAP-Basotect® composite samples were weighted and placed in the swelling solu-tion (usually demineralized water). Periodically, the samples were removed from the solvent, the surface dabbed with industrial paper towel and weighted. Afterwards, the samples were immersed in new swelling medium immediately to continue the swelling. The swelling was stopped when there was no further change of the sample weight for hours. The mean value was used to determine the equilibrium swelling degree. For some samples, the equilibrium could not be determined because the composites disintegrated or short chains of crosslinked poly(acrylic acid) were washed out.

For a re-run of swelling measurements, the swollen samples were dried in a vacuum drying oven at 40 °C and the measurements were replicated.

6.3.3   Removal of Interstitial Solvent

The removal of interstitial solvent in the swollen samples was carried out by applying vacu-um with a water jet pump for 5 min on both sides of the sample.

6.3.4 Solvent Exchange

A solvent exchange with ethanol or dimethyl sulfoxide (DMSO) was carried out after the swelling equilibrium in demineralized water had been reached. A content of organic solvent of 30 % (24 h), 60 % (24 h), 90 % (24 h) and 100 % (> 48 h) was gradually adjusted.

6.3.5 Drying Process

The composites swollen in ethanol or DMSO were dried by fluid extraction with supercritical carbon dioxide. The composites swollen in demineralized water were dried in a vacuum drying oven at 40 °C or by lyophilization.

7. List of Hazardous Substances used according to GHS

The chemicals used in this work are listed with safety instructions in Table 8.

Table 8. Safety instructions of the chemicals used.[4]

Substances	GHS pictograms	Hazard Sentences	Precaution Sentences
Acetic acid	GHS02, GHS05 **Danger**	H226–H314	P210–P260–P280–P303 + P361 + P353–P305 + P351 + P338–P370 + P378
Acrylic acid	GHS02, GHS05, GHS07, GHS09 **Danger**	H226–H302 + H312 + H332–H314–H335–H400	P210–P260–P280–P303 + P361 + P353–P305 + P351 + P338–P370 + P378
Aluminum oxide	No hazardous substance.		
Azobisisobutyronitrile	GHS02, GHS07 **Danger**	H242–H302 + H332–H412	P210–P220–P234–P261–P280–P370 + P378
Basotect®	No hazardous substance.		
Benzyl bromide	GHS07 **Warning**	H315–H319–H335	P261–P305 + P351 + P338
1,2-Bis(2-(4,5-dihydro-1H-imidazol-2-yl)propan-2-yl)diazene dihydrochloride[140]	GHS07 **Warning**	H302–H315–H319–H332–H335	P264–P302 + P352–P304 + P340–P305 + P351 + P338–P332 + P313–P337 + P313
3-Bromopropionic acid	GHS05 **Danger**	H314	P280–P305 + P351 + P338–P310
Carbon disulfide	GHS02, GHS07, GHS08 **Danger**	H225–H315–H319–H332–H361fd–H372	P201–P210–P261–P280–P304 + P340 + P312–P308 + P313

Substances	GHS pictograms	Hazard Sentences	Precaution Sentences
Chloroform	GHS06, GHS08 **Danger**	H302–H315–H319–H331–H336–H351–H361d–H372	P260–P280–P301 + P312 + P330–P304 + P340 + P312–P305 + P351 + P338–P403 + P233
Chloroform-*d*	GHS06, GHS08 **Danger**	H302–H315–H319–H331–H351–H361d–H372	P260–P280–P301 + P312 + P330–P304 + P340 + P312–P305 + P351 + P338–P403 + P233
Deuterium oxide	No hazardous substance.		
Dichloromethane	GHS07, GHS08 **Warning**	H315–H319–H335–H336–H351–H371	P260–P280–P305 + P351 + P338
Diethyl ether	GHS02, GHS07 **Danger**	H224–H302–H336	P210–P261
Dimethyl sulfoxide	No hazardous substance.		
Dimethylformamide	GHS02, GHS07, GHS08 **Danger**	H226–H312 + H332–H319–H360D	P201–P280–P305 + P351 + P338–P308 + P313
1,4-Dioxane	GHS02, GHS07, GHS08 **Danger**	H225–H319–H335–H351	P210–P280–P305 + P351 + P338–P370 + P378–P403 + P235
N-Ethyl-*N*′-(3-dimethyl-aminopropyl)carbodi-imide hydrochloride	GHS05, GHS07 **Danger**	H315–H318–H335	P261–P280–P305 + P351 + P338
Ethanol	GHS02, GHS07 **Danger**	H225–H319	P210–P305 + P351 + P338–P370 + P378–P403 + P235

Substances	GHS pictograms	Hazard Sentences	Precaution Sentences
Furfurylamine	GHS02, GHS05, GHS07 **Danger**	H226–H302 + H312–H314	P280–P305 + P351 + P338–P310
Hydrochloric acid, 37 %	GHS05, GHS07 **Danger**	H290–H314–H335	P261–P280–P305 + P351 + P338–P310
N-Isopropylacrylamide	GHS07 **Warning**	H302–H319	P305 + P351 + P338
Lithium bromide	GHS07 **Warning**	H302–H315–H317–H319	P280–P305 + P351 + P338
Magnesium sulfate	No hazardous substance.		
Methanol	GHS02, GHS06, GHS08 **Danger**	H225–H301 + H311 + H331–H370	P210–P280–P302 + P352 + P312–P304 + P340 + P312–P370 + P378–P403 + P235
Methyl α-ᴅ-glucopyranoside	No hazardous substance.		
Methyl α-ᴅ-mannopyranoside	No hazardous substance.		
Petroleum ether	GHS02, GHS07, GHS08, GHS09 **Danger**	H224–H304–H315–H336–H411	P210–P301 + P310–P331–P370 + P378–P403 + P235
Poly(ethylene glycol) diacrylate	GHS05, GHS07 **Danger**	H315–H317–H318	P280–P305 + P351 + P338

Substances	GHS pictograms	Hazard Sentences	Precaution Sentences
Potassium persulfate	GHS03, GHS07, GHS08 **Danger**	H272–H302–H315–H317–H319–H334–H335	P220–P261–P280–P305 + P351 + P338–P342 + P311
Silica gel	No hazardous substance.		
Sodium acetate	No hazardous substance.		
Sodium chloride	No hazardous substance.		
Sodium hydroxide	GHS05 **Danger**	H290–H314	P280–P301 + P330 + P331–P305 + P351 + P338–P308 + P310
Tetramethylsilane	GHS02 **Danger**	H224	P210
N-Vinyl pyrrolidone	GHS05, GHS07, GHS08 **Danger**	H302 + H312 + H332–H318–H335–H351–H373	P260–P280–P301 + P312 + P330–P305 + P351 + P338 + P310

The CMR substances used are listed in Table 9.

Table 9. List of CMR substances used (category 1A and 1B).[4]

CAS Number	Substances	Procedure	Used Amount	Category
68-12-2	Dimethylformamide	SEC	1 L	1b

8. Bibliography

[1]   P. C. Hiemenz, *Polymer Chemistry – The Basic Concepts*, Marcel Dekker, New York/Basel **1984,** 346 ff.

[2]   H.-G. Elias, *Makromoleküle – Band 1: Chemische Struktur und Synthesen,* 6th Ed., Wiley-VCH Verlag GmbH & Co. KGaA, Weinheim, Germany **1999,** 148–152, 214 ff., 262 ff., 299 ff.

[3]   Wako, *Azo Initiators,* www.wako-chem.co.jp/english, accessed on **24.08.2017**.

[4]   Sigma-Aldrich, *Safety Data Sheet,* www.sigmaaldrich.com, accessed on **19.01.2018**.

[5]   C. J. Hawker, *J. Am. Chem. Soc.* **1994**, *116*, 11185–11186.

[6]   J.-S. Wang, K. Matyjaszewski, *J. Am. Chem. Soc.* **1995**, *117*, 5614–5615.

[7]   K. Matyjaszewski, T. Pintauer, S. Gaynor, *Macromolecules* **2000**, *33*, 1476–1478.

[8]   J. Chiefari, Y. K. Chong, F. Ercole, J. Krstina, J. Jeffery, T. P. T. Le, R. T. A. Mayadunne, G. F. Meijs, C. L. Moad, G. Moad, E. Rizzardo, S. H. Thang, *Macromolecules* **1998**, *31*, 5559–5562.

[9]   Y. K. Chong, T. P. T. Le, G. Moad, E. Rizzardo, S. H. Thang, *Macromolecules* **1999**, *32*, 2071–2074.

[10]   L. Albertin, M. Stenzel, C. Barner-Kowollik, L. J. R. Foster, T. P. Davis, *Macromolecules* **2004**, *37*, 7530–7537.

[11]   L. Albertin, M. H. Stenzel, C. Barner-Kowollik, L. J. R. Foster, T. P. Davis, *Macromolecules* **2005**, *38*, 9075–9084.

[12]   G. Gody, T. Maschmeyer, P. B. Zetterlund, S. Perrier, *Nat. Commun.* **2013**, *4*, 2505.

[13]   G. Gody, T. Maschmeyer, P. B. Zetterlund, S. Perrier, *Macromolecules* **2014**, *47*, 639–649.

[14]   V. Darcos, A. Duréault, D. Taton, Y. Gnanou, P. Marchand, A.-M. Caminade, J.-P. Majoral, M. Destarac, F. Leising, *Chem. Commun. (Camb.)* **2004**, 2110–2111.

[15]   J. Bernard, A. Favier, L. Zhang, A. Nilasaroya, T. P. Davis, C. Barner-Kowollik, M. H. Stenzel, *Macromolecules* **2005**, *38*, 5475–5484.

[16]   J. Bernard, X. Hao, T. P. Davis, C. Barner-Kowollik, M. H. Stenzel, *Biomacromolecules* **2006**, *7*, 232–238.

[17]   M. H. Stenzel-Rosenbaum, T. P. Davis, A. G. Fane, V. Chen, *Angew. Chem. Int. Ed.* **2001**, *40*, 3428–3432.

[18]   G. Moad, J. Chiefari, Y. K. Chong, J. Krstina, R. T. A. Mayadunne, A. Postma, E. Rizzardo, S. H. Thang, *Polym. Int.* **2000**, *49*, 993–1001.

[19]   C. Barner-Kowollik, T. P. Davis, J. P. A. Heuts, M. H. Stenzel, P. Vana, M. Whittaker, *J. Polym. Sci., Part A: Polym. Chem.* **2003**, *41*, 365–375.

[20]   S. Perrier, P. Takolpuckdee, *J. Polym. Sci., Part A: Polym. Chem.* **2005**, *43*, 5347–5393.

[21]   G. Moad, *Macromol. Chem. Phys.* **2014**, *215*, 9–26.

[22]   P. Vana, T. P. Davis, C. Barner-Kowollik, *Macromol. Theory Simul.* **2002**, *11*, 823–835.

[23]   C. Barner-Kowollik, M. Buback, B. Charleux, M. L. Coote, M. Drache, T. Fukuda, A. Goto, B. Klumperman, A. B. Lowe, J. B. McLeary, G. Moad, M. J. Monteiro, R. D. Sanderson, M. P. Tonge, P. Vana, *J. Polym. Sci., Part A: Polym. Chem.* **2006**, *44*, 5809–5831.

[24] M. Destarac, W. Bzducha, D. Taton, I. Gauthier-Gillaizeau, S. Z. Zard, *Macromol. Rapid Commun.* **2002**, *23*, 1049–1054.

[25] D. J. Keddie, C. Guerrero-Sanchez, G. Moad, E. Rizzardo, S. H. Thang, *Macromolecules* **2011**, *44*, 6738–6745.

[26] D. Charmot, P. Corpart, H. Adam, S. Z. Zard, T. Biadatti, G. Bouhadir, *Macromol. Symp.* **2000**, *150*, 23–32.

[27] M. H. Stenzel, L. Cummins, G. E. Roberts, T. P. Davis, P. Vana, C. Barner-Kowollik, *Macromol. Chem. Phys.* **2003**, *204*, 1160–1168.

[28] C. Wei, K. Wu, J. Li, W. Ma, J. Guo, J. Hu, C. Wang, *Macromol. Chem. Phys.* **2012**, *213*, 557–565.

[29] W. Meiser, J. Barth, M. Buback, H. Kattner, P. Vana, *Macromolecules* **2011**, *44*, 2474–2480.

[30] C. Li, J. He, Y. Zhou, Y. Gu, Y. Yang, *J. Polym. Sci., Part A: Polym. Chem.* **2011**, *49*, 1351–1360.

[31] F. Ganachaud, M. J. Monteiro, R. G. Gilbert, M.-A. Dourges, S. H. Thang, E. Rizzardo, *Macromolecules* **2000**, *33*, 6738–6745.

[32] K. Nilles, P. Theato, *Polym. Chem.* **2011**, *2*, 376–384.

[33] F. Ran, S. Nie, J. Li, B. Su, S. Sun, C. Zhao, *Macromol. Biosci.* **2012**, *12*, 116–125.

[34] T. Qu, A. Wang, J. Yuan, J. Shi, Q. Gao, *Colloids Surf., B* **2009**, *72*, 94–100.

[35] J. Ma, C. Yang, J. Luo, T. Shen, M. Lu, *J. Macromol. Sci. A* **2012**, *49*, 321–329.

[36] A. Sogabe, J. D. Flores, C. L. McCormick, *Macromolecules* **2010**, *43*, 6599–6607.

[37] K. Chang, Z. T. Dicke, L. J. Taite, *J. Polym. Sci., Part A: Polym. Chem.* **2012**, *50*, 976–985.

[38] G. Pound, J. B. McLeary, J. M. McKenzie, R. F. M. Lange, B. Klumperman, *Macromolecules* **2006**, *39*, 7796–7797.

[39] S. Aroua, E. G. V. Tiu, M. Ayer, T. Ishikawa, Y. Yamakoshi, *Polym. Chem.* **2015**, *6*, 2616–2619.

[40] A. Guinaudeau, S. Mazières, D. J. Wilson, M. Destarac, *Polym. Chem.* **2012**, *3*, 81–84.

[41] H. Mori, H. Ookuma, S. Nakano, T. Endo, *Macromol. Chem. Phys.* **2006**, *207*, 1005–1017.

[42] M. Benaglia, M. Chen, Y. K. Chong, G. Moad, E. Rizzardo, S. H. Thang, *Macromolecules* **2009**, *42*, 9384–9386.

[43] S. J. Stace, G. Moad, C. M. Fellows, D. J. Keddie, *Polym. Chem.* **2015**, *6*, 7119–7126.

[44] T. F. Tadros, *Rheology of dispersions – Principles and applications*, Wiley-VCH Verlag GmbH & Co. KGaA, Weinheim **2010,** 149–150.

[45] N. A. Peppas, J. Z. Hilt, A. Khademhosseini, R. Langer, *Adv. Mater.* **2006**, *18*, 1345–1360.

[46] D. S. Kryndushkin, I. M. Alexandrov, M. D. Ter-Avanesyan, V. V. Kushnirov, *J. Biol. Chem.* **2003**, *278*, 49636–49643.

[47] J. C. Moore, *J. Polym. Sci. A Gen. Pap.* **1964**, *2*, 835–843.

[48] S. Banerjee, S. Bhattacharya, *Crit. Rev. Food Sci. Nutr.* **2012**, *52*, 334–346.

[49] D. A. Loy, E. M. Russick, S. A. Yamanaka, B. M. Baugher, K. J. Shea, *Chem. Mater.* **1997**, *9*, 2264–2268.

[50] M. D. Lechner, K. Gehrke, E. H. Nordmeier, *Makromolekulare Chemie – Ein Lehrbuch für Chemiker, Physiker, Materialwissenschaftler und Verfahrenstechniker,* 4th Ed., Birkhäuser, Basel/Boston/Berlin **2010,** 24–25.

[51] E. M. Ahmed, *J. Adv. Res.* **2015**, *6*, 105–121.

[52] C. Seidel, *Dissertation*, Universität Hamburg, Hamburg **2003**.

[53] G. Deepa, A. K. T. Thulasidasan, R. J. Anto, J. J. Pillai, G. S. V. Kumar, *Int. J. Nanomedicine* **2012**, *7*, 4077–4088.

[54] R. Skouri, F. Schosseler, J. P. Munch, S. J. Candau, *Macromolecules* **1995**, *28*, 197–210.

[55] C. Seidel, W.-M. Kulicke, C. Heß, B. Hartmann, M. D. Lechner, W. Lazik, *Starch/Stärke* **2004**, *56*, 157–166.

[56] G. Panariello, R. Favaloro, M. Forbicioni, E. Caputo, R. Barbucci, *Macromol. Symp.* **2008**, *266*, 68–73.

[57] F. Lim, A. M. Sun, *Science* **1980**, *210*, 908–910.

[58] H. Wokalek, W. Strasser, US 4905700 (A), **1990**.

[59] N. Efron, G. Young, *Oph. Phys. Optics* **1988**, *8*, 253–256.

[60] S. Ladet, L. David, A. Domard, *Nature* **2008**, *452*, 76–79.

[61] M. J. Zohuriaan-Mehr, K. Kabiri, *Iran. Polym. J.* **2008**, *17*, 451–477.

[62] W. Chen, J. Ma, L. Zhu, Y. Morsi, H. Ei-Hamshary, S. S. Al-Deyab, X. Mo, *Colloids Surf., B* **2016**, *142*, 165–172.

[63] C. de Las Heras Alarcon, S. Pennadam, C. Alexander, *Chem. Soc. Rev.* **2005**, *34*, 276–285.

[64] A. Pourjavadi, S. Barzegar, F. Zeidabadi, *React. Funct. Polym.* **2007**, *67*, 644–654.

[65] H. Omidian, K. Park, *J. Drug Delivery Sci. Technol.* **2008**, *18*, 83–93.

[66] H. Li, J. Yang, X. Hu, J. Liang, Y. Fan, X. Zhang, *J. Biomed. Mater. Res. A* **2011**, *98*, 31–39.

[67] R. Lalani, L. Liu, *Biomacromolecules* **2012**, *13*, 1853–1863.

[68] A. Das, V. K. Kothari, S. Makhija, K. Avyaya, *J. Appl. Polym. Sci.* **2008**, *107*, 1466–1470.

[69] F. F. Montesano, A. Parente, P. Santamaria, A. Sannino, F. Serio, *Agric. Agric. Sci. Procedia* **2015**, *4*, 451–458.

[70] D. Hermeling, B. Steinmetz, DE 102004062457 (A1), **2005**.

[71] G. Burillo, E. Bucio, E. Arenas, G. P. Lopez, *Macromol. Mater. Eng.* **2007**, *292*, 214–219.

[72] J. Hu, S. Liu, *Macromolecules* **2010**, *43*, 8315–8330.

[73] H. G. Schild, *Prog. Polym. Sci.* **1992**, *17*, 163–249.

[74] A. B. Kinney, A. B. Scranton, *Formation and Structure of Cross-Linked Polyacrylates,* in: F. L. Buchholz, N. A. Peppas (Eds.), *ACS Symposium Series: Superabsorbent Polymers – Science and Technology*, American Chemical Society, Washington, DC **1994**, 2–26.

[75] K. Kabiri, H. Omidian, M. J. Zohuriaan-Mehr, S. Doroudiani, *Polym. Compos.* **2011**, *32*, 277–289.

[76] K. M. Raju, M. P. Raju, *Polym. Int.* **2001**, *50*, 946–951.

[77] M. J. Zohuriaan-Mehr, H. Omidian, S. Doroudiani, K. Kabiri, *J. Mater. Sci.* **2010**, *45*, 5711–5735.

[78] S. Friedrich, *Superabsorbent Polymers (SAP),* in: V. Mechtcherine, H.-W. Reinhardt (Eds.), *RILEM State of the Art Reports: Application of super absorbent polymers (SAP) in concrete construction*, Springer, Dordrecht **2012**, 13–19.

[79]   H. Omidian, S. A. Hashemi, P. G. Sammes, I. Meldrum, *Polymer* **1998**, *39*, 6697–6704.

[80]   F. L. Buchholz, *Preparation Methods of Superabsorbent Polyacrylates,* in: F. L. Buchholz, N. A. Peppas (Eds.), *ACS Symposium Series: Superabsorbent Polymers – Science and Technology*, American Chemical Society, Washington, DC **1994**, 27–38.

[81]   K. Kabiri, M. J. Zohuriaan-Mehr, *Polym. Adv. Technol.* **2003**, *14*, 438–444.

[82]   R. Kumar, A. Srivastava, K. Behari, *J. Appl. Polym. Sci.* **2007**, *105*, 1922–1929.

[83]   D. R. Chambers, H. H. Fowler, Y. Fujiura, F. Masuda, US 5145906 (A), **1992**.

[84]   T. Tsubakimoto, T. Shimomura, Y. Irie, Y. Masuda, US 4286082 (A), **1981**.

[85]   Z. Chen, M. Liu, S. Ma, *React. Funct. Polym.* **2005**, *62*, 85–92.

[86]   M. J. Zohuriaan-Mehr, A. Pourjavadi, *J. Polym. Mater.* **2003**, *20*, 113–120.

[87]   K. Kabiri, S. Faraji-Dana, M. J. Zohuriaan-Mehr, *Polym. Adv. Technol.* **2005**, *16*, 659–666.

[88]   H. J. Haehnle, H. Baumgartl, N. Herfert, DE 10034505 A1, **2002**.

[89]   S. Hintz, H. Brüggemann, DE 10231356 A1, **2004**.

[90]   P. Rudolf, WO 2011/032862 A1, **2011**.

[91]   H. J. Quadbeck-Seeger, U. Licht, E. J. Bauer, T. Baumgärtner, A. Ziemer, A. Alteheld, WO 2009/056543 A1, **2009**.

[92]   L. D. Whitmore, F. Engelhardt, WO 01/56625 A2, **2001**.

[93]   S. Himori, K. Itoh, Y. Sugyo, Y. Mori, T. Ishii, US 2006/0252899 A1, **2006**.

[94]   B. Fugmann, M. Dietze, WO 2006/066752 A1, **2006**.

[95]   M. Stork, M. Ehrenstein, T. Breiner, A. Poppe, A. Alteheld, V. Warzelhan, WO 2005/103107 A1, **2005**.

[96]   H.-J. Quadbeck-Seeger, WO 2007/118803 A1, **2007**.

[97]   BASF, *Basotect, The versatile melamine resin foam,* www.basotect.de, accessed on **28.11.2017**.

[98]   F. Askari, S. Nafisi, H. Omidian, S. A. Hashemi, *J. Appl. Polym. Sci.* **1993**, *50*, 1851–1855.

[99]   F. Rosa, J. Bordado, M. Casquilho, *Polymer* **2002**, *43*, 63–70.

[100] J. Chen, H. Park, K. Park, *J. Biomed. Mater. Res.* **1999**, *44*, 53–62.

[101] I. C. Alupei, M. Popa, M. Hamcerencu, M. J. M. Abadie, *Eur. Polym. J.* **2002**, *38*, 2313–2320.

[102] Y. Zhao, H. Su, L. Fang, T. Tan, *Polymer* **2005**, *46*, 5368–5376.

[103] E. Selic, W. Borchard, *Macromol. Chem. Phys.* **2001**, *202*, 516–520.

[104] K. Kimura, T. Hatsuda, K. Nagasuna, EP 0450924 A2, **1991**.

[105] A. R. Berens, *Polymer* **1977**, *18*, 697–704.

[106] A. R. Berens, H. B. Hopfenberg, *Polymer* **1978**, *19*, 489–496.

[107] J. Crank, *The mathematics of diffusion,* 2nd Ed., Clarendon Press, Oxford **1975,** 91.

[108] A. S. Hoffman, *Clin. Chem.* **2000**, *46*, 1478–1486.

[109] R. Duncan, *Nat. Rev. Drug Discov.* **2003**, *2*, 347–360.

[110] T. Delair, M.-H. Charles, P. Cros, A. Laayoun, B. Mandrand, C. Pichot, *Polym. Adv. Technol.* **1998**, *9*, 349–361.

[111] P. Pakawanit, S. Ananta, T. K. Yun, J. Y. Bae, W. Jang, H. Byun, J.-H. Kim, *RSC Adv.* **2014**, *4*, 39287–39296.

[112] M. K. Kokufuta, S. Sato, E. Kokufuta, *Colloid Polym. Sci.* **2012**, *290*, 1671–1681.

[113] T. G. Park, A. S. Hoffman, *J. Biomed. Mater. Res.* **1990**, *24*, 21–38.

[114] B. V. Robinson, F. M. Sullivan, J. F. Borzelleca, S. L. Schwartz, *PVP – A critical review of the kinetics and toxicology of polyvinylpyrrolidone (povidone)*, Lewis Publishers, Chelsea **1990,** 1 ff.

[115] A. B. Lowe, B. S. Sumerlin, C. L. McCormick, *Polymer* **2003**, *44*, 6761–6765.

[116] C. Barner-Kowollik, S. Perrier, *J. Polym. Sci., Part A: Polym. Chem.* **2008**, *46*, 5715–5723.

[117] B. Le Droumaguet, J. Nicolas, *Polym. Chem.* **2010**, *1*, 563–598.

[118] G. Moad, E. Rizzardo, S. H. Thang, *Aust. J. Chem.* **2012**, *65*, 985–1076.

[119] L. Albertin, A. Wolnik, A. Ghadban, F. Dubreuil, *Macromol. Chem. Phys.* **2012**, *213*, 1768–1782.

[120] G. Gody, T. Maschmeyer, P. B. Zetterlund, S. Perrier, *Macromolecules* **2014**, *47*, 3451–3460.

[121] S. R. S. Ting, A. M. Gregory, M. H. Stenzel, *Biomacromolecules* **2009**, *10*, 342–352.

[122] L. Liu, J. Zhang, W. Lv, Y. Luo, X. Wang, *J. Polym. Sci., Part A: Polym. Chem.* **2010**, *48*, 3350–3361.

[123] M. Bathfield, F. D'Agosto, R. Spitz, M.-T. Charreyre, T. Delair, *J. Am. Chem. Soc.* **2006**, *128*, 2546–2547.

[124] C. Barner-Kowollik, J. F. Quinn, T. L. U. Nguyen, J. P. A. Heuts, T. P. Davis, *Macromolecules* **2001**, *34*, 7849–7857.

[125] H. Paulsen, *Master Thesis*, Universität Hamburg, Hamburg **2014**.

[126] D. Trimnell, W. M. Doane, C. R. Russell, C. E. Rist, *Carbohydr. Res.* **1967**, *5*, 166–175.

[127] E. Humeres, V. Soldi, M. Klug, M. Nunes, C. M. S. Oliveira, P. J. Barrie, *Can. J. Chem.* **1999**, *77*, 1050–1056.

[128] S. Stürmer, *Bachelor Thesis*, Universität Hamburg, Hamburg **2015**.

[129] S. Houshyar, D. J. Keddie, G. Moad, R. J. Mulder, S. Saubern, J. Tsanaktsidis, *Polym. Chem.* **2012**, *3*, 1879–1889.

[130] T. Arita, M. Buback, P. Vana, *Macromolecules* **2005**, *38*, 7935–7943.

[131] Y. Hu, Z. Du, X. Deng, T. Wang, Z. Yang, W. Zhou, C. Wang, *Macromolecules* **2016**.

[132] T. Nakajima, H. Sato, Y. Zhao, S. Kawahara, T. Kurokawa, K. Sugahara, J. P. Gong, *Adv. Funct. Mater.* **2012**, *22*, 4426–4432.

[133] J. Li, W. R. K. Illeperuma, Z. Suo, J. J. Vlassak, *ACS Macro Lett.* **2014**, *3*, 520–523.

[134] J. Wang, J. Wei, S. Su, J. Qiu, S. Wang, *J. Mater. Sci.* **2015**, *50*, 5458–5465.

[135] T. Wang, S. Zheng, W. Sun, X. Liu, S. Fu, Z. Tong, *Soft Matter* **2014**, *10*, 3506–3512.

[136] D. Xu, D. Bhatnagar, D. Gersappe, J. C. Sokolov, M. H. Rafailovich, J. Lombardi, *Macromolecules* **2015**, *48*, 840–846.

[137] J. A. Beamish, J. Zhu, K. Kottke-Marchant, R. E. Marchant, *J. Biomed. Mater. Res. A* **2010**, *92*, 441–450.

[138] J.-Y. Kim, J.-Y. Song, E.-J. Lee, S.-K. Park, *Colloid Polym. Sci.* **2003**, *281*, 614–623.

[139] C. Kreiner, L. Nachbaur, WO 2009/021526 A1, **2009**.

[140] Fluorochem, *Material Safety Data Sheet,* www.fluorochem.co.uk, accessed on **19.01.2018**.

9. Appendix

9.1 Kinetic Modelling of Swelling Experiments

9.1.1 Code for the Diffusion-Relaxation Model

For 0 ≤ x ≤ 0.5

[General Information]
Function Name = DiffRelaxModell
Brief Description = Diffusion-Relaxation-Model
Function Source = N/A
Number Of Parameters = 3
Function Type = User-Defined
Function Form = Equations
Path =
Number Of Independent Variables = 1
Number Of Dependent Variables = 1
Function Model = Explicit
Analytical Derivatives for User-Defined = 0
FunctionPrev = DiffRelaxModellSummation

[Fitting Parameters]
Names = x,kD,kR
Initial Values = 0(V),0(V),0(V)
Meanings = amount of diffusion controlled processes,rate constant of Fickian diffusion controlled sorption,rate constant of relaxation controlled sorption
Lower Bounds = 0(I, On),0(I, On),0(I, On)
Upper Bounds = 0.5(I, On),--(I, Off),--(I, Off)
Naming Method = User-Defined
Number Of Significant Digits = 0,0,0
Unit = ,1/h,1/h
Format = --,--,--
CustomDisplay = --,--,--

[Independent Variables]
t =

[Dependent Variables]
y =

[Formula]
```
double bb = 0;
  for(int ii =1; ii<=100; ii++)
  {
      bb = 1/(ii^2) * exp(-(ii^2) * kD * t) + bb;
  }
  y = x * (1 - (6/(pi^2)) * bb)
+ (1 - x) * (1 - exp(-kR*t));
```

[Constraints]

[Initializations]

[After Fitting]

[Constants]

[Controls]
General Linear Constraints = 0
Initialization Scripts = 0
Scripts After Fitting = 0
Number Of Duplicates = N/A
Duplicate Offset = N/A
Duplicate Unit = N/A
Generate Curves After Fitting = 1
Curve Point Spacing = Uniform on X-Axis Scale
Generate Peaks After Fitting = 1
Generate Peaks During Fitting = 1
Generate Peaks with Baseline = 1
Paste Parameters to Plot After Fitting = 1
Paste Parameters to Notes Window After Fitting = 1
Generate Residuals After Fitting = 0
Keep Parameters = 0
Compile On Param Change Script = 1
Enable Parameters Initialization = 1
Treat All Numbers As Double = 1

[Compile Function]
Compile = 1
Compile Parameters Initialization = 1
OnParamChangeScriptsEnabled = 0

[Parameters Initialization]
//Code to be executed to initialize parameters

[Origin C Function Header]
#pragma numlittype(push, TRUE)
#pragma numlittype(push, TRUE)
#pragma warning(error : 15618)
#include <origin.h>
// Add your special include files here.
// For example, if you want to fit with functions from the NAG library,
// add the header file for the NAG functions here.
// Add code here for other Origin C functions that you want to define in this file,
// and access in your fitting function.
// You can access C functions defined in other files, if those files are loaded and compiled
// in your workspace, and the functions have been prototyped in a header file that you have
// included above.

// You can access NLSF object methods and properties directly in your function code.
// You should follow C-language syntax in defining your function.
// For instance, if your parameter name is P1, you cannot use p1 in your function code.
// When using fractions, remember that integer division such as 1/2 is equal to 0, and not 0.5
// Use 0.5 or 1/2.0 to get the correct value.
// For more information and examples, please refer to the "User-Defined Fitting Function"
// section of the Origin Help file.

[Origin C Parameter Initialization Header]

[Derived Parameter Settings]
Unit =
Names =
Meanings =

[References]
Rosa et al.

[LabTalk Functions Definition and Initializations]

[QuickCheck]
t=1
x=0
kD=0
kR=0

For 0.5 ≤ x ≤ 1

[General Information]
Function Name = DiffRelaxModell
Brief Description = Diffusion-Relaxation Model
Function Source = N/A
Number Of Parameters = 3
Function Type = User-Defined
Function Form = Equations
Path =
Number Of Independent Variables = 1
Number Of Dependent Variables = 1
Function Model = Explicit
Analytical Derivatives for User-Defined = 0
FunctionPrev = DiffRelaxModellSummation

[Fitting Parameters]
Names = x,kD,kR
Initial Values = 0(V),0(V),0(V)
Meanings = amount of diffusion controlled processes,rate constant of Fickian diffusion controlled sorption,rate constant of relaxation controlled sorption
Lower Bounds = 0.5(I, On),0(I, On),0(I, On)
Upper Bounds = 1(I, On),--(I, Off),--(I, Off)
Naming Method = User-Defined

Number Of Significant Digits = 0,0,0
Unit = ,1/h,1/h
Format = --,--,--
CustomDisplay = --,--,--

[Independent Variables]
t =

[Dependent Variables]
y =

[Formula]
double bb = 0;
  for(int ii =1; ii<=100; ii++)
  {
     bb = 1/(ii^2) * exp(-(ii^2) * kD * t) + bb;
  }
  y = x * (1 - (6/(pi^2)) * bb)
+ (1 - x) * (1 - exp(-kR*t));

[Constraints]

[Initializations]

[After Fitting]

[Constants]

[Controls]
General Linear Constraints = 0
Initialization Scripts = 0
Scripts After Fitting = 0
Number Of Duplicates = N/A
Duplicate Offset = N/A
Duplicate Unit = N/A
Generate Curves After Fitting = 1
Curve Point Spacing = Uniform on X-Axis Scale
Generate Peaks After Fitting = 1
Generate Peaks During Fitting = 1
Generate Peaks with Baseline = 1
Paste Parameters to Plot After Fitting = 1
Paste Parameters to Notes Window After Fitting = 1
Generate Residuals After Fitting = 0
Keep Parameters = 0
Compile On Param Change Script = 1
Enable Parameters Initialization = 1
Treat All Numbers As Double = 1

[Compile Function]
Compile = 1
Compile Parameters Initialization = 1

OnParamChangeScriptsEnabled = 0

[Parameters Initialization]
//Code to be executed to initialize parameters

[Origin C Function Header]
#pragma numlittype(push, TRUE)
#pragma warning(error : 15618)
#include <origin.h>
// Add your special include files here.
// For example, if you want to fit with functions from the NAG library,
// add the header file for the NAG functions here.
// Add code here for other Origin C functions that you want to define in this file,
// and access in your fitting function.
// You can access C functions defined in other files, if those files are loaded and compiled
// in your workspace, and the functions have been prototyped in a header file that you have
// included above.
// You can access NLSF object methods and properties directly in your function code.
// You should follow C-language syntax in defining your function.
// For instance, if your parameter name is P1, you cannot use p1 in your function code.
// When using fractions, remember that integer division such as 1/2 is equal to 0, and not 0.5
// Use 0.5 or 1/2.0 to get the correct value.
// For more information and examples, please refer to the "User-Defined Fitting Function"
// section of the Origin Help file.

[Origin C Parameter Initialization Header]

[Derived Parameter Settings]
Unit =
Names =
Meanings =

[References]
Rosa et al.

[LabTalk Functions Definition and Initializations]

[QuickCheck]
t=1
x=0
kD=0
kR=0

Declaration on Oath

I hereby declare on oath that I have written the present dissertation by my own and have not used other than the acknowledged resources and aids. I hereby declare that I have not previously applied or pursued for a doctorate (Ph.D. studies).

Hamburg, 27.04.2018